IMAGE-GUIDED THERAPEUTIC DELIVERY TO SOLID TUMORS WITH HPMA COPOLYMERS

by

Brandon Buckway

A dissertation submitted to the faculty of
The University of Utah
in partial fulfillment of the requirements for the degree of

Doctor of Philosophy

Department of Pharmaceutics and Pharmaceutical Chemistry

The University of Utah

December 2013

The University of Utah Graduate School

STATEMENT OF DISSERTATION APPROVAL

The dissertation of **Brandon Buckway**

has been approved by the following supervisory committee members:

Hamidreza Ghandehari	, Chair	**6/12/2013** Date Approved
John Hoffman	, Member	**6/4/2013** Date Approved
Sunil Sharma	, Member	**6/12/2013** Date Approved
James Herron	, Member	**6/12/2013** Date Approved
Jindrich Kopecek	, Member	**6/11/2013** Date Approved

and by **David Grainger** , Chair/Dean of

the Department/College/School of **Pharmaceutics and Pharmaceutical Chemistry**

and by David B. Kieda, Dean of The Graduate School.

ABSTRACT

Treatment of cancer is a significant challenge due to the heterogeneity of both tumors and patients. This realization has led to the field of personalized medicine in which patients can be selected for a therapy based on the specific needs. One potential area for personalized medicine is utilizing medical imaging to predict and monitor the therapeutic efficacy and safety of a particular targeted therapy. Development of image-guided therapeutics based on macromolecular carriers such as *N*-(2-hydroxypropyl)methacrylamide (HPMA) copolymers is advantageous because they are water-soluble and can contain a wide range of comonomers to confer multifunctionality. HPMA copolymers are water-soluble nano-sized constructs which can improve the delivery of therapeutics to tumors by passive targeting via the enhanced permeability and retention effect. They can also increase tumor uptake using targeting ligands that are conjugated to the backbone of the copolymer. This dissertation focuses on the development of targeted HPMA copolymers for delivery of both therapeutics and imaging agents to solid tumors. Barriers to delivery of these constructs were addressed in various tumor models. In pancreatic tumors, the desmoplastic response, or dense extracellular matrix prevents delivery of drugs and macromolecules alike. Treating hyaluronic acid, a component of desmoplasia, with hyaluronidase allowed for increased delivery of HPMA copolymers based on HER2 and $\alpha_v\beta_3$ integrin targeting strategies for HPMA copolymers. Based on the selection of HER2 as a viable tumor targeting strategy,

an image-guided drug delivery (IGDD) system was synthesized, characterized and evaluated in vitro in pancreatic tumor cell lines. In vitro results suggest that the designed construct was potentially capable of targeting, binding, treating and imaging pancreatic tumors for an IGDD approach. Lastly, a study was conducted in a prostate tumor model for localized tumor delivery of a ^{90}Y radiolabeled HPMA copolymers for radiotherapy. Imaging tumor localization and biodistribution was accomplished using an equivalent ^{111}In radiolabeled HPMA copolymer. Targeting and efficacy were accomplished via gold nanorod (GNR)-mediated hyperthermia and demonstrated antitumor efficacy in the prostate tumor mouse model. The combined studies demonstrate the current progress for development of an HPMA copolymer conjugate for image-guided therapy of solid tumors.

To my wife and kids…

For your love, patience and support.

CONTENTS

LIST OF FIGURES

Figure

LIST OF TABLES

Table

LIST OF SCHEMES

Scheme

ABBREVIATIONS

^{111}In	^{111}In - Indium
^{131}I	^{131}I-Iodine
^{18}F	^{18}F-Fluorine
^{19}F	^{19}F-Fluorine
3D	Three dimensional
^{64}Cu	^{64}Cu-Copper
^{90}Y	^{90}Y-Yttrium
AIC	Akaike information criterion
ANOVA	One-way analysis of variance
APMA	*N*-(3-Aminopropyl)methacrylamide hydrochloride
APMA-CHX-A"-DTPA	*N*-methacryloylaminopropyl-2-amino-3-(isothiourea-phenyl)propyl-cyclohexane-1,2-diamine-*N,N-N',N',N''*-pentaacetic acid
APMA-DOTA	1, 4, 7, 10-tetraazacyclododecane-1,4,7,10-tetraacetic acid mono (*N*-(3-aminopropyl)methacrylamide
AUC	Area under the curve
CD	Cluster of differentiation
CML	Chronic Myeloid Leukemia
CPDT	2-cyano-2-propyl dodecyl trithiocarbonate
CPP	Cell penetrating peptides
CT	X-ray computed tomography

CTAB	hexadecyltrimethylammonium bromide
DCM	Dichloromethane
DIPEA	Diisopropylethylamine
DMF	Dimethylformamide
DMM	Dulbecco's Modified Medium
DMSO	Dimethylsulfoxide
DNA	Deoxyribonucleic acid
DOTA	1, 4, 7, 10-tetraazacyclododecane-1,4,7,10-tetraacetic acid
EDTA	Ethylenediaminetetraacetic acid
EGFR	Epidermal growth factor receptor
EPR	Enhanced permeability and retention
FBS	Fetal bovine serum
FDA	Food and drug administration
FDG	^{18}F-Fluorodeoxyglucose
FFPE	Formalin-fixed parrafin-embedded
FISH	Fluorescence in situ hybridization
FMT	Fluorescence molecular tomography
FPLC	Fast protein liquid chromatography
FRET	Fluorescence resonance energy transfer
Gem	Gemcitabine
GFLG	Gly-Phe-Leu-Gly
GMP	Good manufacturing practices
GNR	Gold nanorod
GRP78	Glucose-regulated protein 78
H&E	Hemotoxylin and Eosin

HA	Hyaluronic acid
HAMA	Human anti-mouse antibodies
HBTU	*O*-Benzotriazole-N,N,N',N'-tetramethyl-uronium-hexafluoro-phosphate
HCl	Hydrochloric acid
HER2	Human epidermal growth factor receptor 2
HIFU	High Intensity Focused Ultrasound
HPLC	High- performance liquid chromatography
HPMA	*N*-(2-hydroxypropyl)methacrylamide
IACUC	Institutional Animal Care and Use Committee
IFP	Intratumoral fluidic pressure
IGDD	Image guided drug delivery
IGT	Image guided therapeutics
IHC	Immunohistochemistry
IMDM	Iscove's Modified Dulbecco's Medium
KCCYSL	Lys-Cys-Cys-Tyr-Ser-Leu
KYLCSC	Scramble sequence for KCCYSL targeted peptide comparisons
MA	Methacrylic acid
MA-GG-TT	*N*-methacryloyl-glycyl-glycyl-thiazolidine-2-thione
MALS	Multi-angle light scattering
MoAbs	Monoclonal antibodies
mol%	Mole percent
MR-HIFU	Magnetic Resonance High Intensity Focused Ultrasound
MRI	Magnetic Resonance Imaging
MW	Molecular weight
MWCO	Molecular weight cutoff

NCI	National Cancer Institute
PAMAM	Poly(amido amine)
PBS	Phosphate buffered saline
PCR	Polymerase chain reaction
PDAC	Pancreatic ductal adenocarcinoma
PDT	Photodynamic therapy
PE	Phycoerythrin
PEG	Poly(ethylene glycol)
PEHAM	Poly(etherhydroxylamine)
PEI	Polyethylenimine
PET	Positron emission tomography
PGA	Poly(glutamic acid)
PPTT	Plasmonic photothermal therapy
RAFT	Reversible addition-fragmentation transfer
RES	Reticuloendothelial system
RGD	Arg-Gly-Asp
RGDfK	Arg-Gly-Asp-d-Phe-Lys
RGEfK	Non-targeted control peptide for RGDfK peptide comparisons
RNA	Ribonucleic acid
SEC	Size exclusion chromatography
SEM	Standard error of the mean
siRNA	Small interfering ribonucleic acid
SMA	Smooth muscle actin
SMANCS	Polystyrene-co-maleic acid-half-butylate copolymer
SNR	Signal to noise ratio

SPECT	Single photon emission computed tomography
SPIONs	Superparamagnetic iron oxide nanoparticles
SPR	Surface plasmon resonance
T½	Half-life
TFA	Tetrafluoro acetic acid
UV	Ultraviolet
VA-044	2,2'-Azobis[2-(2-imidazolin-2-yl)propane] dihydrochloride
wt%	Weight percent
α	Alpha particle
β^-	Beta particle
β^+	Positron

ACKNOWLEDGEMENTS

The ideas and work presented in this dissertation would not have been possible without the support, contribution and guidance of many people. These people have influenced my life immensely, for which I am thankful.

Primarily I need to thank my wife, Amanda Buckway, who has honestly worked harder than anyone I know at raising our family of five wonderful children. Through it all, she continually supported, encouraged and cared for me and our family. Her continued support of my goals and educational directions never faltered, even after the struggles of changing research directions and lengthening my time away from home. Her warm smile and embrace could melt away an entire day of frustrating results from experiments. I could not have done it without her.

My advisor, Dr. Hamid Ghandehari, provided a new and exciting direction half-way through my graduate studies and took me to a new level of understanding. He also allowed me to work in an area of research that took a new direction in his lab here in Utah. His time and dedication to his work were an example to me of what it takes to be a successful researcher. I admire his ability to direct such a large and successful laboratory. I have learned so much under his tutelage and greatly adore his loyalty to his students.

My thesis committee has been instrumental in providing the direction needed to accomplish the research of this project. Dr. James Herron was very supportive and made sure that my data were always scientifically sound. Under his tutelage, as a teaching

assistant, I learned a great deal about what it takes to manage a classroom and teach effectively. His observation and feedback on all my endeavors have made me a better scientist.

Dr. Jindrich Kopeček, another member of my committee, provided the expertise and suggestions in polymer chemistry. His knowledge in this area is unsurpassed. I appreciate his support and friendship. I admire his dedication to his work and career as a scientist and hope I can perhaps follow in his footsteps that so greatly have influenced the world of polymer therapeutics.

Dr. Sunil Sharma has provided some of the most useful direction in my research. His knowledge in current research in the area of pancreatic cancer was extremely helpful in accomplishing an impactful result in my studies. I appreciate the multiple sessions of research direction he provided and for assuring that whatever direction I took had a translational goal in mind.

To Dr. John Hoffman I owe a substantial amount of gratitude. He was both a member on my committee and my current employer in the Molecular Imaging Program at the Huntsman Cancer Institute who allowed me to take the necessary time to accomplish this work. His lifetime experience with imaging was an essential part of my research. I greatly appreciate his advice and for incorporating my education into my job as a radiochemist. I appreciate his mentorship in learning the regulatory aspects of radiopharmaceuticals. I was fortunate to have this opportunity, unlike many of my student colleagues. He has been very patient and willing to always work with me and I especially appreciate the time he dedicated out of his busy schedule during this process.

Dr. Abhijit Ray played a very key role in my learning of polymer chemistry. His guidance taught me new skills in organic synthesis and various techniques that I could not have learned by myself. His friendship was also helpful in and outside of the lab. His support and encouragement were extremely helpful when things were not going well. I acknowledge his support during my educational career.

I also cannot hesitate to thank Dr. Yongjian Wang, visiting scientist from Nankai University in China. She worked for a whole year on synthesis of some of the conjugates for image-guided drug delivery. There is no way I could have completed the amount of work that needed to be done without her help. I appreciate her patience, encouragement and friendship and for teaching me a little about the culture of China. Her dedication to the research and effort deserves a significant amount of praise.

I would also like to thank my first mentor, Dr. Zheng-Rong Lu, who was extremely supportive of my goals for image-guided therapeutics. During my time in his lab, I learned a great deal about chemistry and how to manage my time. Although his transfer to Case Western Reserve University was not advantageous for my education, he has been continually supportive and always had my best interests at mind.

I need to especially thank my parents, Dallas and Shirlene Buckway, for always encouraging me to do my best. Being raised as the oldest child of a large family of ten was what shaped my aspirations today. They taught me how to work hard and were always encouraging me to be the best example I could be for my family. I am a first-generation college graduate and Ph.D. graduate. They have always been excited to hear my latest results in my research, even though they probably understand very little of what

I was working on. They have been extremely supportive and proud of all my accomplishments and I will be always in debt to them for helping find my way in life.

I have made many lasting friendships that have helped me to accomplish this research. Dr. Nate Larson integrated me into the Ghandehari lab when I first joined and showed me a good example of how to balance family, work and research. Dr. Giridhar Thiagarajan always had big ideas for research and encouraged me to pursue them. John Gibby is a fellow radiochemist at the Cyclotron Lab at Huntsman Cancer Institute who would always lend an ear when I needed it and was always willing to help me out if I had experiments that took me away from my employment. Dr. Adam Gormley provided guidance in the gold nanorod mediated hyperthermia studies. Dr. Venkata Yellepeddi and Dallin Hubbard were both always willing and able to lend a hand when I needed it with experiments.

I would also like to acknowledge the seed funding grant support for my research from the Imaging, Diagnostics, and Therapeutics Program at the Huntsman Cancer Institute and the University's assistance in partially funding my graduate tuition.

CHAPTER 1

INTRODUCTION

1.1. Introduction

Cancer is the second leading cause of death in the United States[1]. Recent statistics estimate that nearly 12 million Americans with a history of cancer were alive in January of 2008[2]. 1 in 2 men and 1 in 3 women risk developing or dying from cancer during their lifetime[2,3]. The prevalence of cancer is expansive. However, some progress has been made during the past few decades in treating this difficult disease. The 5-year survival rate for all cancers diagnosed in the United States was 49% in the years 1975-1977 and has increased to 67% during 2001-2007[2]. This rate increase represents improvements in both aspects of the disease from diagnosis to treatment. There remains a substantial need to improve the standard of care for patients with cancer.

Cancer is a very complicated disease to treat. This may be due to the fact that each type of cancer is actually its own specific disease. The website for Cancer Research (UK) reported that more than 200 cancer malignancies can develop in over 60 organs of the human body[4]. Each type comes with its own set of causes, symptoms, characteristics and limitations to treatment. This creates quite an array of problems for clinicians in knowing exactly how to treat each malignancy. Not only is the vast library of individual cancer diseases a problem, but each individual patient with cancer may have different

responses to the disease as well. Still, this is not all. Each tumor developed in a patient is heterogeneous which will affect the patient's ability to be successfully cured. Clearly, options must be developed with which we can assess this disease on a case-by-case basis in regards to individual needs.

Historically, a patient diagnosed with cancer is given a scripted treatment plan based on their cancer staging and what has worked in the past for other patients with the same cancer, a 'one-size-fits-all' approach[5]. Recently, due to medical advances in diagnosis of cancer, a person's treatment is more and more tailored to their specific cancer characteristics. One area that clinicians are finding to be very helpful in diagnosing cancer is imaging. Imaging in cancer patients is growing at an ever-increasing rate because it gives more accurate assessment of tumor staging and treatment response[6]. High-resolution techniques such as x-ray computerized tomography (CT) and magnetic resonance imaging (MRI) can enable anatomical placement of tumors along with size and shape that can be progressively measured during treatment to monitor response. Through the advanced molecular imaging techniques used in nuclear medicine modalities such as single photon emission computerized tomography (SPECT) and positron emission tomography (PET) imaging, clinicians can also understand the underlying processes effecting tumor treatment response, including metabolic state, hypoxia or proliferation that are occurring in each tumor within an individual[7,8]. Each of these modalities can be combined to give a more accurate and precise treatment plan for patients, leading to better overall treatment.

Theranostics is defined as medical treatment which combines both diagnostics and therapeutics for personalized therapy of an individual's disease status. This includes

the use of any diagnostic test including genetic testing, histology and/or imaging which can estimate potential response, predict safety and monitor progress of a specific therapy. One simple example is the use of an excised biopsy tissue being evaluated for HER2 expression using the HercepTest®[9] and other HER2 assays from the tumor of a breast cancer patient which gives prognostic information when treating with Herceptin®. The patient can then be qualified or disqualified for the therapy, thus assuring that the patient is receiving a treatment that has a much greater chance of efficacy. However, diagnostics such as HER2 assays for breast cancer have their limitations. They rely on invasive tissue biopsies, sometimes leading to false negative results simply because of the limited sampling of tissue[10]. The use of modern imaging technologies can more accurately assess the tumors for prognostic factors because the entire tumor is visualized.

For example, ^{18}F-Fluorodeoxyglucose (FDG) imaging using PET has been widely used to influence treatment planning in cancer patients[11]. FDG localization in a tumor is a result of high metabolic activity or viability of a tumor. Imaging before and after use of an anticancer therapy can measure the therapeutic response and lead to maintenance of the particular therapy or change in treatment plan if there is no response. Even though the measure of glucose metabolism in tumors is not directly related to a particular therapeutic, it represents how a very simple imaging diagnostic can be utilized in conjunction with therapeutic treatments. Another simple case of a theranostic use has been in practice for decades. ^{131}I therapy, a beta emitter for thyroid cancer, has been used in conjunction with ^{123}I imaging using gamma scintigraphic techniques since the mid-1940s[12]. Imaging the patient with ^{123}I gamma scintigraphy predicts whether the thyroid is iodine sensitive. This prevents the use of the therapeutic in patients who will not see any

effect from the therapeutic ^{131}I which can be more harmful for the patient. Image-guided therapy is becoming a more widely used concept based on the benefit to the patient.

Imaging-based theranostics can be developed on an array of different materials. One area of increasing promise is the use of multifunctional nanomaterials as image-guided platforms. Nanoconstructs can be used for treatment and/or diagnosis with a size generally in the 1-100 nm range[13]. Their size, shape and density can be matched to the biological properties of the body, including cell surfaces, pores and channels. The main common property of these materials is their large surface area-to-volume ratio which allows for their surface to be coated with various molecules, including drugs, targeting ligands and imaging agents. Designing a nanomaterial with multiple functionalities is important to the development of an image-guided therapeutic system. The properties of a nanomaterial influence the pharmacokinetics, drug release, stability and payload for delivery to diseased tissue. Therefore, selecting the proper material for theranostic applications needs to be tailored for the needs of the disease.

Water-soluble polymers such as *N*-(2-hydroxypropyl)methacrylamide (HPMA) copolymers are promising platforms for image-guided therapies[14,15]. HPMA copolymers are biocompatible, nonimmunogenic and can be synthesized with a variety of comonomers to attach imaging agents, drugs and targeting ligands in a nano-sized range. The various functionalities can be conjugated to the side chains of the HPMA copolymer backbone, as shown schematically in *Figure 1*. HPMA copolymers can be tailored to the proper size in order to control biodistribution and pharmacokinetic profiles needed to successfully target tumors. Due to their macromolecular nature, these copolymers passively target tumors based on the enhanced permeability and retention (EPR) effect[16].

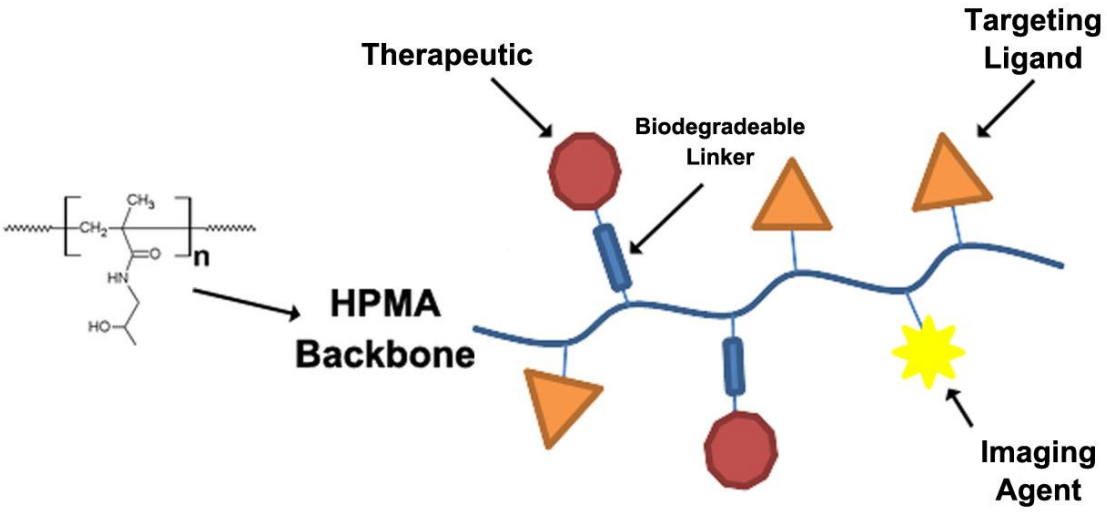

Figure 1.1. Schematic representation of HPMA copolymer for image-guided therapy

Many studies have shown that HPMA copolymer-drug conjugates successfully increase delivery to tumors via passive targeting[17-19]. However, accumulation in the tumor can be further enhanced by incorporating targeting ligands to the HPMA copolymer construct.

Active targeting of tumors can be accomplished by adding various tumor targeting ligands to HPMA copolymer side chains such as sugars, small peptide sequences and antibody fragments that are recognized by the surface of tumor cells[20-24]. Increased uptake leads to increased localization of drug or imaging agents, thereby increasing the efficacy of cancer treatment. For example, the use of RGD peptide, which targets the $\alpha_v\beta_3$ integrin receptors overexpressed on tumor vasculature, has been shown to increase the accumulation and antitumor efficacy in prostate cancer models [25,26]. The combination of both active targeting and passive targeting via the EPR effect with targeted HPMA copolymers creates a promising platform for their development as an image-guided therapeutic or theranostic platform.

The **ultimate goal** of this dissertation is to design an HPMA copolymer system for image-guided delivery to solid tumors. Ideally, the HPMA copolymer will have an effective targeting ligand for the recognition of overexpressed tumor cells. Therapeutics will be selected based on the ability of HPMA copolymers to improve their efficacy, stability and release within the targeted tumor mass. Many drugs are rapidly metabolized in the bloodstream and conjugation to the backbone can prevent enzymatic access to the metabolism of the drug. Site-specific drug release will be incorporated into the polymer via biodegradable spacers that retain drug activity after tumor localization. Barriers to solid tumor delivery will also be considered in the development of targeted approaches. Tumor delivery will be assessed using nuclear medicine imaging techniques

in order to provide quantitative relationships between areas of conjugate localization. SPECT will be used because of its high sensitivity to commercially available radionuclides with radioactive half-lives that match biological half-lives of HPMA copolymers in the body such as ^{111}In (2.8 day ½-life)[27]. Incorporation of both imaging and therapeutics will allow the correlation of biodistribution of the HPMA copolymer with potential efficacy and safety of a combined image-guided theranostic system.

1.2. Aims and Scope of This Dissertation

The overall rationale for developing image-guided therapeutics based on HPMA copolymers begins with the knowledge that many barriers exist to delivery of therapeutics to solid tumors. Lack of efficacy in tumor treatment with therapeutics can be attributed to several factors; these include therapeutic instability in the bloodstream, lack of tumor penetration, dose-limiting toxicity due to off-target accumulation in various organs, low solubility or low bioavailability of the therapeutic dose. All of these factors essentially lead to insufficient therapeutic concentration in the tumor to overcome the rapid tumor growth. HPMA copolymers can be designed to overcome these barriers.

The **hypothesis** of this research is that image-guided therapeutics using HPMA copolymers can overcome the barriers to tumor treatment. Many studies involving imaging demonstrated the ability to visualize localization of HPMA copolymers in tumors[15]. Successful delivery of therapeutics to the tumor has also been demonstrated using HPMA copolymers[28]. What remains is further development in matching these constructs with the combined imaging and therapeutic that can correlate efficacy and safety in a patient. By using HPMA copolymer conjugates in this manner, patients can

be evaluated in real-time whether a therapeutic agent is working or will work based on the imaging results. Development of these systems has great potential for improving the quality of cancer treatment. In this dissertation, two model tumors of pancreatic and prostate were utilized to evaluate targeting, imaging and therapy. Three aims were investigated.

1.2.1. Specific Aim 1: Compare and evaluate HPMA-based targeting strategies and overcome the barriers to pancreatic tumor delivery

In **Aim 1**, two targeting strategies were used to investigate the ability of HPMA copolymers to target pancreatic cancer. HPMA copolymers with side-chain terminated in KCCYSL or cyclic RGDfK peptides which bind to HER2 or $\alpha_v\beta_3$ integrin receptors, respectively, were used as tumor targeting strategies. Synthesis and characterization of the HPMA copolymers for pancreatic tumor targeting were established. Pancreatic cancer is a difficult disease to treat and evidence suggested this may be due to the desmosplastic response that creates a dense interstitial tissue with high intratumoral fluidic pressure (IFP) preventing small molecular weight drug and macromolecular delivery to the tumor. Targeted HPMA copolymer tumor localization was investigated, after reducing tumor stromal effects with hyaluronidase, a stromal treating enzyme for hyaluronic acid prevalent in pancreatic tumor stroma. Biodistribution and imaging of the targeting strategies using ^{111}In radiolabeled targeted HPMA copolymers were compared in pancreatic CAPAN-1 tumor bearing mice before and after stromal treatment. Results of these studies are discussed in Chapter 3[29].

1.2.2. Specific Aim 2: Evaluate a HER2 targeted image-guided drug delivery system based on HPMA copolymers for pancreatic cancer treatment

In **Aim 2**, the synthesis of HPMA comonomers and subsequent HPMA copolymer construct with targeting ligand, drug and imaging agent by reversible-addition fragmentation transfer (RAFT) polymerization were established. A method for solid phase synthesis of peptide-containing comonomers was described. Gemcitabine, the first line therapeutic drug for pancreatic cancer, was conjugated via a lysosomally degradable linker and incorporated into the HPMA copolymer along with a chelator for ^{111}In isotopes for quantitative SPECT imaging. HPMA copolymers were evaluated for binding affinity using a receptor blocking experiment. Radiostability of the ^{111}In complexed with HPMA copolymers were tested in mouse serum at physiologically relevant parameters. Drug release was investigated in pH 5.0, 7.0 and cell culture media. Cytotoxicity of gemcitabine was also evaluated against CAPAN-1 (HER2 positive) and PANC-1 (HER2 negative) pancreatic tumor cell lines. The results are reported in Chapter 4[30].

1.2.3. Specific Aim 3: Correlate the in-vivo imaging and efficacy of gold nanorod-mediated hyperthermia with a HPMA copolymer-^{90}Y conjugates

In **Aim 3**, HPMA copolymers containing 1, 4, 7, 10-tetraazacyclododecane-1,4,7,10-tetraacetic acid (DOTA) were synthesized by reversible addition-fragmentation transfer (RAFT) copolymerization. Subsequently, labeling was performed with either ^{111}In for imaging or ^{90}Y for efficacy studies. Radiolabeled complexes were assayed for

stability in vitro in the presence of mouse serum. Imaging using SPECT of the ^{111}In conjugates was performed in order to determine the pharmacokinetics and biodistribution of the HPMA copolymer conjugates when tumors were treated with gold nanorod mediated hyperthermia. Localized mild tumor hyperthermia was achieved by plasmonic photothermal therapy using gold nanorods. Efficacy studies evaluating the combination of hyperthermia and radiotherapy with ^{90}Y radiolabeled HPMA copolymers were conducted in DU145 prostate tumor-bearing mice. The results of this study are found in Chapter 5[31]. The overall conclusion and future directions are discussed in Chapter 6.

1.3. References

1. Minino AM, Murphy SL. Death in the United States, 2010. NCHS Data Brief. 2012:1-8.

2. American Cancer Society. Cancer Facts and Figures 2012. Atlanta, GA: American Cancer Society; 2012.

3. Siegel R, DeSantis C, Virgo K, et al. Cancer treatment and survivorship statistics, 2012. CA Cancer J Clin. 2012; 62:220-241.

4. Cancer Research UK. How many different types of cancer are there? Available from URL: http://www.cancerresearchuk.org/cancer-help/about-cancer/cancer-questions/how-many-different-types-of-cancer-are-there [accessed 03/25/2013].

5. Sumer B, Gao J. Theranostic nanomedicine for cancer. Nanomedicine (Lond). 2008; 3:137-140.

6. Weissleder R. Molecular imaging in cancer. Science. 2006; 312:1168-1171.

7. Bailey DL. Positron emission tomography : basic sciences. New York: Springer, 2005.

8. Chowdhury FU, Scarsbrook AF. The role of hybrid SPECT-CT in oncology: current and emerging clinical applications. Clin Radiol. 2008; 63:241-251.

9. Jacobs TW, Gown AM, Yaziji H, Barnes MJ, Schnitt SJ. Specificity of HercepTest in determining HER-2/neu status of breast cancers using the United States Food and Drug Administration-approved scoring system. J Clin Oncol. 1999; 17:1983-1987.

10. Jenner K, Darnton SJ, Billingham L, Warfield AT, Matthews HR. Tumour heterogeneity: a problem in biopsy assessment of the proliferation index of oesophageal adenocarcinomas. Clin Mol Pathol. 1996; 49:M61-63.

11. Hillner BE, Siegel BA, Shields AF, et al. The impact of positron emission tomography (PET) on expected management during cancer treatment: findings of the National Oncologic PET Registry. Cancer. 2009; 115:410-418.

12. Lee DY, Li KC. Molecular theranostics: a primer for the imaging professional. AJR Am J Roentgenol. 2011; 197:318-324.

13. Kim BY, Rutka JT, Chan WC. Nanomedicine. N Engl J Med. 2010; 363:2434-2443.

14. Kopecek J, Kopeckova P. HPMA copolymers: origins, early developments, present, and future. Adv Drug Deliv Rev. 2010; 62:122-149.

15. Lu ZR. Molecular imaging of HPMA copolymers: visualizing drug delivery in cell, mouse and man. Adv Drug Deliv Rev. 2010; 62:246-257.

16. Noguchi Y, Wu J, Duncan R, et al. Early phase tumor accumulation of macromolecules: a great difference in clearance rate between tumor and normal tissues. Jpn J Cancer Res. 1998; 89:307-314.

17. Etrych T, Strohalm J, Chytil P, Rihova B, Ulbrich K. Novel star HPMA-based polymer conjugates for passive targeting to solid tumors. J Drug Target. 2011; 19:874-889.

18. Kopecek J. Polymer-drug conjugates: origins, progress to date and future directions. Adv Drug Deliv Rev. 2013; 65:49-59.

19. Etrych T, Chytil P, Mrkvan T, Sirova M, Rihova B, Ulbrich K. Conjugates of doxorubicin with graft HPMA copolymers for passive tumor targeting. J Control Release. 2008; 132:184-192.

20. Pike DB, Ghandehari H. HPMA copolymer-cyclic RGD conjugates for tumor targeting. Adv Drug Deliv Rev. 2010; 62:167-183.

21. Larson N, Ray A, Malugin A, Pike DB, Ghandehari H. HPMA copolymer-aminohexylgeldanamycin conjugates targeting cell surface expressed GRP78 in prostate cancer. Pharm Res. 2010; 27:2683-2693.

22. Pola R, Studenovsky M, Pechar M, et al. HPMA-copolymer conjugates targeted to tumor endothelium using synthetic oligopeptides. J Drug Target. 2009; 17:763-776.
23. Johnson RN, Kopeckova P, Kopecek J. Biological activity of anti-CD20 multivalent HPMA copolymer-Fab' conjugates. Biomacromolecules. 2012; 13:727-735.

24. Yang Y, Zhou Z, He S, et al. Treatment of prostate carcinoma with (galectin-3)-targeted HPMA copolymer-(G3-C12)-5-Fluorouracil conjugates. Biomaterials. 2012; 33:2260-2271.

25. Borgman MP, Aras O, Geyser-Stoops S, Sausville EA, Ghandehari H. Biodistribution of HPMA copolymer-aminohexylgeldanamycin-RGDfK conjugates for prostate cancer drug delivery. Mol Pharm. 2009; 6:1836-1847.

26. Ray A, Larson N, Pike DB, et al. Comparison of active and passive targeting of docetaxel for prostate cancer therapy by HPMA copolymer-RGDfK conjugates. Mol Pharm. 2011; 8:1090-1099.

27. Kupinski MA, Barrett HH. Small-animal SPECT imaging. New York: Springer, 2005.

28. Kopecek J, Kopeckova P, Minko T, Lu Z. HPMA copolymer-anticancer drug conjugates: design, activity, and mechanism of action. Eur J Pharm Biopharm. 2000; 50:61-81.

29. Buckway B, Wang Y, Ray A, Ghandehari H. Overcoming the stromal barriers to targeted delivery of HPMA copolymers to pancreatic tumors. Int J Pharm. (2013); Accepted.

30. Buckway B, Wang Y, Ray A, Ghandehari H. In vitro evaluation of HPMA-copolymers targeted to HER2 expressing pancreatic tumor cells for image guided drug delivery Macromol Biosci. (2013); Accepted.

31. Buckway B, Frazier N, Gormley AJ, Ray A, Ghandehari H. Gold nanorod-mediated hyperthermia enhances the efficacy of HPMA copolymer - ^{90}Y conjugates in treatment of prostate tumors. Nucl Med Biol. (2013); Submitted.

CHAPTER 2

LITERATURE BACKGROUND

2.1. Introduction

This chapter provides the underlying background for the hypothesis and aims of the dissertation. Focus will be derived on how cancer treatment can be improved through the use of image-guided therapeutics (IGT) which can assess an individual's disease status and relate the most effective treatment for optimal success. A breakdown of the key characteristics for design of an IGT will be explained with details about choosing the proper material, target, imaging modality and therapeutic for cancer treatment. Examples of systems being currently used in clinic will be presented, as well as those that are under preclinical evaluation.

2.2. Challenges to Traditional Cancer Therapy

Cancer is the second leading cause of death in the United States[3]. The prevalence of cancer is well documented. In fact, about 1 in 2 men and 1 in 3 women risk developing or dying of cancer in their lifetime.[4] Death from cancer related to obesity accounted for approximately 1/3 of all cancer deaths in 2012 and due to increasing rates of obesity is expected to increase[4]. Chance for development of cancer also increases with age[4]. With an ever-increasing average lifetime and growing proportion of aged individuals, we can

expect cancer treatment to continue to be a major part of treatment for the foreseeable future.

The challenge to find a cure for cancer was accelerated in the early 70s with passing of the National Cancer Act. Since then, billions of dollars have been spent on cancer research. A recent study reported that from the years 1995-2005, a total amount of $65.3 billion was spent on cancer research[5]. The NCI is primarily responsible for about 52% of the total research support for academic oncology centers in the U.S.[5]. This is an enormous amount of money and effort in order to cure the disease. However, this effort has only led to a modest improvement of the overall 5-year survival rates for all tumor sites by about 37% (49% to 67%) over the past 25-30 years[4].

A large amount of progress has been made in prevention of the disease, as in the case of lowered lung cancer death rates due to the emphasis on public campaigning of the dangers of smoking tobacco[6]. Advances in earlier detection have also improved the outcomes of several tumor treatments. Breast cancer death rates have slowly decreased over time due to earlier detection using methods such as mammography[7]. Decreased cancer deaths related to both colorectal and prostate cancer have also decreased based on early diagnosis through screening[4]. Treatment options have also expanded for cancer, and have been responsible for a modest reduction in overall cancer deaths. In certain cancer types, novel treatments have made exceptional impacts on survival of patients. For example, Imatinib, a tyrosine kinase inhibitor has made a significant impact in treating chronic myeloid leukemia (CML), even on survival rates beyond 5 years[8]. One of the main reasons for success in therapeutic treatments of cancer is the increased understanding that it is heterogeneous[9], leading to a growing understanding among clinicians that the traditional one-size-fits-all approach to treatment does not work.

2.3. History of Personalized Medicine

Clinicians have found that each individual can respond differently to any particular therapeutic agent based on genetic differences in the individual, in the individual tumor site response to therapy or in the magnitude of the side effects related to a given therapeutic. Therefore, treatments which can be tailored to an individual in order to minimize toxicity and increase therapeutic efficacy are desirable, especially in cancer treatment.

Traditionally, a patient enters a clinician's care and is diagnosed for a given disease based on prevalent symptoms, risk factors and diagnostic tests. Once diagnosed, the patient is given the most effective medicine known by the clinician that has worked for the entire population. Like any population, there are outliers who will not respond like the majority of patients. An outlier patient, who will not respond well to the normal treatment, is susceptible to enhanced risks (i.e., side effects) associated with the treatment without having any beneficial effect. On another note, the patient suffers the disease risks for an extended period of time because the treatment effects are usually latent and time is wasted for both the patient and clinician.

Personalized medicine is beneficial to a patient because it provides the best chance of success for disease treatment in the most efficient manner. One of the first examples of a personalized medicine approach was discovered in 1902[10] in the treatment with primaquine, an antimalarial drug. A genetic deficiency of the enzyme glucose-6-phosphate dehydrogenase led to primaquine-induced hemolytic anemia. Testing for this deficiency led to increased safety of primaquine administration. Since then, many advances have been made in the area of diagnostics, allowing for more rapid, accurate and reliable tests which can be utilized to personalize medicine. Information about the

patient's disease status cannot only be utilized to select or qualify a patient for a particular therapy, but can be used to influence dosing or co-administration of drugs to limit known side effects.

2.4. Definition of Theranostics and Image-Guided Therapy

The term "theranostic" was first described by Funkhouser and his company in 2002[11]. It is defined as a material that combines diagnostic testing with a specific therapeutic in order to increase its safety or efficacy[12]. Diagnostic testing provides genomic, proteomic and anatomical information related to a disease state. These tests come from a wide range of sources, including tissue biopsies and blood tests for in vitro diagnostics or even more sophisticated methods such as imaging. Diagnostic testing utilizes these results to assay the disease status in order to take advantage of weak points in the disease that can be treated by a particular drug or therapeutic intervention. Pharmacogenetics is a field of study that utilizes genetic testing to provide information of patient's susceptibility to a disease or treatment[13]. Despite the ethical concerns of predicting human disease from genetic testing, the information from a genetic test can be used to give patients preventative care that may help avoid the disease occurrence.

The information obtained from theranostic testing is especially suited for the study of cancer. As mentioned before, heterogeneity in cancer reduces the ability to find appropriate treatments[9,14]. Targeted therapies under development to treat cancer are only effective when certain biomarkers are overexpressed in the tumor. However, expression of these biomarkers is variable in a patient population and also within the individual tumors of a particular patient. The ability to assay for the specific biomarker before the patient is given a matching therapeutic can prevent unnecessary wasteful treatments that

are not effective or unnecessarily dangerous to the patient. Thus, in the case of targeted therapeutics for tumor treatment, theranostics can provide a better strategy than traditional methods.

Successful implementation of theranostics not only has the potential of improving the treatment of cancer, but also potentially lowers healthcare costs and streamlines regulatory approval of targeted therapies[15]. This concept of combining treatment with a diagnostic is gaining the attention of pharmaceutical companies. Many therapeutic companies are able to partner with diagnostic companies to accelerate the drug development process by improving clinical trial outcomes. This is done by selecting patients based on potential therapeutic success on a "companion diagnostic." Early examples of this were Herceptin® and the HercepTest®[16]. The FDA simultaneously approved both Genentech's Herceptin® and Dako's HercepTest® for treatment and diagnosis of Stage IV breast cancer. Other examples of FDA approved theranostics are contained in *Table 2.1*

In vitro diagnostics for receptor expression have been found to be useful in qualifying patients for various targeted therapies. However, these assays are invasive and suspect to false positive or false negative results due to sampling error. Typically, tumor samples are collected by biopsy and subsequently tested in assays similar to those contained in *Table 2.1*. A sample may or may not be reflective of the entire tumors' expression profile. Also some tumors may be too small and not detected within the patient and therefore, tissue sampling for a diagnostic test cannot be performed in this case. Therefore, other diagnostic methods are needed that accurately assess the whole tumor for target expression.

Table 2.1. Examples of FDA approved theranostics[19-21].

Trade Name	Manufacturer	Diagnostic Description	Companion Therapeutic
HercepTest	Dako Denmark A/S	Semiquantitative immunocytochemical assay to determine HER2 protein overexpression in breast cancer tissues for histological evaluation and formalin-fixed, paraffin-embedded cancer tissue from patients with metastatic gastric or gastroesophageal junction adenocarcinoma.	Hercepta Perjeta
DAKO C-KIT PharmDx	Dako North America, Inc.	Qualitative immunohistochemical (IHC) kit system for the identification of c-kit protein/CD 117 antigen (c-kit protein) expression in normal and neoplastic formalin-fixed paraffin-embedded tissues for histological evaluation.	Gleevec
VYSIS ALK Break Apart FISH Probe Kit	Abbott Molecular Inc.	Qualitative test to detect rearrangements involving the ALK gene via fluorescence in situ hybridization (FISH) in formalin-fixed, paraffin-embedded (FFPE) non-small cell lung cancer (NSCLC) tissue specimens	Xalkori
COBAS 4800 BRAF V600 Mutation Test	Roche Molecular Systems, Inc.	In vitro diagnostic device intended for the qualitative detection of the BRAF V600E mutation in DNA by PCR extracted from formalin-fixed, paraffin-embedded human melanoma tissue and is intended to be used as an aid in melanoma	Vemurafenib
therascreen KRAS RGQ PCR Kit	Qiagen Manchester, Ltd.	Real-time qualitative PCR assay used for the detection of seven somatic mutations in the human KRAS oncogene, using DNA extracted from formalin fixed paraffin-embedded (FFPE) colorectal cancer	Erbitux
Bexxar	GlaxoSmithKline	Bexxar Dosimetric: a low dose ^{131}I-Tositumomab monoclonal antibody for imaging biodistribution for selection of B-cell Lymphoma patients for radioimmunotherapy	Bexxar Therapeutic: High dose ^{131}I-Tositumomab
Zevalin	Spectrum Pharmaceuticals, Inc.	^{111}In-Ibritumomab Tiuxetan monoclonal antibody for imaging biodistribution for selection of B-cell Lymphoma patients for radioimmunotherapy	^{90}Y-Ibritumomab Tiuxetan

Modern advances in medical imaging have brought theranostics to a whole new level of potential possibilities. Molecular imaging methods such as magnetic resonance imaging (MRI), x-ray computed tomography (CT), ultrasound, single photon emission computerized tomography (SPECT) and positron emission tomography are prevalent in many medical centers today and can accurately monitor tumor progression, stage cancer and detect small lesions[1,17,18]. Image-guided therapies are being accelerated in development with these imaging modalities. Imaging provides noninvasive and real-time information for diagnosis of a patient. MRI and CT are used for anatomical information and can be combined with other nuclear medicine modalities (SPECT and PET) to provide quantification of radiolabeled targeted probes and determine their localization within the patient. Another advantage to image guided therapies is the potential to use platforms which include both diagnostic and therapeutic on one material. Real-time assessment of both target and therapeutic can be measured simultaneously. One example of an image-guided therapy is the use of Bexxar® and Zevalin®[22]. This radioimmunotherapy is based on two targeting monoclonal antibodies (tositumomab and ibritumomab tiuxetan, respectively) which recognize CD20 receptors highly expressed on B-cells. Both agents have an imaging version and a therapeutic version. For Bexxar®, the patients are administered a low dose of ^{131}I-tositumomab to confirm normal biodistribution observed by gamma camera imaging. ^{131}I has both gamma and beta emission that can be used for imaging and radiotherapy. If no abnormal biodistribution is observed, the patient is administered a high dose of ^{131}I-tositumomab. For Zevalin®, a similar approach is used but the imaging version uses ^{111}In and ^{90}Y for radiotherapy. ^{111}In is a pure gamma emitter for imaging and ^{90}Y is a pure beta emitter effective for radiotherapy. Both agents are clinical examples of how image-guided therapy can

improve the treatment of cancer. It improves the safety of radioimmunotherapy because the imaging reduces the risk of more radiation exposure to patients who would not see any benefit from the therapeutic version due to abnormal biodistribution. This strategy was also helpful for regulatory approval because it qualifies a patient for therapy and increases the overall chance for efficacious treatment of lymphoma.

Image-guided therapy can be used in a multitude of methods which help to increase the safety and efficacy of therapeutics. Image-guided drug delivery uses the advantages of imaging to monitor drug delivery within the targeted tumor. It has been suggested that image-guided drug delivery can be incorporated in a multitude of ways including: visualizing of biodistribution in real-time, analyzing drug distribution at the target site, predicting drug response, evaluating longitudinal drug efficacy, combining disease diagnosis with therapy, facilitating triggered drug release, monitoring and quantifying drug release and noninvasively assessing target site accumulation[23]. Drug delivery systems improve the delivery of anticancer drugs that suffer from poor water-solubility and poor pharmacokinetic profiles through the use of passive targeting or active targeting[24-28]. Passive targeting occurs with macromolecular drug delivery systems that selectively accumulate in tumors due to the enhanced permeability and retention (EPR) effect. Active targeting of these systems involves the use of conjugated targeting ligands such as small peptides, sugars or monoclonal antibody fragments which increases recognition and uptake by the targeted cell type. However, targeted drug delivery systems have had many challenges in getting approval for use in the clinic[29]. This can be attributed to the differences in patient responses to both active and passive targeting. However, drug delivery systems are increasingly being developed with imaging agents in order to improve their likelihood of success for treating cancer.

Image-guided therapies have great potential for improving the treatment of cancer. Many strategies can be utilized with these systems. However, there are several challenges for the development and successful use of these conjugates when treating cancer. A wide range of carriers, imaging modalities, targeting strategies and therapeutics have been studied and currently only a select few have overcome the hurdles required for clinical use. Therefore, the next sections will focus on the design criteria and components of image-guided therapeutics for the treatment of cancer. Each section will present several examples of image-guided therapeutics that embody the characteristics of each design criteria. The presentation of each design characteristic will be summarized in the last section and will attempt to provide a picture of the ideal image-guided therapeutic system for cancer treatment.

2.5. Design Criteria for Image-Guided Therapeutics

This section will focus on the different aspects of therapeutic delivery in combination with imaging starting with a discussion of materials and carriers. One of the most challenging aspects of drug delivery is choice of vehicle for delivering the therapeutic, targeting agent and imaging agent.

2.5.1. Type of material and carrier

A large investment in research has been focused on the design and development of materials for targeted delivery to tumors. Each has their advantages and disadvantages for delivery of imaging and therapeutics. Some have had extensive clinical experience or testing. Recently, constructs based on nanomaterials have become a promising area of research[30-32]. The of nano-scale constructs of 1-100 nm in size as therapeutic delivery

systems has generated a promising venue for image-guided theranostics[33-35]. This property allows for multiple components to be incorporated on the surface or within these materials for targeted delivery of both imaging agents and therapeutics. They are also able to be tailored in ways as to interact with the body's pores, channels and surfaces in unique ways because of their small size[31]. Many types of carriers are synthesized in the nano-size range. *Figure 2.1* displays some of the most investigated systems that have been utilized for image-guided delivery. The following are examples of nanomaterials that can be used as image-guided therapeutics for the treatment of cancer.

2.5.1.1. Linear polymers

Some examples of linear polymers that have been extensively studied are poly(ethylene glycol) (PEG), *N*-(2-hydroxypropyl)methacrylamide (HPMA) and poly-*L*-glutamic acid (PGA)[36-38]. A wide body of research has been conducted using these particular linear polymers. PEG and HPMA copolymers are nonbiodegradable where PGA is biodegradable in the body. The main advantage of linear polymer carriers is the ease to control their size[38]. Linear polymers such as those described above are biocompatible and have limited recognition by the immune system[39,40]. This provides an advantage because they can circulate in the body for an extensive amount of time, thus increasing the likelihood of their ability to interact with the targeted tumor sites. PEG and HPMA copolymers also have properties which impart steric hindrance to degradation of their attached payload of drug and targeting moieties[41]. One advantage that HPMA copolymers have is the ability to incorporate multiple therapeutics and targeting agents into the side chains. Linear PEG has limitations in the amount of payload because it is limited to end group functionalization[37]. Some of the main disadvantages to traditional

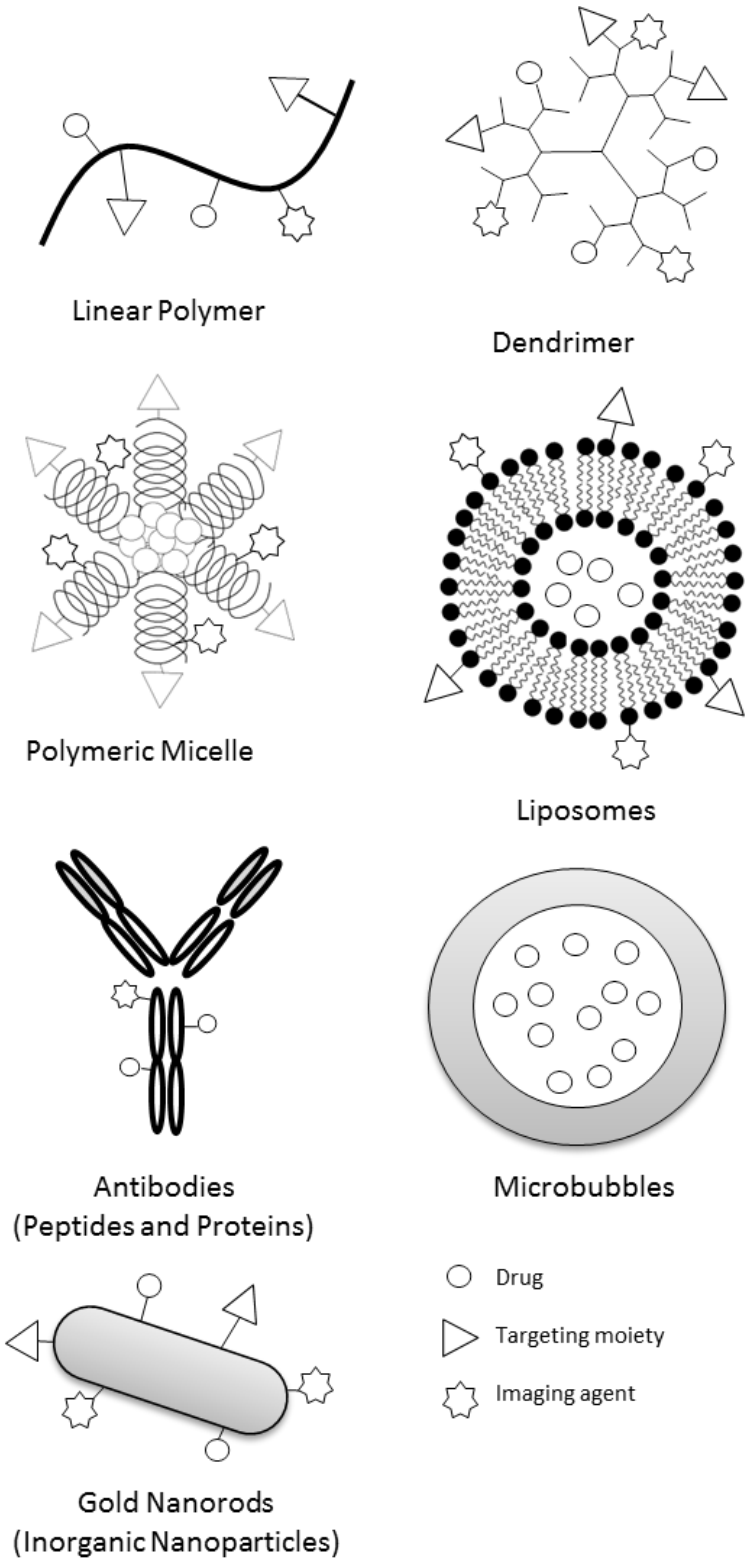

Figure 2.1. Examples of carriers for image-guided therapeutic delivery.

HPMA copolymers are nonbiodegradability and potential long-term exposure in the body leading to possible toxicity effects[42,43]. PGA is biodegradable; however, this may not be ideal for a combined image-guided therapeutic because breakdown of the PGA backbone will eventually lead to imaging agent being separated from the carrier. HPMA copolymer doxorubicin drug conjugates were evaluated in clinical trials[44]. A matching HPMA copolymer was available with attached radioisotopes for imaging the biodistribution of the copolymers in patients[45]. The drug conjugate failed based on lack of efficacy in some patients[46]. However, the trial may have had more success if they had used the imaging version of the HPMA copolymer for preselection of patients that would have been more susceptible to the HPMA copolymer-drug conjugate[23].

2.5.1.2. Polymeric micelles

Polymeric micelles are constructed from a combination of hydrophobic and hydrophilic components or segments[47-49]. The structure is formed in aqueous solutions by self-assembly of a hydrophobic core and hydrophilic shell. Many chemotherapeutics are hydrophobic leading to solubility issues[47]. Hydrophobic drugs can be associated with the hydrophobic core and improve their solubility and protect them from metabolic enzymes in the blood stream while associated with the nanoparticle[50]. Imaging agents and targeting groups can be associated with the hydrophilic components and allow for imaging of micelle biodistribution within the body[50,51]. Another unique advantage that micelles have is their ability to have triggered therapeutic release based on pH change[50,52]. Micelles however, have limited stability in the body and progressively breakdown to their initial components especially when encountering biological milieu[31]. Therefore, imaging of the nanoparticle has limitations due to the eventual breakdown of

the micelle. One example of a block copolymer micelle image-guided drug delivery system incorporated folate targeting, pH sensitive drug release of doxorubicin and Cy5.5 for optical imaging[53]. The polymeric conjugate was able to successfully image targeted conjugate localization and treatment in HeLa tumor cell bearing nude mice[53].

2.5.1.3. Dendrimers

Dendrimers are multibranched polymeric systems with a central initiator core[54,55]. Dendrimer size can be precisely controlled by successive additions of layers of branched units. Dendrimers have exceptionally low polydispersity and in some cases can be unimolecular[56]. Because of their unimolecular structure, regulatory hurdles to clinical approval can be significantly less challenging compared to other polydisperse polymers[57]. The branched structure allows for specific control of the amount and density of functional groups on the surface of the dendrimer. This can be utilized for surface decoration with various imaging agents, targeting moieties and drugs. With larger generations of dendrimers, a hollow core can be formed which can also be loaded with hydrophobic drugs. Several limitations are prevalent with dendrimers. Large dendrimers become difficult to synthesize, because the larger the dendrimers become the more steric hindrance prevents chemical ligation of the branching units and surface modifications[58]. The dendrimer that has had a substantial amount of investigation for clinical development is poly(amino amine) or PAMAM[55,59]. PAMAM dendrimers have had challenges with toxicity based on the charge density of the surface when reacting with cells[60,61]. One of the key aspects of PAMAM dendrimers are the alternating generations terminating with either primary amines or carboxyl groups. One limitation with dendrimers is that their typical branched layered structure contains only one type of surface group for

conjugation of targeting moieties, imaging agents and drugs. This limits the degree of control over how much of each component is incorporated. However, several groups have begun strategically synthesizing "Janus" dendrimers which are able to have several different types of surface functional groups, thereby providing better surface conjugation control[62]. One particular example shows great promise as a platform for a theranostic[63]. Although the study only demonstrated the dendrimer with a near-infrared agent for optical imaging, the conjugate did not show any toxicity in presence of T98G human cells and the unique trifunctional surface groups showed potential for development in image-guided therapy for cancer treatment.

2.5.1.4. Liposomes

Liposomes are spherical lipid bilayer constructs with an aqueous core which can contain drugs or other therapeutic agents[64,65]. Their lipid bilayer structure mimics the biological environment of a cell but can be made of many different materials with the majority using phospholipids. Liposomes are among the most studied drug delivery systems with many clinically approved formulations[66,67]. They are primarily formulated to entrap hydrophilic drugs within their aqueous core or associate hydrophobic drugs into their lipid bilayer[64]. Due to their macromolecular nature, they can passively target tumors via the EPR effect[68]. Of particular mention is Doxil®, a liposome-based formulation of doxorubicin for treatment of advanced ovarian cancer[66]. Liposomes protect their encapsulated drugs from metabolism in the blood stream and fuse with their biologically similar membranes of targeted cells. Once fused with cells, they release their payload into the cell for increased therapeutic efficacy. Phospholipids can be modified with different imaging agents and targeting moieties and be inserted into the lipid bilayer in order to

make theranostic nanoparticle systems[65]. One particular challenge recognized by the FDA with liposomes is reproducibly controlling the size and polydispersity[69]. They are also subject to rapid degradation or reticuloendothelial system (RES) clearance from the body[70]. Methods are being developed to overcome some of the issues such as incorporation of PEG for "stealth" liposomes[71]. However, the biodegradability of these systems in-vivo remains a particular challenge when considered for image guided therapy. Regardless, complex systems have been attempted to overcome these issues. For example, magnetic resonance high-intensity focused ultrasound (MR-HIFU) has been used with temperature sensitive liposomes loaded with doxorubicin[72]. MR imaging was used to guide the placement of localized hyperthermia within the tumor for triggered release of the liposomes in Vx2 rabbit models. This study showed the potential translation of a liposomal formulation for image guided therapy.

2.5.1.5. Microbubbles

Microbubbles for therapeutic delivery are a special case of liposome structure which encompasses gas and can be designed for image-guided therapeutic delivery[73]. Small gas bubbles, typically perfluorocarbons, are imaged via ultrasound based on their difference in echogenicity than liquid media[74]. In most cases, microbubbles are stabilized by a lipid bilayer which surrounds the gas bubble. The surrounding liposome can be loaded with drugs and targeting agents for tumor delivery. With increased sonic waves these liposomal bubbles can burst, thus releasing their contents. This can be focused in the areas where the microbubbles are accumulating, including tumors. Imaging and drug release is therefore controlled by ultrasound, and thus is a promising method of image-guided delivery. One such example is the stabilization of perfluorocarbon nanodroplets

using block copolymers with paclitaxel[75]. Because of their high ^{19}F-fluorine content, they were able to utilize ^{19}F-MR spectroscopy in conjunction with ultrasound to determine precise anatomical location of the nanoconstructs. Complete tumor regression was observed on a pilot study with tumor focusing ultrasound in breast tumor bearing mice. The promise of ultrasound-mediated delivery using microbubbles is being investigated in several clinical trials[76]. However, challenges remain in reproducibly manufacturing these constructs, especially when complicated by associating targeting agents and drugs into their structure. Their size distribution also remains a challenge. Microbubbles span a large range in sizes affecting their distribution in the body. Strategies are needed to refine microbubble manufacturing process for more reproducible formulations, smaller size and less polydispersity.

2.5.1.6. Antibodies and proteins

Antibodies are of particular interest in therapeutic delivery because of their biocompatibility and intrinsic ability to target antigens within the body, including those highly expressed in tumors. Many monoclonal antibodies (MoAbs) can be therapeutically active and have been approved or are in clinical trials for the treatment of cancer[77]. Therapeutics such as drugs and radionuclides conjugated to MoAbs have been shown to be effective for targeted delivery and image guided therapy[78]. One of the major concerns in using antibodies as image-guided therapies is their method of manufacture. MoAbs are produced from nonhuman sources (typically mice) and this can cause immune recognition within a patient by human anti-mouse antibodies (HAMA) that can either reduce the effectiveness of the therapeutic conjugate or cause severe life-threatening immune reactions[79]. Image guidance helps to select patients which may suffer from this

effect as demonstrated in radioimmunotherapy[22]. Antibodies are not the only proteins that are used in therapeutic delivery. Albumin, a native protein in the blood stream, serves as a macromolecular delivery system that is biocompatible and capable of being imaged. For example, a photosensitizer, chlorin e6, covalently linked to albumin formed nanoparticles that were used for image guided drug delivery[80]. Tumor localization was observed by optical imaging of the photosensitizer and then subsequently irradiated with light in the tumor for anticancer treatment in a mouse model.

2.5.1.7. Inorganic nanoparticles

The last platform to discuss as carriers for image-guided therapeutics encompasses an array of inorganic materials such as quantum dots, gold and iron oxide nanoparticles. Metal elements exhibit interesting properties when synthesized in the nano-size ranges. For example, gold nanoparticles can absorb light in the near infrared spectrum and produce heat for localized hyperthermia[81]. Quantum dots are semiconductor nanocrystals made of transition metals that have tunable emission spectra that are much stronger than organic dyes[82]. Iron-oxide nanoparticles can be detected using MRI. All of these materials can be decorated with targeting agents, imaging agents and therapeutics for image-guided therapeutic delivery in cancer[83]. One of the main concerns with these constructs is their toxicity. Typically, these constructs do not breakdown in the body and therefore are deposited in tissues for an extended period of time[83]. The nature of their toxicity is still being investigated, but the long-term effects of some of these materials raise many questions to whether they can be used safely in the clinic.

2.5.2. Imaging modalities

Imaging modalities are becoming more sensitive, accurate and precise at detecting tracers in the body. Availability of sophisticated imaging devices is increasing; therefore, there is a growing need to rapidly develop probes for use in these different imaging modalities, especially in the area of image-guided therapy. Personalized medicine is the ultimate goal of imaging in the clinic and its full potential is yet to be realized. This section will present the different strengths and weaknesses associated with different imaging modalities. Many of the modalities can be combined in such a way as to compensate for lack of sensitivity or accuracy in detection of different probes. In fact, many groups have focused on the development of nanoparticles which have multiple methods of detection for multimodality imaging that can provide a variety of information that is not possible with the use of one alone. *Table 2.2* shows a brief summary comparison of the different modalities. A more in-depth discussion is provided for each modality in the following subsections.

2.5.2.1. Magnetic resonance imaging

Magnetic resonance imaging (MRI) is primarily used in the clinic for anatomical imaging. MRI signals are produced from changes in magnetic orientation from radiofrequency pulses of aligned protons in a strong magnetic field[84]. Signals from MRI are measured based on two typical responses, T1 and T2 relaxation demonstrated in *Figure 2.2*. Typical use of MRI measures proton T1 or T2 relaxation signals in the body for high resolution images containing soft-tissue anatomical information. Differences in each proton's environment influence the T1 or T2 relaxation rate which in turn causes the variations that can be converted into an image. Different materials used as MRI contrast

Table 2.2. Summarized comparison of the main imaging modalities[1,2]

Modality	Temporal Resolution	Spatial Resolution	Quantitation	Depth of Penetration	Probe Sensitivity	Imaging agents	Clinical Use	Relative Cost
X-ray computed tomography (CT)	Minutes	0.5-1 mm	No	Limitless	Not determined	Iodine, Barium suspensions	YES	$$
Magnetic resonance imaging (MRI)	Minutes-hours	~ 1 mm	Semi-quantitative	Limitless	10^{-3} to 10^{-5} M	Gadolinum, Iron oxide nanoparticles, 19F-Fluorine	YES	$$$
Fluorescence molecular tomography (FMT)	Seconds-minutes	1-3 mm	Quantitative	< 2 cm	~10^{-9} to 10^{-12} M	NIR Fluorochromes	NO	$
Ultrasound (US)	Seconds-minutes	0.01 to 2 mm	No	mm-cm	~10^{-12} M	Microbubbles	YES	$
Single photon emission computed tomography (SPECT)	Minutes	8-10 mm	Semi-quantitative	Limitless	10^{-10} to 10^{-11} M	Gamma emitting isotopes	YES	$$
Positron emission tomography (PET)	Seconds-minutes	5-7 mm	Quantitative	Limitless	10^{-11} to 10^{-12} M	Positron emitting isotopes	YES	$$$

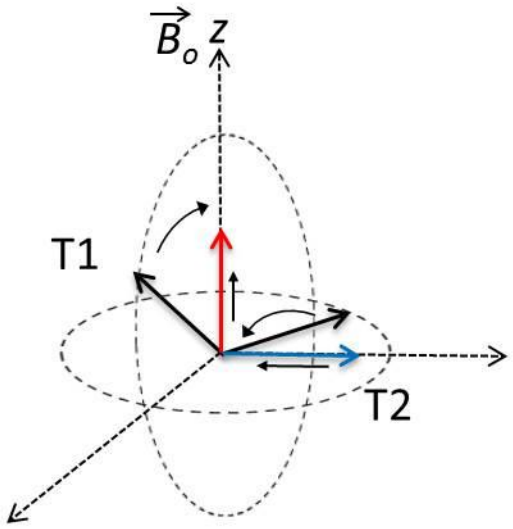

Figure 2.2. Diagram of T1 and T2 relaxation in MRI. T1 relaxation is the rate at which the magnetic vector realigns or net alignment (red arrow) increases on z-axis which aligns with the external magnetic field after a 90º radiofrequency pulse. T2 relaxation is the rate at which the magnetic vector disappears or net x-y vector (blue) decreases in the x-y plane after a 90º radiofrequency pulse[87].

agents also have various effects on protons in the body with these two relaxation signals[1,84]. Gadolinium has been used as a contrast agent for T1 relaxation in image guided therapeutics[85]. An additional method for MRI imaging is the detection of other paramagnetic elements such as ^{19}F called magnetic resonance spectroscopy[86]. ^{19}F has been incorporated into many nanomaterial constructs[88-91]. One example is the system developed by Porsch et al. containing ^{19}F conjugated to amphiphilic polymers[92]. These polymers forming a micelle structure were subsequently loaded with doxorubicin for an image-guided drug delivery approach that exhibited MRI suitable signal-to-noise ratio (SNR) in phantoms[92]. These systems have potential for future study in vivo. However, one of the main challenges for MRI contrast agents is the lack of sensitivity of the MRI scanner. Large amounts of contrast are needed in order to produce a signal distinguishable from background. This makes MRI very difficult to use quantitatively. Although some techniques are in development to improve quantitative capacity of MRI, the physical nature of sensitivity is a large hurdle to overcome. Nonetheless, MRI is a valuable tool for anatomical imaging that can be used in conjunction with other imaging modalities which are more quantitative.

2.5.2.2. X-ray computed tomography

X-ray computed tomography or CT is another method in which anatomical information is provided. CT uses x-ray projections that interact with high electron dense materials through a subject in multiple planes[1]. These planar images can then be reconstructed based on computer algorithms which produce a high-resolution image of the body. Resolution depends on the electron density of the material and therefore primarily returns high-resolution images of hard-tissues. Contrast agents are based on

heavier atoms such as iodine or barium. Iodine contrast agents are commonly used for angiography studies but require large frequent doses for a sustained signal output. The need for highly dense materials for contrast is the main limitation for use of CT with image-guided delivery. Therefore, CT is utilized in a multimodality approach which provides 3D anatomical information in tandem with other imaging information modalities. Risk due to ionizing radiation from prolonged CT exposure is of some concern. However, CT has made a substantial impact in detection and measurement of tumor sizes[93].

2.5.2.3. Optical imaging

Optical imaging is based on light emitting probes which can be detected by camera[94,95]. Optical imaging has been successfully used for many years for the detection of molecular processes in in vitro assays. However, in vivo the challenge becomes increasingly difficult when trying to penetrate tissues which rapidly attenuate light signals. The attenuation of light prevents absolute quantification and limits resolution[96]. A modern technique called fluorescence molecular tomography (FMT) can measure signals from the visible to near-infrared spectrum (500-900 nm) of fluorescent probes in multiple orientations and use mathematical models which predict attenuation in the subject to produce three-dimensional images of probe localization[17,97]. FMT is currently available for small animal imaging research, but clinical translation is yet to be viable. The tissue penetration in a human subject is more difficult. Therefore, FMT and other optical imaging techniques remain at the preclinical level. However, one of the advantages to using fluorescent probes in the development of image-guided therapeutics is the potential to visualize drug release from a nano-construct. Recent developments in

dyes which are conjugated to nanoparticles can be activated once released by targeted mechanisms from the nanoparticle surface[98]. Fluorescent dyes when in proximity (i.e., conjugated to the surface of a nanoparticle) lead to a strong fluorescence quenching due to fluorescence resonance energy transfer (FRET). Once the dyes are released and quenching is stopped, the signal will be visible and the resulting signal can be related to a mechanistic process[98]. Other imaging modalities are not capable of having activatable signals in relation to cellular responses in vivo such as SPECT or PET imaging. Radionuclide signals are constitutively active and cannot be suppressed unlike fluorophores. One example of such a system provides information of cathepsin B protease activity[99]. This is performed by a FRET designed peptide sequence conjugated with two terminal fluorophores. When the peptide sequence is cleaved, FRET interactions cease and the signal representing protease activity can be visualized via FMT imaging. A similar type of system could potentially be used to visualize drug release by containing enzymatically degradable linkers conjugated with drug and FRET capable fluorophores. The released fluorophore would produce the optical signal that could be related to the release of drug from the linker. This objective is yet to be realized but could be a powerful tool for the development of novel drug delivery approaches for treatment of cancer.

2.5.2.4. Ultrasound

Ultrasound is probably the most cost effective and safe imaging modality available in the clinic today[1,2]. Ultrasound utilizes high-intensity ultrasonic waves mechanically produced from a transducer. The sound waves then reflect or scatter from different tissues which can be detected by the transducer and converted into images. One

advantage that ultrasound has is actual real-time imaging. Images are returned within seconds and therefore provide the highest temporal resolution available among the different modalities. Temporal resolution is a term describing the ability to distinguish between individual events[1]. Contrast agents for ultrasound are limited to gas bubbles which have specific properties that resonate in the 1 – 20 MHz frequency range, producing highly specific signals that can be recognized by the ultrasound device[17]. Ultrasound is limited to only microbubbles for visualizing probes and is therefore relatively limited in application to image-guided drug delivery. It also suffers from a lack of penetration (*Table 2.2*) and requires contact of the device to the subject. Ultrasound resolution is highly dependent on the type of tissue and its depth and is therefore difficult to directly compare against other modalities. In the best case scenario, resolution is on the order of 10-100 μm[1]. Microbubbles are used as carriers for image-guided delivery. Further refinement in manufacturing is needed for clinical translation of this approach for image-guided therapeutics.

2.5.2.5. Single photon emission computerized tomography

Nuclear medicine techniques such as single photon emission computerized tomography (SPECT) detect gamma emission from radioisotopes which are administered to a patient for purposes of diagnosis and treatment[100]. SPECT is a descendent of older gamma scintigraphic methods which were only capable of producing planar images that were not quantifiable and had very poor resolution. SPECT imaging takes modern advances in scanner and computer technology to obtain single γ-ray emissions using two to three gamma cameras that rotate around a patient who has been administered a gamma-emitting isotope tracer. Gamma emission is detected through thick collimators,

plates of lead or tungsten, with small holes between the subject and gamma detector, that only allow photons emitted in the 90º direction of the gamma camera to interact with the detector. SPECT relies on reconstructing these multiple projections into a 3D image that gives precise localization of radioisotope biodistribution. Because only a select few gamma emissions are detected by the camera, the sensitivity is compromised to some degree due to a lack of sufficient detector events[100]. Images are also dependent on the energy of the γ-rays emitted from the radioisotope. Lower energy radioisotopes have more attenuation than higher energy radioisotopes. Attenuation increases the scatter and noise detected from the camera, thus compromising the resolution of the image. The quality and usefulness of images for image-guided approaches with SPECT are highly dependent on the type of radioisotope being utilized.

Radioisotopes for SPECT imaging must be selected based on the length of time needed to acquire information; otherwise, the half-life of the radioisotope must match the biological process that is being monitored. A list of clinically utilized radioisotopes for SPECT imaging with their emission properties are described in *Table 2.3*. Many isotopes can be utilized in SPECT for detection and the majority of them can be attached to nanoparticles via metal chelation, ionic interaction or covalent linkage. Transition metal based radioisotopes are easily conjugated to nanoparticles using stable bifunctional chelators of metals[101]. Some radioisotopes can be associated with a nanoparticle by ionic charge interactions[102]. Others, including halides, form stable covalent bonds in order to radiolabel a nanoparticle[103]. Many strategies exist to radiolabel a nanoparticle. Consideration for the method of labeling must not interfere with other functions (i.e., drug and targeting) for image-guided therapies for cancer. One interesting strategy for SPECT imaging is the ability to image two different radionuclides with different energies

Table 2.3. Radioisotopes for SPECT imaging.[17,104,105]

Radionuclides	$T_{1/2}$	γ-ray energy
^{99m}Tc	6.01 h	140 keV
^{111}In	2.83 d	173, 247 keV
^{67}Ga	3.26 d	93, 184, 300, 393 keV
^{123}I	13.3 h	159 keV
^{131}I	8 d	365 keV
^{67}Cu	2.58 d	184.6 keV
^{201}Tl	3 d	69-81, 167 keV
^{133}Xe	5.2 d	81 keV

at the same time. This may allow for imaging of distinct processes within a given construct. For example, a study was conducted using an ^{111}In labeled targeted peptide and ^{177}Lu labeled control nontargeting peptide injected into the same mouse in order to visualize differences in accumulation without interanimal variations[106]. The dual isotope approach could be applied in mixed micelles where the hydrophobic and hydrophilic components are labeled with different isotopes and could potentially give information as to the breakdown and ultimate fate of the two components.

SPECT is a promising modality for image-guided delivery in cancer because it can provide accurate information on the relative location of nanoparticle carriers. However, there is the risk of ionizing radiation exposure that limits the amount of radioactive exposure a patient can receive. It also does not provide anatomical reference. This has been overcome by multimodal approaches such as combining images with both CT and MRI. The combined modalities can more accurately pin-point where the nanoparticles are accumulating and give accurate information predicting both potential efficacy and safety of image guided nanoconstructs. The major challenge for SPECT imaging is obtaining accurate quantitative results. Detection events required for accurate quantitation are limited due to the use of collimators and a large range of gamma emission energies that are scattered and attenuated differently in tissue. Longer imaging times are also required for SPECT which can exaggerate motion effects leading to increased signal noise. There are methods for both attenuation and scatter correction which are being developed to make SPECT more quantitative. However, these methods and capacities vary greatly among scanners and groups. Ideally, further development and common adoption of correction techniques may some day lead to more routine quantitative capability of SPECT.

2.5.2.6. Positron emission tomography

Positron emission tomography (PET) is another nuclear medicine technique which has made a major impact in the field of cancer treatment[107,108]. PET detection is based on radionuclides emitting positrons which interact with nearby electrons and annihilate into two antiparallel gamma photons each with signature 511 keV energy. This allows for coincidence detection by a circular array of detectors that can trace back along the line of response to the origin of emission and produce high-resolution images of radioisotope probes. A basic diagram of PET is shown in *Figure 2.3*. PET can detect radioisotopes down to the pico-molar (10^{-12}) range and has limitless depth penetration due to the high energy of its 511 keV gamma-rays[1]. In comparison with SPECT, PET has a much higher count rate and better resolution, thus providing the ability for accurate quantitation of imaging agents. PET scanners are also combined with CT and other techniques in order to provide attenuation and scatter correction, thus increasing its quantitative ability in comparison to SPECT. Due to the fact that only one gamma energy window is needed for detection around 511 keV, these correction techniques can be simplified when compared to SPECT. Radioisotopes used in the clinic for PET are generally short-lived and for the most part must be produced locally using a cyclotron. This increases the costs and availability of PET radionuclides. Like SPECT, ionizing radiation also limits the ability of patients to be continually administered radioisotopes for research studies. *Table 2.4* lists some of the isotopes used in PET imaging with details of the characteristics and properties. PET also does not provide anatomical reference; thus, almost all PET imaging devices are coupled with CT detectors for precise localization of signals with the patient. The CT images can also be used to correct for attenuation in the imaged subject for improved resolution and quantification.

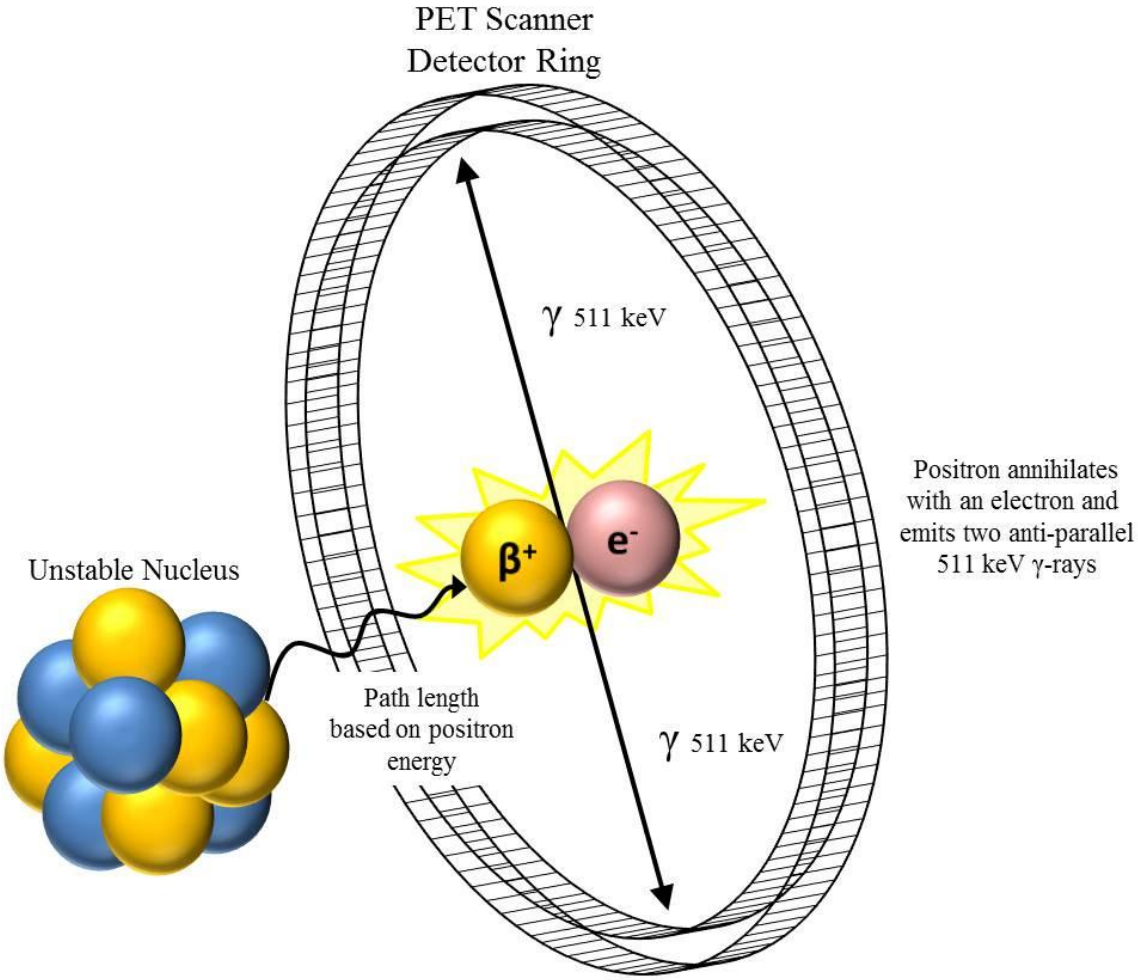

Figure 2.3. Positron emission tomography[108].

Table 2.4. Physical characteristics of common positron emitting radioisotopes[17,108,109].

Radionuclides	$T_{1/2}$	Max β^+ energy (MeV)	Availability*
^{18}F	110 min	0.69	+++
^{11}C	20.4 min	0.96	+++
^{15}O	122.2 sec	1.7	+++
^{13}N	9.97 min	1.20	+++
^{124}I	4.2 d	2.14	+
^{64}Cu	12.7 h	0.65	+
^{89}Zr	3.3 d	0.897	+
^{68}Ga	67.7 min	1.90	++

* Availability based on estimated cost and production facilities

Selection of radionuclides for PET imaging is important in that it can affect the resolution and relevance of the research study. The initial positron energy determines the path-length from the parent nuclide to the annihilation event. The higher the energy, the longer the path-length, thus increasing image noise and reducing resolution[17]. Like SPECT, isotope half-lives must match the relevant biological process intended to be measured. This represents a significant challenge in nanoparticle imaging with PET, since most of the clinically available radionuclides have ½-lives on the order of minutes (^{15}O ~ 2 min ½-life) to a couple of hours (^{18}F ~ 110 min ½-life) which does not match the biological half-life of many nanoparticle systems. However, the majority of these short-lived isotopes are basic elements found in biology and therefore can be incorporated into drugs, sugars and other biological entities without influencing their structure.

A recent study using a positron emitting ^{64}Cu radionuclides conjugated to HPMA copolymers containing angiogenesis targeting peptides demonstrated measurable increased tumor localization by PET imaging in prostate tumor bearing mice[110]. Because ^{64}Cu also has some beta-emission, the radionuclide can serve a dual purpose for imaging and therapy. This is a perfect example of how radioisotopes can be utilized in image guided therapeutic delivery. Clearly, more research and effort in this area needs to be conducted to improve the availability of radionuclides. PET represents the future of nuclear medicine imaging and has already influenced the treatment of cancer profoundly[111]. However, costs and lack of radionuclide availability are detrimental for rapid development of image-guided therapeutics for cancer based on PET imaging.

2.5.3. How to target cancer

One of the main limitations to success with therapeutics for cancer treatment is their lack of specificity. The lack of specificity leads to side effects due to organ toxicity related to uptake of therapeutics. Targeted therapies seek to overcome this problem by changing the pharmacokinetic behavior. Many approaches have been presented to selectively localize a therapeutic to tumors[112]. Image-guided delivery allows researchers to assess whether targeting strategies are working in the given patient. The heterogeneity of tumors and their targets makes it difficult to achieve successful approval of many therapeutics. This can be overcome with image-guided approaches which select and qualify patients. This section will focus on the available methods for targeting nanomaterial platforms for cancer treatment.

2.5.3.1. Passive targeting

Perhaps one of the most important aspects of nanoparticle behavior for oncological targeting is their ability to passively target via the enhanced permeability and retention (EPR) effect[27,28,113]. This was first described by Maeda who found that rapidly growing tumors have large gaps or fenestrations in the vasculature when compared to normal tissues due to uncontrolled tortuous growth related to unregulated tumor angiogenesis[113,114]. Macromolecules accumulate in the tumor because they can easily extravasate through gaps that lack normal lymphatic drainage. Several constructs based on this targeting strategy have been tested in clinical trials with variable success[36,115]. One of the first agents to be tested was SMANCS, polystyrene-co-maleic acid-half-butylate copolymer conjugate with neocarzinostatin for the successful treatment of hepatocarcinoma[115]. Interestingly, a CT contrast Lipiodol® was also administered in

these studies giving an example theranostic approach. However, other trials with macromolecular polymers as drug conjugates were unsuccessful in the clinic. The first HPMA copolymer conjugates containing various drugs were halted during clinical trials due to a variable patient tumor response[46]. The lack of response may be attributed to the variability of the EPR effect in different patients and tumors. It has been suggested that perhaps the use of an imaging version of these conjugates could be used to select patients who may have a better chance of success with the passive targeting strategy[23,46].

2.5.3.2. Small molecules

Many small molecules are recognized by tumor cells. They can be conjugated to the surface of nanoparticles for increased uptake or increased accumulation in the tumor. As with any targeting ligand for therapeutic delivery, one must consider the function of the receptor-ligand interaction. Some receptors bind their ligands and facilitate endocytosis of the ligand cargo. Others may not increase endocytosis but may cause a signaling pathway which may affect cellular functions. These interactions need to be carefully considered when designing a system. If carrying a drug that needs to be internalized for its action, then small molecule ligands must be selected that cause endocytosis. In the case of radionuclides for therapy, uptake may not be necessary in order to facilitate the targeted nanoparticles' anticancer activity. Several small molecules have been utilized for active targeting of cancer. Folate receptors (GP38) are highly expressed on malignant cells and can facilitate tumor targeting[116,117]. For example, a 5th-generation PAMAM dendrimer was conjugated with folic acid and methotrexate and demonstrated enhanced tumor uptake in folic acid receptors[118]. In vivo studies demonstrated an enhanced efficacy compared to controls and minimized the toxic side

effects of methotrexate. Galactosamine has also been used for targeting to tumor cells. It has been used to target HPMA copolymer-doxorubicin conjugates for treatment of hepatocellular carcinoma[45]. Targeting with these molecules and others is possible. However, consideration on the chemical linkage site on the molecule must be evaluated to assure that recognition by the receptor is not compromised.

2.5.3.3. Peptides

Peptides are recognized by a variety of tumor cell receptors. A vast majority of researchers utilize phage display techniques for selection in order to find novel peptides which bind receptors overexpressed in cancer[119,120]. Many candidates used with these techniques have been utilized for imaging and drug targeting in cancer. Because of their small size, more peptides can be incorporated on nanoparticles and possibly facilitate multivalent interactions which potentially can increase their recognition on the targeted cell surface. Peptides do suffer from rapid degradation by proteases in the body, but use of unnatural amino acids, cyclization and conjugation to nanoparticles may restrict protease activity due to steric hindrance. Peptides are constantly being developed as new targeting approaches for active targeting of nanoparticles. RGD-containing peptides mimic the extracellular domains of many proteins that are involved in angiogenesis. It specifically recognizes the $\alpha_v\beta_3$ integrin receptors overexpressed on neovasculature of growing tumors and on the cells of some tumor types[121,122]. HPMA copolymers with RGD containing ligands and radioisotopes for both imaging and radiotherapy demonstrated tumor-specific targeting and antitumor efficacy[123]. GRP78, a heat-shock related protein is overexpressed on tumor cells when the tumor is under stress. Hyperthermia treated tumors were successfully targeted using a GRP78-binding peptide

WIFPWIQL on HPMA copolymers containing anticancer drugs[124]. Cell penetrating peptides (CPPs) have also been used for increasing nanoparticle uptake in cancer cells[125]. However, CPPs are nonspecific and therefore need other methods of targeting in order to increase tumor localization. Peptides also suffer from retention effects in the kidney[126]. This may lead to therapeutic payloads of nanoparticles with peptides causing renal toxicity.

2.5.3.4. Antibody and fragments

Antibodies are immunoglobulins used by the immune system for recognition of foreign materials[127]. However, antibodies have been developed that recognize certain antigens expressed on the surface of cells. They have binding affinities in the nanomolar range. They consist of both heavy and light chains with a single effector region which causes immunological triggers for cell-killing and two binding regions. Antibodies that target antigens expressed on the surface of tumor cells have been utilized in many nanoparticles for targeted delivery. For example, trastuzumab, an antibody that binds HER2 receptors overexpressed in cancer, has been shown to increase the uptake of nanoparticle systems for imaging and drug delivery[128-130]. However, antibodies are large (MW ~150 kDa) and therefore add a considerable amount of size to nanoparticles when conjugated to the surface. The effector region of the antibody can also cause recognition by immune factors, resulting in undesirable immunoreactivity[131]. Therefore, various forms of fragments have been developed from the binding regions of the antibodies[132]. Antibody fragments have smaller size (MW ~27 kDa) and lack the effector region and therefore have less immunoreactivity[131]. In regards to conjugation of both antibodies and fragments, conjugation sites must be selected in a manner that conserves binding affinity.

One challenge for incorporation of antibodies into nanoparticles is that there is lack of a single functional group for conjugation to nanoparticles. Bioconjugation techniques must be carefully performed to prevent cross-linking between nanoparticles.

2.5.3.5. External trigger targeting

One of the main challenges for ligand-directed targeting is that their targeted receptors are rarely expressed only on the targeted tumor. This leads to increased uptake in other organs of the body that leads to toxic effects. Researchers have developed methods to target tumors exogenously. One such method is hyperthermia. Hyperthermia can be utilized to increase blood flow and perfusion to a tumor to potentially augment nanoparticle penetration and accumulation[133]. It can also be used in conjunction with thermal sensitive liposomes which release their therapeutic payload with increased temperature[134,135]. Hyperthermia must be administered locally in order to selectively target tumors with nanoparticles and can be done with a variety of methods. One such method involves gold nanorod (GNR)-mediated plasmonic photothermal therapy (PPTT). PPTT utilizes the surface plasmon resonance of gold nanorods to produce heat when activated at the appropriate laser light wavelength[136,137]. Another method that may be closer to translation is high-intensity focused ultrasound (HIFU). HIFU utilizes ultrasonic waves to generate heat within biological tissues[138]. It can also be combined with MRI imaging with gadolinium thermal sensitive liposome conjugates for precise imaging of the nanoparticle localization within the tumor and subsequent drug release[139-141]. Hyperthermic delivery based on HIFU represents a promising future for targeted delivery of nanoparticles for therapeutics and imaging.

Hyperthermia is not the only method for guided delivery. Magnetic nanoparticles can be guided to tumors using an external magnetic field with the tumor. Magnetic nanomaterials such as superparamagnetic iron oxide nanoparticles (SPIONs) can deliver both imaging and therapeutics to the tumor site[142]. SPIONs form a dual purpose in that they can be visualized by MRI and guided to tumor site using magnetic fields. This represents a promising area for targeted delivery. However, paramagnetic materials like SPIONs are large and remain in the body for long periods of time, leading to concerns in toxicity. Iron is carefully balanced in the body and addition of large amounts can also be detrimental[142]. Thus, the promise for SPIONs in clinical use requires further development to address these concerns.

Passive and active targeting and externally triggered methods are continually being developed to more precisely target tumors. Selecting any of these strategies has their advantages and disadvantages. Selection of the best targeting strategy will rely on considerations of the nanoparticle system and the targeted cancer type. Further investigation into targeting must be conducted with nanoparticle systems to find the optimal strategy for image-guided therapeutic delivery.

2.5.4. Choice of therapeutic

A wide range of therapeutics has been utilized in nanomaterials for cancer treatment. Nanomaterials have been designed to improve the short-falls of chemotherapeutics, radiotherapeutics, oligonucleotides and photosensitizers. These four areas of therapeutics require delivery methods that improve solubility, increase localization, improve efficacy and reduce toxicity. The choice of therapeutic for a particular nanoparticle design is highly dependent on the type of cancer being treated,

clinically available and approved therapeutics and potential for improvement with delivery systems. Examples of each of these therapeutic areas will be discussed and how image-guided delivery can improve their success in cancer treatment.

2.5.4.1. Chemotherapeutics

Chemotherapeutics are the main-stay of treatments for advanced stages of cancer. Of course surgical methods to remove known tumor sites are preferred. However, small invasive tumors are difficult to detect and remove. Therefore, they require small molecule agents to penetrate and destroy tumor sites which are not accessible. However, small molecules are nonspecific in their cytotoxic action. Therefore, they cause a variety of side effects that reduce quality of life and endanger the patient. Most chemotherapeutics can be broken down into a few classes: alkaloids, antibiotics, platinates, antimetabolites, topoisomerase inhibitors, mitosis inhibitors and others[143]. In discussing chemotherapeutics for image-guided drug delivery it becomes necessary to discuss what has been performed in the past. Chemotherapeutic selection for drug delivery systems has been based primarily on clinically approved drugs which have limitations due to solubility, dose limiting toxicity, instability in the bloodstream or poor efficacy. For FDA approval, selecting drugs that are already approved for use is one less hurdle to cross and is therefore beneficial in image-guided therapeutics.

One of the many challenges for chemotherapeutic delivery using nanoparticles are methods of conjugation and subsequent release. Some carriers entrap the chemotherapeutic cargo like liposomes, microbubbles and potentially micelles. The important part of image-guided drug delivery is that the formulated nanoparticle drug complex must stay intact until it arrives at the targeted tumor site. Otherwise, the imaging

of the carrier does not represent the actual drug localization. This is a challenge for nanoparticle formulations which have limited stability over time and "leak" drug. Covalent linkages to nanoparticles can overcome this but methods must be developed in order to realize site-specific drug release. Linear carriers such as HPMA copolymers have utilized lysosomally degradable GFLG peptide sequences for drug release once the nanoparticle has been endocytosed into the cell[144]. Success of site-specific drug release has been variable using this approach. In the case of HPMA copolymers conjugated with docetaxel, rapid release was observed in cell culture media and therefore expected to observe similar behavior in vivo[145]. In another study, release kinetics were variable when HPMA copolymer was conjugated with both gemcitabine and doxorubicin via GFLG linkers[146]. Gemcitabine was rapidly released in the presence of cathepsin-B, a lysosomal enzyme, but docetaxel showed a very slow release even with the enzyme. These examples demonstrate the balance that is needed with site-specific drug release. Drugs must be stable enough before getting to the targeted site but have the ability to empty its payload rapidly for a maximally effective image-guided delivery.

2.5.4.2. Radiotherapeutics

Radioisotopes have been utilized for cancer treatment for a considerable amount of time. Some of the first clinically used radioisotopes were produced in the 1930s such as ^{131}I iodine[147]. Radiotherapy is primarily performed using isotopes which emit alpha and beta radiation. Both forms of radiation are efficient at forming radicals (usually with water) which exert damage to the DNA of cells and cause irreversible damage leading to cell death. However, the range of tissue in which these effects occur is different depending on the type and energy of particle[105]. Many of the radioisotopes in the clinic

for radiotherapy have beta emission with a range of 50-5000 μm. More rare isotopes with alpha emission have a much shorter range of 40-90 μm. Radioisotopes with auger electrons have the shortest range of 0.01-1.0 μm. The greater the range the more risk to nontargeted tissues near tumors. However, for larger tumors, a larger range may be more advantageous. Selecting the proper isotope is a matter of ½-life and the range of emission that is ideal for the targeted tumor. *Table 2.5* is a list of radioisotopes for potential use in radiotherapy. The key aspect required for successful radioisotopes is site-specific localization and ample radiation dose to cause sufficient irreversible DNA damage leading to tumor cell death. This is a challenge that requires tumor-targeted approaches which do not cause off-site accumulation. One of the first clinically available theranostic delivery systems is based on a radiotherapeutic approach. Iodine uptake is especially high in the thyroid and for more than 50 years, radiation oncologists have exploited this feature to treat thyroid cancer with ^{131}I-iodine[149]. Imaging can be performed using SPECT or simple gamma scintigraphy of ^{123}I, a gamma emitter, which gives information on the areas of accumulating iodine in the patient. Safety and efficacy concerns can be utilized to select the patient for the subsequent ^{131}I therapy. Another example was discussed early on in this chapter about Bexxar® and Zevalin® which are radioimmunotherapies used in image-guided therapy for lymphoma patients. Image-guided approaches have been extremely useful in the approval of these therapeutics in the clinic. Selecting the proper isotope is highly dependent on the ability to stably link the radionuclide to the nanoparticle platform. For efficacious and safe radiotherapy, loss of the radioisotope must not occur. Using nanoparticles to carry isotopes prevents them from accumulating in radiation sensitive areas such as bone marrow as long as the chelated radioisotope is stable in the blood stream. The main advantage of using

Table 2.5. Isotopes for image-guided radiotherapy[105,148]

Radionuclides	$T_{1/2}$	Type of emission	Average energy (keV)
^{131}I	8.0 d	β^-	181
^{90}Y	2.7 d	β^-	935
^{153}Sm	1.94 d	β^-	280
^{64}Cu	12.7 h	β^-	1670 (max)
^{67}Cu	2.58 d	β^-	141
^{211}At	7.2 h	α	5867
^{213}Bi	46 min	α	6000 (max)
^{67}Ga	3.26 d	Auger	0.04-9.5
^{125}I	60.5 d	Auger	27 (max)

radioisotopes in nanoparticles is that their effect on cancer is independent of release, unlike chemotherapeutics. Nanoparticles in this case do not need to penetrate deep within the tumor to exert their anticancer effects. This advantage is profound because typically nanomedicines cannot penetrate deep within tumor tissues.

Several successful image guided radiotherapeutics have been developed and have shown promising results in treating cancer[148]. Wang et al. synthesized a multifunctional lipid-polymer hybrid nanoparticle that contained docetaxel and chelator for both ^{111}In and ^{90}Y radioisotopes[150]. The prostate tumor-targeting nanoparticle was able to demonstrate superior antitumor efficacy of the combination chemotherapy and radiotherapy particle. Although the approach has promise, control over all components especially between loaded drug and ^{90}Y may prevent reproducible synthesis required for eventual translation.

2.5.4.3. Antisense oligonucleotides

A promising area still in development for therapeutics is antisense oligonucleotides. This can include short strands of either DNA or RNA which are complementary to a chosen sequence. When introduced into the cell, they can knock-down expression of a cancer-related gene and thus treat tumors. One such technology involves small interference RNA or siRNA which has the higher therapeutic index when compared to other gene modifying therapies[151]. Due to the siRNA charge, it cannot cross biological membranes and therefore, nanomaterials have been utilized to shield the charge, protect the oligonucleotides in the bloodstream from nucleases and transport them into the cytosol of tumor cells. Optical imaging offers an interesting opportunity with FRET-like systems based on siRNA delivery. Cationic quantum dots were conjugated with polyethylenimine (PEI) in order to complex with siRNA that had been labeled with

a fluorochrome[152]. Once complexed the fluorescence signal was quenched and upon siRNA release, an increase in fluorescence was observed. This system could potentially be utilized to observe release and essentially be correlated with efficacy within tumor cells. However, systems such as these are in early-development. No siRNA therapies have been approved to date and therefore, these studies offer only a proof-of-concept for now.

2.5.4.4. Photosensitizers

Photosensitizers are a class of molecules which are able to absorb light and transfer it to local electrons to singlet oxygen species[153]. Singlet oxygen species are highly reactive with biological molecules and can cause damage to the cell resulting in cell death. Use of photosensitizers is promising in cancer therapy because their anti-cancer action can be restricted to tumors that have been radiated with appropriate wavelength for photodynamic therapy (PDT)[154]. One challenge is sensitization based on photosensitizers nonspecifically localizing to the skin and being activated by normal sunlight. This can cause severe reactions in the skin. Conjugation of photosensitizers to nanoparticles can help prevent skin accumulation and reduce this toxicity. Nanoparticles can also improve tumor localization through means of passive and active targeting, thereby increasing the therapeutic index of the photosensitizer. Many photosensitizers are hydrophobic as well; therefore, incorporation into water-soluble nanoparticles can improve their solubility. Another benefit of some photosensitizers is that their fluorescence emission can be observed by optical imaging; therefore, they can both provide an imaging and therapeutics on a single nanoparticle. The potential for PDT is attractive; however, limitations in tissue penetration of light limit this therapy to

superficial tumors or through endoscopically accessible organs such as the lung[155]. There is potential to use small light emitting optical fiber probes through guided needles into deeper tissues such as the pancreas, but this remains challenging and invasive[156]. Multimodality imaging using PET is also a possibility using nanoparticles conjugated with photosensitizers, thus describing accurately the location and depth of required light penetration for PDT[157]. PDT is a promising area of research with one photosensitizer already approved for use. However, PDT is generally limited to superficial and local treatment and is thus limited against metastatic cancer[158]. Despite this, PDT can be used for cancers which are not restricted by the limitations of this approach.

2.6. Ideal Image-Guided Therapeutic System for Treating Cancer

The previous few sections have presented the different aspects, advantages and disadvantages of the different requirements for image-guided therapeutics in cancer. Unfortunately, there is no system that satisfies the demands of all types and stages of cancer disease. One must also consider for clinical translation the regulatory hurdles that need to be overcome for manufacturing of nanoparticles with imaging agent, therapeutic and targeting.

Generally, the simpler the design is, the better is the approach. Good manufacturing practices (GMP) required for FDA approval require that each component of the formulation have complete characterization at the full range of possibilities within the nanoparticle formulation. With multiple components having multiple cross-interactions possible, the regulatory hurdle for just one image-guided approach is significant. Thus, a simpler approach is more likely going to be logistically and economically feasible. Selecting components especially drugs with more individual

clinical experience will also lessen the burden because previous experience can yield much information in regards to potential problems.

The ideal system is therefore dependent on needs of the particular tumor type. Development of delivery systems for pancreatic cancer treatment is the focus in Chapters 3 and 4 of this dissertation. Current progress in treatment of this disease is very slow. Variable results have been observed for targeted strategies. The anticancer drug gemcitabine is the first line drug for advanced pancreatic cancer but it lacks in efficacy due to its metabolism in the blood and could be potentially improved by water-soluble polymer delivery. Chapter 4 examines the utilization of HPMA copolymers as carriers to improve delivery to pancreatic tumors. A study regarding pancreatic targeting strategies with small ligands for both $\alpha_v\beta_3$ integrin and HER2 receptors is discussed in Chapter 3. This chapter also seeks to observe how the treatment of the dense stroma associated with pancreatic cancer can be overcome using hyaluronic acid. Both studies include a chelator for ^{111}In for multimodal SPECT and CT imaging.

Chapter 5 seeks to provide a different approach via gold nanorod-mediated hyperthermia for HPMA radiotherapeutic polymers containing ^{90}Y. This particular type of approach may not be ideal for pancreatic cancer. Therefore, prostate cancer was selected based on patients with advanced local disease. Hyperthermia in this method requires irradiation of light on gold nanorods and the source of light has limits on its penetration. The prostate is potentially accessible for this type of approach and therefore makes logical sense as a viable treatment.

Image-guided therapeutics are in their earliest stages of development. With more advances on the horizon in imaging modalities, nanomaterials and targeting methods, it

can be expected that these types of approaches are going to contribute to cancer treatment in future.

2.7. References

1. James ML, Gambhir SS. A molecular imaging primer: modalities, imaging agents, and applications. Physiol Rev. 2012; 92:897-965.

2. Rudin M, Weissleder R. Molecular imaging in drug discovery and development. Nat Rev Drug Discov. 2003; 2:123-131.

3. Minino AM, Murphy SL. Death in the United States, 2010. NCHS Data Brief. 2012:1-8.

4. American Cancer Society. Cancer Facts and Figures 2012. Atlanta, GA: American Cancer Society; 2012.

5. Dorsey ER, Thompson JP, Carrasco M, et al. Financing of U.S. biomedical research and new drug approvals across therapeutic areas. PLoS One. 2009; 4:e7015.

6. Alberg AJ, Ford JG, Samet JM, American College of Chest P. Epidemiology of lung cancer: ACCP evidence-based clinical practice guidelines (2nd edition). Chest. 2007; 132:29S-55S.

7. Berry DA, Cronin KA, Plevritis SK, et al. Effect of screening and adjuvant therapy on mortality from breast cancer. N Engl J Med. 2005; 353:1784-1792.

8. Moen MD, McKeage K, Plosker GL, Siddiqui MA. Imatinib: a review of its use in chronic myeloid leukaemia. Drugs. 2007; 67:299-320.

9. Heppner GH, Miller BE. Therapeutic implications of tumor heterogeneity. Semin Oncol. 1989; 16:91-105.

10. Issa AM. Personalized medicine and the practice of medicine in the 21st century. Mcgill J Med. 2007; 10:53-57.

11. Funkhouser J. Reintroducing pharma: Theranostic revolution. Curr. Drug Discovery. 2002; 2.

12. Kelkar SS, Reineke TM. Theranostics: combining imaging and therapy. Bioconjug Chem. 2011; 22:1879-1903.

13. Haga SB, Burke W. Using pharmacogenetics to improve drug safety and efficacy. JAMA. 2004; 291:2869-2871.

14. Marusyk A, Polyak K. Tumor heterogeneity: causes and consequences. Biochim Biophys Acta. 2010; 1805:105-117.

15. Blair ED, Stratton EK, Kaufmann M. The economic value of companion diagnostics and stratified medicines. Expert Rev Mol Diagn. 2012; 12:791-794.

16. Zieba A, Grannas K, Soderberg O, Gullberg M, Nilsson M, Landegren U. Molecular tools for companion diagnostics. N Biotechnol. 2012; 29:634-640.

17. Weissleder R. Molecular imaging : principles and practice. Shelton, Conn.: People's Medical Pub. House, 2009.

18. Gambhir SS. Molecular imaging of cancer with positron emission tomography. Nat Rev Cancer. 2002; 2:683-693.

19. U.S. Food and Drug Administration. In Vitro Companion Diagnostic Devices. [accessed 04/04/2013].

20. Capizzi RL. Targeted radio-immunotherapy with Bexxar produces durable remissions in patients with late stage low grade non-Hodgkin's lymphomas. Trans Am Clin Climatol Assoc. 2004; 115:255-272.

21. Chapuy B, Hohloch K, Trumper L. Yttrium 90 ibritumomab tiuxetan (Zevalin): a new bullet in the fight against malignant lymphoma? Biotechnol J. 2007; 2:1435-1443.

22. Goldsmith SJ. Radioimmunotherapy of lymphoma: Bexxar and Zevalin. Semin Nucl Med. 2010; 40:122-135.

23. Lammers T, Kiessling F, Hennink WE, Storm G. Nanotheranostics and image-guided drug delivery: current concepts and future directions. Mol Pharm. 2010; 7:1899-1912.

24. Hirsjarvi S, Passirani C, Benoit JP. Passive and active tumour targeting with nanocarriers. Curr Drug Discov Technol. 2011; 8:188-196.

25. Seymour LW, Miyamoto Y, Maeda H, et al. Influence of molecular weight on passive tumour accumulation of a soluble macromolecular drug carrier. Eur J Cancer. 1995; 31A:766-770.

26. Prabhakar U, Blakey DC, Maeda H, et al. Challenges and key considerations of the enhanced permeability and retention effect (EPR) for nanomedicine drug delivery in oncology. Cancer Res. 2013.

27. Iyer AK, Khaled G, Fang J, Maeda H. Exploiting the enhanced permeability and retention effect for tumor targeting. Drug Discov Today. 2006; 11:812-818.

28. Maeda H. The enhanced permeability and retention (EPR) effect in tumor vasculature: the key role of tumor-selective macromolecular drug targeting. Adv Enzyme Regul. 2001; 41:189-207.

29. Lammers T, Kiessling F, Hennink WE, Storm G. Drug targeting to tumors: principles, pitfalls and (pre-) clinical progress. J Control Release. 2012; 161:175-187.

30. Prabhu P, Patravale V. The upcoming field of theranostic nanomedicine: an overview. J Biomed Nanotechnol. 2012; 8:859-882.

31. Zhang XQ, Xu X, Bertrand N, Pridgen E, Swami A, Farokhzad OC. Interactions of nanomaterials and biological systems: Implications to personalized nanomedicine. Adv Drug Deliv Rev. 2012; 64:1363-1384.

32. Farokhzad OC, Langer R. Nanomedicine: developing smarter therapeutic and diagnostic modalities. Adv Drug Deliv Rev. 2006; 58:1456-1459.

33. Zhang H. Multifunctional nanomedicine platforms for cancer therapy. J Nanosci Nanotechnol. 2012; 12:4012-4018.

34. Liu Y, Miyoshi H, Nakamura M. Nanomedicine for drug delivery and imaging: a promising avenue for cancer therapy and diagnosis using targeted functional nanoparticles. Int J Cancer. 2007; 120:2527-2537.

35. Lee PY, Wong KK. Nanomedicine: a new frontier in cancer therapeutics. Curr Drug Deliv. 2011; 8:245-253.

36. Kopecek J, Kopeckova P, Minko T, Lu ZR, Peterson CM. Water soluble polymers in tumor targeted delivery. J Control Release. 2001; 74:147-158.

37. Torchilin VP. Multifunctional pharmaceutical nanocarrires. New York: Springer, 2008.

38. Kopecek J, Kopeckova P. HPMA copolymers: origins, early developments, present, and future. Adv Drug Deliv Rev. 2010; 62:122-149.

39. Rihova B, Kovar M. Immunogenicity and immunomodulatory properties of HPMA-based polymers. Adv Drug Deliv Rev. 2010; 62:184-191.

40. Pasut G, Veronese FM. PEG conjugates in clinical development or use as anticancer agents: an overview. Adv Drug Deliv Rev. 2009; 61:1177-1188.

41. Ulbrich K, Subr V. Structural and chemical aspects of HPMA copolymers as drug carriers. Adv Drug Deliv Rev. 2010; 62:150-166.

42. Duncan R. Polymer therapeutics as nanomedicines: new perspectives. Curr Opin Biotechnol. 2011; 22:492-501.

43. Webster R, Elliott V, Park BK, Walker D. PEG and PEG conjugate toxicity: towards an understanding of toxicity of PEG and its relevance to Pegylated biologicals. In: Veronese FM, editor. PEGylated Protein Drugs: Basic Science and Clinical Applications: Birkhauser Basel, 2009:127-146.

44. Duncan R, Vicent MJ. Do HPMA copolymer conjugates have a future as clinically useful nanomedicines? A critical overview of current status and future opportunities. Adv Drug Deliv Rev. 2010; 62:272-282.

45. Julyan PJ, Seymour LW, Ferry DR, et al. Preliminary clinical study of the distribution of HPMA copolymers bearing doxorubicin and galactosamine. J Control Release. 1999; 57:281-290.

46. Duncan R. Development of HPMA copolymer-anticancer conjugates: clinical experience and lessons learnt. Adv Drug Deliv Rev. 2009; 61:1131-1148.

47. Gong J, Chen M, Zheng Y, Wang S, Wang Y. Polymeric micelles drug delivery system in oncology. J Control Release. 2012; 159:312-323.

48. Li G, Liu J, Pang Y, et al. Polymeric micelles with water-insoluble drug as hydrophobic moiety for drug delivery. Biomacromolecules. 2011; 12:2016-2026.

49. Kedar U, Phutane P, Shidhaye S, Kadam V. Advances in polymeric micelles for drug delivery and tumor targeting. Nanomedicine. 2010; 6:714-729.

50. Oerlemans C, Bult W, Bos M, Storm G, Nijsen JF, Hennink WE. Polymeric micelles in anticancer therapy: targeting, imaging and triggered release. Pharm Res. 2010; 27:2569-2589.

51. Lee HJ, Ponta A, Bae Y. Polymer nanoassemblies for cancer treatment and imaging. Ther Deliv. 2010; 1:803-817.

52. Liu Z, Zhang N. pH-Sensitive polymeric micelles for programmable drug and gene delivery. Curr Pharm Des. 2012; 18:3442-3451.

53. Tsai HC, Chang WH, Lo CL, et al. Graft and diblock copolymer multifunctional micelles for cancer chemotherapy and imaging. Biomaterials. 2010; 31:2293-2301.

54. Fr chet J J, Tomalia DA. Dendrimers and other dendritic polymers. Chichester ; New York: Wiley, 2001.

55. Tomalia DA, Baker H, Dewald J, et al. A new class of polymers: starburst-dendritic macromolecules. Polym. J. 1985; 17:117-132.

56. Gillies ER, Frechet JM. Dendrimers and dendritic polymers in drug delivery. Drug Discov Today. 2005; 10:35-43.

57. Zolnik BS, Sadrieh N. Regulatory perspective on the importance of ADME assessment of nanoscale material containing drugs. Adv Drug Deliv Rev. 2009; 61:422-427.

58. Walter MV, Malkoch M. Simplifying the synthesis of dendrimers: accelerated approaches. Chem Soc Rev. 2012; 41:4593-4609.

59. Yellepeddi VK, Kumar A, Palakurthi S. Surface modified poly(amido)amine dendrimers as diverse nanomolecules for biomedical applications. Expert Opin Drug Deliv. 2009; 6:835-850.

60. Sadekar S, Ghandehari H. Transepithelial transport and toxicity of PAMAM dendrimers: implications for oral drug delivery. Adv Drug Deliv Rev. 2012; 64:571-588.

61. Duncan R, Izzo L. Dendrimer biocompatibility and toxicity. Adv Drug Deliv Rev. 2005; 57:2215-2237.

62. Caminade AM, Laurent R, Delavaux-Nicot B, Majoral JP. "Janus" dendrimers: syntheses and properties. New Journal of Chemistry. 2012; 36:217-226.

63. Ornelas C, Pennell R, Liebes LF, Weck M. Construction of a well-defined multifunctional dendrimer for theranostics. Org Lett. 2011; 13:976-979.

64. Kumar P, Gulbake A, Jain SK. Liposomes a vesicular nanocarrier: potential advancements in cancer chemotherapy. Crit Rev Ther Drug Carrier Syst. 2012; 29:355-419.

65. Al-Jamal WT, Kostarelos K. Liposomes: from a clinically established drug delivery system to a nanoparticle platform for theranostic nanomedicine. Acc Chem Res. 2011; 44:1094-1104.

66. Barenholz Y. Doxil(R)--the first FDA-approved nano-drug: lessons learned. J Control Release. 2012; 160:117-134.

67. Meyerhoff A. U.S. Food and Drug Administration approval of AmBisome (liposomal amphotericin B) for treatment of visceral leishmaniasis. Clin Infect Dis. 1999; 28:42-48; discussion 49-51.

68. Sawant RR, Torchilin VP. Challenges in development of targeted liposomal therapeutics. AAPS J. 2012; 14:303-315.

69. FDA. Guidance for Industry: Liposome Drug Products, 2002. http://www.fda.gov/downloads/Drugs/GuidanceComplianceRegulatoryInformation/Guidances/ucm070570.pdf

70. Desai N. Challenges in development of nanoparticle-based therapeutics. AAPS J. 2012; 14:282-295.

71. Immordino ML, Dosio F, Cattel L. Stealth liposomes: review of the basic science, rationale, and clinical applications, existing and potential. Int J Nanomedicine. 2006; 1:297-315.

72. Ranjan A, Jacobs GC, Woods DL, et al. Image-guided drug delivery with magnetic resonance guided high intensity focused ultrasound and temperature sensitive liposomes in a rabbit Vx2 tumor model. J Control Release. 2012; 158:487-494.

73. Kiessling F, Fokong S, Koczera P, Lederle W, Lammers T. Ultrasound microbubbles for molecular diagnosis, therapy, and theranostics. J Nucl Med. 2012; 53:345-348.

74. Liang HD, Blomley MJ. The role of ultrasound in molecular imaging. Br J Radiol. 2003; 76 Spec No 2:S140-150.

75. Rapoport N, Nam KH, Gupta R, et al. Ultrasound-mediated tumor imaging and nanotherapy using drug loaded, block copolymer stabilized perfluorocarbon nanoemulsions. J Control Release. 2011; 153:4-15.

76. Castle J, Butts M, Healey A, Kent K, Marino M, Feinstein SB. Ultrasound-mediated targeted drug delivery: recent success and remaining challenges. Am J Physiol Heart Circ Physiol. 2013; 304:H350-357.

77. Oldham RK, Dillman RO. Monoclonal antibodies in cancer therapy: 25 years of progress. J Clin Oncol. 2008; 26:1774-1777.

78. Barbet J, Bardies M, Bourgeois M, et al. Radiolabeled antibodies for cancer imaging and therapy. Methods Mol Biol. 2012; 907:681-697.

79. Mirick GR, Bradt BM, Denardo SJ, Denardo GL. A review of human anti-globulin antibody (HAGA, HAMA, HACA, HAHA) responses to monoclonal antibodies. Not four letter words. Q J Nucl Med Mol Imaging. 2004; 48:251-257.

80. Jeong H, Huh M, Lee SJ, et al. Photosensitizer-conjugated human serum albumin nanoparticles for effective photodynamic therapy. Theranostics. 2011; 1:230-239.

81. Kennedy LC, Bickford LR, Lewinski NA, et al. A new era for cancer treatment: gold-nanoparticle-mediated thermal therapies. Small. 2011; 7:169-183.

82. Fernandez-Fernandez A, Manchanda R, McGoron AJ. Theranostic applications of nanomaterials in cancer: drug delivery, image-guided therapy, and multifunctional platforms. Appl Biochem Biotechnol. 2011; 165:1628-1651.

83. Huang HC, Barua S, Sharma G, Dey SK, Rege K. Inorganic nanoparticles for cancer imaging and therapy. J Control Release. 2011; 155:344-357.

84. Plewes DB, Kucharczyk W. Physics of MRI: a primer. J Magn Reson Imaging. 2012; 35:1038-1054.

85. Koh TS, Bisdas S, Koh DM, Thng CH. Fundamentals of tracer kinetics for dynamic contrast-enhanced MRI. J Magn Reson Imaging. 2011; 34:1262-1276.

86. Chen J, Lanza GM, Wickline SA. Quantitative magnetic resonance fluorine imaging: today and tomorrow. Wiley Interdiscip Rev Nanomed Nanobiotechnol. 2010; 2:431-440.

87. Brown MA, Semelka RC. MRI : basic principles and applications. 4th ed. Hoboken, N.J.: Wiley-Blackwell/John Wiley & Sons, 2010.

88. Zhang H, Zhang L, Myerson J, et al. Quantifying the evolution of vascular barrier disruption in advanced atherosclerosis with semipermeant nanoparticle contrast agents. PLoS One. 2011; 6:e26385.

89. Kok MB, de Vries A, Abdurrachim D, et al. Quantitative (1)H MRI, (19)F MRI, and (19)F MRS of cell-internalized perfluorocarbon paramagnetic nanoparticles. Contrast Media Mol Imaging. 2011; 6:19-27.

90. Neubauer AM, Myerson J, Caruthers SD, et al. Gadolinium-modulated 19F signals from perfluorocarbon nanoparticles as a new strategy for molecular imaging. Magn Reson Med. 2008; 60:1066-1072.

91. Waters EA, Chen J, Allen JS, Zhang H, Lanza GM, Wickline SA. Detection and quantification of angiogenesis in experimental valve disease with integrin-targeted nanoparticles and 19-fluorine MRI/MRS. J Cardiovasc Magn Reson. 2008; 10:43.

92. Porsch C, Zhang Y, Ostlund A, et al. In vitro evaluation of non-protein adsorbing breast cancer theranostics based on 19F-polymer containing nanoparticles. Part. Part. Syst. Charact. (2013).

93. Hricak H. Oncologic imaging: a guiding hand of personalized cancer care. Radiology. 2011; 259:633-640.

94. Bremer C, Ntziachristos V, Weissleder R. Optical-based molecular imaging: contrast agents and potential medical applications. Eur Radiol. 2003; 13:231-243.

95. Ntziachristos V, Bremer C, Weissleder R. Fluorescence imaging with near-infrared light: new technological advances that enable in vivo molecular imaging. Eur Radiol. 2003; 13:195-208.

96. Hielscher AH. Optical tomographic imaging of small animals. Curr Opin Biotechnol. 2005; 16:79-88.

97. Ntziachristos V, Ripoll J, Wang LV, Weissleder R. Looking and listening to light: the evolution of whole-body photonic imaging. Nat Biotechnol. 2005; 23:313-320.

98. Licha K, Olbrich C. Optical imaging in drug discovery and diagnostic applications. Adv Drug Deliv Rev. 2005; 57:1087-1108.

99. Ntziachristos V, Tung CH, Bremer C, Weissleder R. Fluorescence molecular tomography resolves protease activity in vivo. Nat Med. 2002; 8:757-760.

100. Prekeges J. Nuclear medicine instrumentation. 2nd ed. Burlington, Mass.: Jones & Bartlett Learning, 2013.

101. Brechbiel MW. Bifunctional chelates for metal nuclides. Q J Nucl Med Mol Imaging. 2008; 52:166-173.

102. Khalil MM. Basic sciences of nuclear medicine. Heidelberg: Springer, 2011.

103. Seevers RH, Counsell RE. Radioiodination techniques for small organic molecules. Chem Rev. 1982; 82:575-590.

104. Saha GB. Fundamentals of Nuclear Pharmacy. 6th ed. New York: Springer, 2010.

105. Srivastava SC. Paving the way to personalized medicine: production of some promising theragnostic radionuclides at Brookhaven National Laboratory. Semin Nucl Med. 2012; 42:151-163.

106. Hijnen NM, de Vries A, Nicolay K, Grull H. Dual-isotope 111In/177Lu SPECT imaging as a tool in molecular imaging tracer design. Contrast Media Mol Imaging. 2012; 7:214-222.

107. Alberini JL, Edeline V, Giraudet AL, et al. Single photon emission tomography/computed tomography (SPET/CT) and positron emission tomography/computed tomography (PET/CT) to image cancer. J Surg Oncol. 2011; 103:602-606.

108. Bailey DL. Positron emission tomography : basic sciences. New York: Springer, 2005.

109. Liu Y, Welch MJ. Nanoparticles labeled with positron emitting nuclides: advantages, methods, and applications. Bioconjug Chem. 2012; 23:671-682.

110. Yuan J, Zhang H, Kaur H, Oupicky D, Peng F. Synthesis and characterization of theranostic poly(HPMA)-c(RGDyK)-DOTA-64Cu copolymer targeting tumor angiogenesis: tumor localization visualized by positron emission tomography. Mol Imaging. 2012; 12:203-212.

111. Fass L. Imaging and cancer: a review. Mol Oncol. 2008; 2:115-152.

112. Gu FX, Karnik R, Wang AZ, et al. Targeted nanoparticles for cancer therapy. Nanotoday. 2007; 2:14-21.

113. Noguchi Y, Wu J, Duncan R, et al. Early phase tumor accumulation of macromolecules: a great difference in clearance rate between tumor and normal tissues. Jpn J Cancer Res. 1998; 89:307-314.

114. Folkman J. Tumor angiogenesis: therapeutic implications. N Engl J Med. 1971; 285:1182-1186.

115. Maeda H, Sawa T, Konno T. Mechanism of tumor-targeted delivery of macromolecular drugs, including the EPR effect in solid tumor and clinical overview of the prototype polymeric drug SMANCS. J Control Release. 2001; 74:47-61.

116. Gruner BA, Weitman SD. The folate receptor as a potential therapeutic anticancer target. Invest New Drugs. 1998; 16:205-219.

117. Weitman SD, Lark RH, Coney LR, et al. Distribution of the folate receptor GP38 in normal and malignant cell lines and tissues. Cancer Res. 1992; 52:3396-3401.

118. Majoros IJ, Williams CR, Becker A, Baker JR, Jr. Methotrexate delivery via folate targeted dendrimer-based nanotherapeutic platform. Wiley Interdiscip Rev Nanomed Nanobiotechnol. 2009; 1:502-510.

119. Trepel M, Pasqualini R, Arap W. Chapter 4. Screening phage-display Peptide libraries for vascular targeted peptides. Methods Enzymol. 2008; 445:83-106.

120. Deutscher SL. Phage display in molecular imaging and diagnosis of cancer. Chem Rev. 2010; 110:3196-3211.

121. Ruoslahti E, Pierschbacher MD. New perspectives in cell adhesion: RGD and integrins. Science. 1987; 238:491-497.

122. Haubner R, Wester HJ, Burkhart F, et al. Glycosylated RGD-containing peptides: tracer for tumor targeting and angiogenesis imaging with improved biokinetics. J Nucl Med. 2001; 42:326-336.

123. Mitra A, Nan A, Papadimitriou JC, Ghandehari H, Line BR. Polymer-peptide conjugates for angiogenesis targeted tumor radiotherapy. Nucl Med Biol. 2006; 33:43-52.

124. Larson N, Ray A, Malugin A, Pike DB, Ghandehari H. HPMA copolymer-aminohexylgeldanamycin conjugates targeting cell surface expressed GRP78 in prostate cancer. Pharm Res. 2010; 27:2683-2693.

125. Vives E, Schmidt J, Pelegrin A. Cell-penetrating and cell-targeting peptides in drug delivery. Biochim Biophys Acta. 2008; 1786:126-138.

126. Briat A, Wenk CH, Ahmadi M, et al. Reduction of renal uptake of 111In-DOTA-labeled and A700-labeled RAFT-RGD during integrin alphavbeta3 targeting using single photon emission computed tomography and optical imaging. Cancer Sci. 2012; 103:1105-1110.

127. Elloumi J, Jellali K, Jemel I, Aifa S. Monoclonal antibodies as cancer therapeutics. Recent Pat Biotechnol. 2012; 6:45-56.

128. Taheri A, Dinarvand R, Atyabi F, Ghahremani MH, Ostad SN. Trastuzumab decorated methotrexate-human serum albumin conjugated nanoparticles for targeted delivery to HER2 positive tumor cells. Eur J Pharm Sci. 2012; 47:331-340.

129. Yousefpour P, Atyabi F, Vasheghani-Farahani E, Movahedi AA, Dinarvand R. Targeted delivery of doxorubicin-utilizing chitosan nanoparticles surface-functionalized with anti-Her2 trastuzumab. Int J Nanomedicine. 2011; 6:1977-1990.

130. Anhorn MG, Wagner S, Kreuter J, Langer K, von Briesen H. Specific targeting of HER2 overexpressing breast cancer cells with doxorubicin-loaded trastuzumab-modified human serum albumin nanoparticles. Bioconjug Chem. 2008; 19:2321-2331.

131. Karra N, Benita S. The ligand nanoparticle conjugation approach for targeted cancer therapy. Curr Drug Metab. 2012; 13:22-41.

132. Cardoso MM, Peca IN, Roque AC. Antibody-conjugated nanoparticles for therapeutic applications. Curr Med Chem. 2012; 19:3103-3127.

133. Landon CD, Park J, Needham D, Dewhirst MW. Nanoscale drug delivery and hyperthermia: the materials design and preclinical and clinical testing of low temperature-sensitive liposomes used in combination with mild hyperthermia in the treatment of local cancer. The Open Nanomedicine Journal. 2011; 3:38-64.

134. Koning GA, Eggermont AM, Lindner LH, ten Hagen TL. Hyperthermia and thermosensitive liposomes for improved delivery of chemotherapeutic drugs to solid tumors. Pharm Res. 2010; 27:1750-1754.

135. Ponce AM, Vujaskovic Z, Yuan F, Needham D, Dewhirst MW. Hyperthermia mediated liposomal drug delivery. Int J Hyperthermia. 2006; 22:205-213.

136. Link S, El-Sayed MA. Shape and size dependence of radiative, non-radiative and photothermal properties of gold nanocrystals. Int Rev Phys Chem. 2000; 19:409-453.

137. Gormley AJ, Greish K, Ray A, Robinson R, Gustafson JA, Ghandehari H. Gold nanorod mediated plasmonic photothermal therapy: a tool to enhance macromolecular delivery. Int J Pharm. 2011; 415:315-318.

138. Lynn JG, Zwemer RL, Chick AJ. The biological application of focused ultrasonic waves. Science. 1942; 96:119-120.

139. Grull H, Langereis S. Hyperthermia-triggered drug delivery from temperature-sensitive liposomes using MRI-guided high intensity focused ultrasound. J Control Release. 2012; 161:317-327.

140. Yudina A, de Smet M, Lepetit-Coiffe M, et al. Ultrasound-mediated intracellular drug delivery using microbubbles and temperature-sensitive liposomes. J Control Release. 2011; 155:442-448.

141. de Smet M, Heijman E, Langereis S, Hijnen NM, Grull H. Magnetic resonance imaging of high intensity focused ultrasound mediated drug delivery from temperature-sensitive liposomes: an in vivo proof-of-concept study. J Control Release. 2011; 150:102-110.

142. Wahajuddin, Arora S. Superparamagnetic iron oxide nanoparticles: magnetic nanoplatforms as drug carriers. Int J Nanomedicine. 2012; 7:3445-3471.

143. Espinosa E, Zamora P, Feliu J, Gonzalez Baron M. Classification of anticancer drugs--a new system based on therapeutic targets. Cancer Treat Rev. 2003; 29:515-523.

144. Ulbrich K, Zacharieva EI, Obereigner B, Kopecek J. Polymers containing enzymatically degradable bonds V. Hydrophilic polymers degradable by papain. Biomaterials. 1980; 1:199-204.

145. Ray A, Larson N, Pike DB, et al. Comparison of active and passive targeting of docetaxel for prostate cancer therapy by HPMA copolymer-RGDfK conjugates. Mol Pharm. 2011; 8:1090-1099.

146. Lammers T, Subr V, Ulbrich K, et al. Simultaneous delivery of doxorubicin and gemcitabine to tumors in vivo using prototypic polymeric drug carriers. Biomaterials. 2009; 30:3466-3475.

147. Kramer-Marek G, Capala J. The role of nuclear medicine in modern therapy of cancer. Tumour Biol. 2012; 33:629-640.

148. Zhang L, Chen H, Wang L, et al. Delivery of therapeutic radioisotopes using nanoparticle platforms: potential benefit in systemic radiation therapy. Nanotechnol Sci Appl. 2010; 3:159-170.

149. Griggs WS, Divgi C. Radioiodine imaging and treatment in thyroid disorders. Neuroimaging Clin N Am. 2008; 18:505-515, viii.

150. Wang AZ, Yuet K, Zhang L, et al. ChemoRad nanoparticles: a novel multifunctional nanoparticle platform for targeted delivery of concurrent chemoradiation. Nanomedicine (Lond). 2010; 5:361-368.

151. Whitehead KA, Langer R, Anderson DG. Knocking down barriers: advances in siRNA delivery. Nat Rev Drug Discov. 2009; 8:129-138.

152. Lee H, Kim IK, Park TG. Intracellular trafficking and unpacking of siRNA/quantum dot-PEI complexes modified with and without cell penetrating peptide: confocal and flow cytometric FRET analysis. Bioconjug Chem. 2010; 21:289-295.

153. Celli JP, Spring BQ, Rizvi I, et al. Imaging and photodynamic therapy: mechanisms, monitoring, and optimization. Chem Rev. 2010; 110:2795-2838.

154. Ackroyd R, Kelty C, Brown N, Reed M. The history of photodetection and photodynamic therapy. Photochem Photobiol. 2001; 74:656-669.

155. Vergnon JM, Huber RM, Moghissi K. Place of cryotherapy, brachytherapy and photodynamic therapy in therapeutic bronchoscopy of lung cancers. Eur Respir J. 2006; 28:200-218.

156. Bown SG, Rogowska AZ, Whitelaw DE, et al. Photodynamic therapy for cancer of the pancreas. Gut. 2002; 50:549-557.

157. Pandey SK, Gryshuk AL, Sajjad M, et al. Multimodality agents for tumor imaging (PET, fluorescence) and photodynamic therapy. A possible "see and treat" approach. J Med Chem. 2005; 48:6286-6295.

158. Capella MA, Capella LS. A light in multidrug resistance: photodynamic treatment of multidrug-resistant tumors. J Biomed Sci. 2003; 10:361-366.

CHAPTER 3

OVERCOMING THE STROMAL BARRIER FOR TARGETED DELIVERY OF HPMA COPOLYMERS TO PANCREATIC TUMORS*

3.1. Introduction

Pancreatic cancer is the 4th leading cause of cancer-related deaths in the United States[1]. Recently, the incidence rate has begun to increase, possibly related to the increase in rates of obesity[1]. Patients that receive this diagnosis have little hope of a cure with only a 6% statistical chance for more than a 5-year survival. Typically, this cancer is not discovered early on in its development and has already rapidly spread by the time it is discovered[2,3]. Advanced stages of pancreatic cancer have little to no response to treatment because of the challenge to deliver drugs in sufficient amounts to the pancreatic tumors[4]. Novel methods of delivery to the pancreatic tumor need to be developed.

Water-soluble polymers such as *N*-(2-hydroxypropyl)methacrylamide copolymers have the potential to increase the delivery of drugs, imaging agents and targeting ligands to pancreatic tumors. HPMA copolymers are water-soluble polymers which can be synthesized in a wide range of sizes and with a large selection of comonomers that can

* Buckway B, Wang Y, Ray A, Ghandehari H. Overcoming the stromal barriers to targeted delivery of HPMA copolymers to pancreatic tumors. Int J Pharm. (2013); Accepted.

afford multifunctionality for enhanced delivery and monitoring[5,6]. Several studies have shown that these polymers can increase tumor localization based on both passive targeting, via the enhanced permeability and retention (EPR) effect[7], and active targeting by side chain conjugation to small peptides and monoclonal antibody fragments[8].

Active targeting is accomplished by attaching various targeting ligands to the side chains of the HPMA copolymer backbone which recognize receptors overexpressed in tumors[9-12]. HPMA copolymer systems conjugated with short peptide ligands containing the arg-gly-asp (RGD) sequence, which bind to $\alpha_v\beta_3$ integrins overexpressed on the neovasculature and surface of many tumor types, have shown to actively target tumors, thus increasing the concentration of polymer carriers conjugated with imaging agents and drugs[13-18]. Pancreatic tumors undergoing angiogenesis express this receptor on the vasculature and on the surface of some cells[19-21]. Therefore, HPMA copolymer-RGD conjugates could be potentially used as a targeted platform for delivery of both imaging agents and drugs for pancreatic cancer treatment. However, pancreatic cancers are known to have low vascularity which may be insufficient for vascular targeting[22].

Another receptor that has been shown to overexpress in pancreatic tumors is the human epidermal growth factor receptor 2 (HER2)[23]. HER2 also known as Neu, ErbB-2 is a protein of the family of epidermal growth factor receptor (EGFR/ErbB). 16-61% of pancreatic tumors in patients have high HER2 expression[23-26]. The peptide sequence KCCYSL was found by phage display technology to specifically recognize and bind to HER2 receptors[27]. KCCYSL can be conjugated to the backbone of HPMA copolymers and potentially allow for HER2 recognition, providing another targeting strategy to improve delivery.

Macromolecular carriers, however, have a significant challenge to penetrate pancreatic tumors. Pancreatic tumors are known to have a highly dense extracellular matrix which prevents the diffusion of large and even small molecules such as gemcitabine[28,29]. This effect is more pronounced with large macromolecules severely limited by diffusion in a dense tissue[30-32]. Recently, the effects of treating the stromal tissue in conjunction with drug to increase its concentration within the tumor has been investigated using drugs and enzymes which breakdown the dense stroma[28]. By breaking this barrier or causing "stromal collapse," it has been found that the barriers to diffusion caused by the dense stroma in pancreatic cancers can be overcome and improve therapy[33].

One of the stromal treating agents that has been investigated is hyaluronidase[4]. Hyaluronic acid is one of the main components of the dense interstitial tissues of the stroma and causes high intratumoral fluidic pressure (IFP). High IFP prevents the diffusion of both small and macromolecular constructs into the tumor. Several studies have been conducted along with clinical trials using hyaluronidase enzymes to breakdown hyaluronic acid which results in a lowering of IFP[4,34]. After treatment with hyaluronidase, it has been found that they can increase the localization of gemcitabine and other drugs into the tumor[4]. For example, 40 kDa and 2,000 kDa dextrans demonstrated increased tumor accumulation after administration of a PEGylated hyaluronidase treatment to the tumor[35]. The barriers to macromolecular delivery based on HPMA copolymers if combined with hyaluronidase treatment to the tumor can therefore potentially increase localization within the tumor. The goal of the study described in this Chapter is to compare the increased tumor localization of HPMA copolymer systems for either $\alpha_v\beta_3$ integrin or HER2 targeting in pancreatic cancer in conjunction with

hyaluronidase administration to the stromal tissue. The comparison between targeting strategies combined with stromal collapse were investigated in a pancreatic tumor mouse model.

3.2. Materials and Methods

3.2.1. Chemicals

Amino acids for peptide synthesis were obtained from AAPPTec (Louisville, KY). *N*-[(*R*)-2-Amino-3-(*p*-isothiocyanatophenyl)propyl]-*trans*-(S,S)-cyclohexane-1,2-diamine-*N,N-N',N',N''N''*-pentaacetic acid (*p*-SCN-CHX-A"-DTPA) was obtained from Macrocyclics (Dallas, TX). *N*-(3-Aminopropyl)methacrylamide hydrochloride (APMA) was acquired from Polysciences (Warrington, PA). 2,2'-Azobis[2-(2-imidazolin-2-yl)propane] dihydrochloride (VA-044) was obtained from Wako Chemicals (Richmond, VA). $^{111}InCl_3$ was obtained from the Intermountain Radiopharmacy (Salt Lake City, UT). All other reagents were of reagent grade and were obtained from Sigma-Aldrich (St. Louis, MO).

3.2.2. Cell lines

CAPAN-1 pancreatic adenocarcinoma cells (ATCC, Manassas, VA) were cultured in Iscove's Modified Dulbecco's Medium (IMDM) (ATCC, Manassas, VA) supplemented with 20% (v/v) fetal bovine serum (FBS) and 1:100 penicillin/streptomycin at 37ºC in a humidified atmosphere of 5% CO_2 (v/v). PANC-1 pancreatic duct carcinoma cells (ATCC, Manassas, VA) were cultured in Dulbecco's Modified Medium (DMM) (ATCC, Manassas, VA) supplemented with 10% FBS at 37ºC in a humidified atmosphere of 5% CO_2 (v/v). For all experimental procedures, the confluent cultures

were harvested by treatment with TrypLE™ Express (Invitrogen, Grand Island, NY) and subsequent dilution in their respective medium or phosphate buffered saline (PBS).

3.2.3. Synthesis and characterization of comonomers and peptides

N-(2-hydroxypropyl)methacrylamide comonomer (HPMA), *N*-methacryloyl-glycyl-glycyl thiazolidine-2-thione (MA-GG-TT) and *N*-methacryloylaminopropyl-2-amino-3-(isothiourea-phenyl)propyl-cyclohexane-1,2-diamine-*N,N-N',N',N'',N''*-pentaacetic acid (APMA-CHX-A"-DTPA) were synthesized according to published methods[36-38] (structures shown in *Figure 3.1*). A brief synthesis and characterization is described for HPMA, MA-GG-TT and APMA-CHX-A"-DTPA in Appendix A. The peptide sequences for cyclic Arg-Gly-Asp-D-Phe-Lys (cRGDfK), cyclic Arg-Gly-Glu-D-Phe-Lys (cRGEfK), Lys-Cys-Cys-Tyr-Ser-Leu (KCCYSL) and Lys-Tyr-Leu-Cys-Ser-Cys (KYLCSC) were synthesized via solid phase synthesis on a PS3 Peptide Synthesizer (Protein Technologies, Inc., Tucson, AZ). Products were confirmed by electrospray ionization mass spectroscopy. cRGDfK electrospray ionization mass spectroscopy (ESI-MS) *m/z* calculated for $C_{27}H_{41}N_9O_7$ 603.6705, found 604 $[M+H]^+$. cRGEfK ESI-MS *m/z* calculated for $C_{28}H_{43}N_9O_7$ 617.6971, found 617 $[M]^+$. KCCYSL ESI-MS *m/z* calculated for $C_{30}H_{49}N_7O_9S_2$ 715.8816, found 716 $[M]^+$. KYLCSC ESI-MS *m/z* calculated for $C_{30}H_{49}N_7O_9S_2$ 715.8816, found 716 $[M]^+$.

3.2.4. Synthesis of HPMA copolymers

Copolymerization was performed using the reversible addition-fragmentation chain transfer (RAFT) method in order to control the size and polydispersity. Briefly, HPMA, MA-GG-TT and APMA-CHX-A"-DTPA comonomers were combined with the

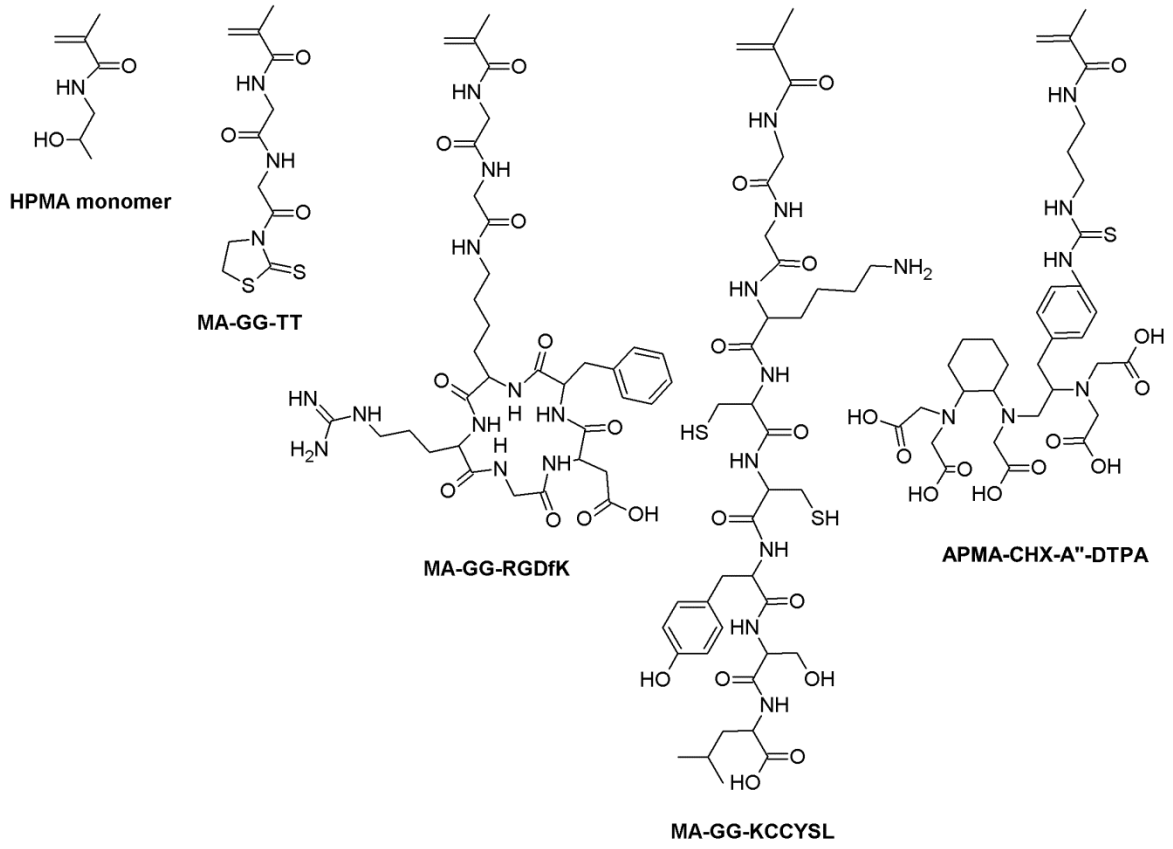

Figure 3.1. HPMA comonomers for imaging and targeting of pancreatic cancer. HPMA monomer affords the backbone and water-solubility of the polymer. MA-GG-TT is an active ester linker for postpolymerization addition of peptides by aminolysis. MA-GG-RGDfK and MA-GG-KCCYSL are the monomers responsible for $\alpha_v\beta_3$ integrin and HER2 targeting, respectively. APMA-CHX-A"-DTPA chelates $^{111}In^{+3}$ were used for imaging and biodistribution studies.

initiator VA-044 and the chain transfer agent 2-cyano-2-propyl dodecyl trithiocarbonate (CPDT) in methanol in a nitrogen purged sealed glass ampule (*Scheme 3.1*). The feed ratio of comonomers was kept constant at 88:10:2 (mol%), respectively. In order to control the polymerization, a ratio of 175:1:0.67 monomers:CPDT:VA-044 was used with total monomer concentration at 1 M. The ampule was placed in a 50ºC oil bath for 24 hs, after which the resulting polymer was collected by precipitation and washed with diethyl ether. The precursor HPMA-GGTT-DTPA copolymer apparent weight average molecular weight (M_w) and polydispersity (M_w/M_n) were estimated by size exclusion chromatography (SEC) using a Fast Protein Liquid Chromatography (FPLC) system (GE Healthcare) equipped with a Superose 12 column calibrated with fractions of known molecular weight HPMA homopolymers. MA-GG-TT content was quantified by UV spectrophotometry at 305 nm (ε_{305} = 10,800 $mol^{-1}cm^{-1}$). APMA-CHX-A"-DTPA content was estimated based on the 2 mol% feed ratio.

3.2.5. Peptide conjugation by aminolysis

Peptide sequences were added to the polymer via aminolysis. Briefly, a molar ratio of 1.5:1 peptides to MA-GG-TT content was dissolved in anhydrous methanol under nitrogen atmosphere overnight at room temperature. The resulting copolymer was precipitated from ether and purified by dialysis against deionized water using dialysis tubes with a molecular weight cutoff (MWCO, 3500, SpectraPor) to remove small molecular weight impurities. Amino acid analysis was performed in the Health Sciences Core Lab and the University of Utah School of Medicine in order to determine the amount of each peptide per HPMA copolymer.

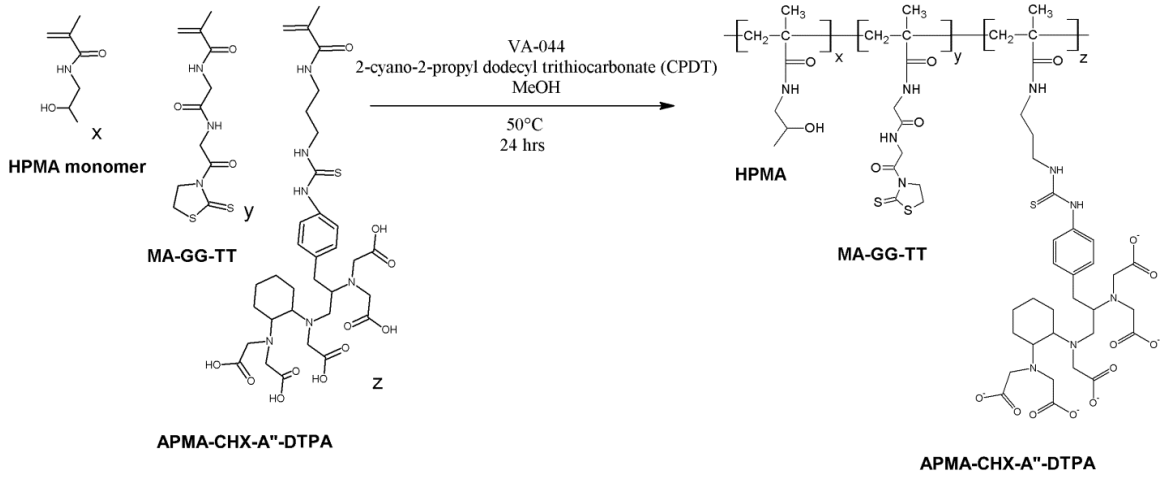

Scheme 3.1. RAFT polymerization of HPMA-GGTT-DTPA copolymer. Polymerization using RAFT synthesis with CPDT as the chain transfer agent and VA-044 as the azo-initiator. Synthesis provides the precursor polymer for addition of peptides by aminolysis of the TT group on the side chains. Precursor polymerization allows for an accurate comparison of targeting strategies based on the exact same HPMA copolymer backbone.

3.2.6. Flow cytometry analysis

Anti-HER2 (Neu), anti-$\alpha_v\beta_3$ Integrin and normal mouse IgG_1 (negative control) monoclonal antibodies labeled with phycoerythrin (PE) were obtained from Santa Cruz Biotechnology (Santa Cruz, CA). Samples of CAPAN-1 and PANC-1 cells were removed, washed with fresh media followed by PBS and then incubated with antibodies for 30 min at 4°C. Cells were washed with PBS and then fixed in 1% formaldehyde in PBS. Samples were analyzed by flow cytometry using a FACScan System (BD Biosciences, San Jose, CA).

3.2.7. Binding affinity

Competitive binding of the $\alpha_v\beta_3$ integrin receptor with free cRGDfK and cRGDfK containing copolymers was assessed as described previously except PANC-1 cell lines were used for the assay[13]. KCCYSL-containing copolymers were assayed by performing a blocking experiment. CAPAN-1 cells were harvested and resuspended in serum-free IMDM media. Each sample was combined with ^{111}In labeled KCCYSL polymers and increasing concentrations of free KCCYSL peptide or saline as control. The samples were incubated at 4ºC for 24 hs and then cells were centrifuged and the supernatant removed. The cells were then washed five times with saline. The resulting cell pellet was then counted using the CAPTUS 3000 gamma counter.

3.2.8. Radiolabeling with ^{111}In

Each copolymer was dissolved in 400 µl of 1.0 M sodium acetate buffer pH 5.0 and added to 5.0 µ (185 MBq) of $^{111}InCl_3$ stock solution which was also previously treated with 200 µl of 1.0 M sodium acetate buffer pH 5.0. The reaction was heated at

50ºC for 45 min after which 50 µl of 0.05 M ethylenediaminetetraacetic acid (EDTA) solution was added to scavenge any free ^{111}In ions. The radiolabeled copolymer was then purified using Sephadex G-25 PD-10 columns (GE Lifesciences, Piscataway, NJ). Radiostability was evaluated by incubating radiolabeled copolymer at 37ºC in the presence of mouse serum. Comparison between ^{111}In labeled copolymers and free $^{111}In^{+3}$ was performed by size exclusion chromatography and subsequent measurement of each fraction using a Cobra II Auto-gamma-counter (Canberra Industries, Inc., Meriden, CT).

3.2.9. Biodistribution

Female Nu/Nu athymic mice (Charles River Laboratories, Wilmington, MA) were subcutaneously inoculated with 5 x 10^6 CAPAN-1 cells in PBS in the lower left and right flank of the animal. After tumors had reached 5-8 mm in diameter, the mice were injected via lateral tail vein with 100-250 µCi (3.7-9.25 MBq) of ^{111}In labeled targeted copolymers or controls. Animals were euthanized at 2, 24, 72 h postinjection and blood, heart, lung, liver, spleen, kidney and tumor were collected, weighed and counted by a CAPTUS 3000 multichannel analyzer (Canberra Industries, Inc. Meriden, CT). All biodistribution studies were performed with 3-4 mice per group. All procedures were conducted under an approved protocol by the Institutional Animal Care and Use Committee (IACUC) at the University of Utah.

3.2.10. Imaging

Single Photon Emission Computerized Tomography and X-ray Computerized Tomography Imaging (SPECT/CT) was conducted on another group of CAPAN-1 tumor bearing mice prepared as described above. Animals were administered anesthesia via

nose cone using 2.5% Isoflurane and placed in an Inveon microPET/SPECT/CT scanner (Siemens Medical Solutions USA, Inc., Malvern, PA) and imaged at 2, 24, 48 and 72 h postinjection. Images were reconstructed and visualized using the Inveon Research Workplace software from Siemens Medical Solutions. Qualitative comparisons between conjugates were determined from the obtained images.

3.2.11. Immunohistochemistry

In order to assay the desmoplasia, neovasculature and the expression of HER2 in the in vivo mouse model, samples of CAPAN-1 xenograft tumor tissue were collected and fixed in normalized formalin buffer and embedded in paraffin. Slides were prepared and stained for HER2, CD31, smooth muscle actin (SMA), hyaluronic acid (HA) and Masson's Trichrome performed by ARUP Laboratories, Salt Lake City, UT.

3.2.12. Hyaluronidase treatment

In order to examine the stromal tissue breakdown effects to pancreatic tumors, Nu/Nu mice with CAPAN-1 xenograft tumors were administered 1600 U of Type 1 hyaluronidase (Sigma-Aldrich, St. Louis, MO) per tumor daily for three consecutive days before each biodistribution study. Biodistribution studies were then conducted in a similar manner as above and compared to nonhyaluronidase treated groups.

3.3. Results

3.3.1. Characteristics of HPMA copolymer conjugates

Characteristics of the synthesized HPMA copolymer conjugates are shown in *Table 3.1*. The precursor HPMA copolymer-GGTT-DTPA was synthesized with

Table 3.1. Polymer Characteristics

Polymer	M_w	M_n	PDI	CHX-A"-DTPA (mol%)	MA-GG-TT content (wt%)[c]	Peptide content (wt%)[b]	Peptides Per Polymer Backbone	^{111}In Radioactivity (μCi/mg)[d]
HPMA-GGTT-^{111}In DTPA	33 kDa	30 kDa	1.1	2.0[a]	7.3[c] (MA-GG-TT)	---	---	---
HPMA-RGDfK-^{111}In DTPA	-	-	-	-	-	21.5	11.7	169.4
HPMA-RGEfK-^{111}In DTPA	-	-	-	-	-	19.8	10.6	162.6
HPMA-KCCYSL-^{111}In DTPA	-	-	-	-	-	18.9	8.7	214.3
HPMA-KYLCSC-^{111}In DTPA	-	-	-	-	-	21.5	9.9	239.7

a) Based on feed ratio during polymerization
b) Based on amino acid analysis
c) Based on UV spectroscopy at $\varepsilon_{305} = 10{,}800\ mol^{-1}cm^{-1}$
d) Measured by γ-counter

approximately 7.3 wt% of the activated ester. The copolymers contained 8-12 peptides per polymer backbone. This is similar in content to studies performed previously which demonstrated effective targeting in prostate tumor xenografts[15,39]. The measurement of APMA-CHX-A"-DTPA was estimated to be 8.6 wt% based on the feed ratio during polymerization and reproducibly chelated ^{111}In with average of 196.5 ± 36.8 μCi/mg of polymer.

3.3.2. Relative receptor expression by flow cytometry

There are limited reports on the amounts of HER2 and $\alpha_v\beta_3$ integrin expression on the surface of pancreatic cell lines. Therefore, several cell lines were selected for this study based on literature reports that had high and low expression of HER2 receptors[40]. To our knowledge, levels of $\alpha_v\beta_3$ integrin expression on the various pancreatic tumor cell lines have not been widely investigated. Therefore, we performed flow cytometry experiments using PE labeled antibodies and found CAPAN1 had relatively high expression as compared to controls with respect to HER2 ($p < 0.0001$), but little to no significant difference with respect to controls versus $\alpha_v\beta_3$ integrin expression (*Figure 3.2*). PANC-1 cell lines were opposite to that of CAPAN-1 with higher expression of $\alpha_v\beta_3$ integrin ($p < 0.001$), but little to no expression of HER2 (*Figure 3.2*). The HER2 levels found between these two cell lines correlated well with previously reported values[40].

3.3.3. Binding affinity of targeted conjugates

Binding affinity of the different targeted HPMA copolymer conjugates was examined against their respective cell lines CAPAN1 for HER2 and PANC1 for $\alpha_v\beta_3$ integrin binding for each KCCYSL and RGDfK peptide species of polymer,

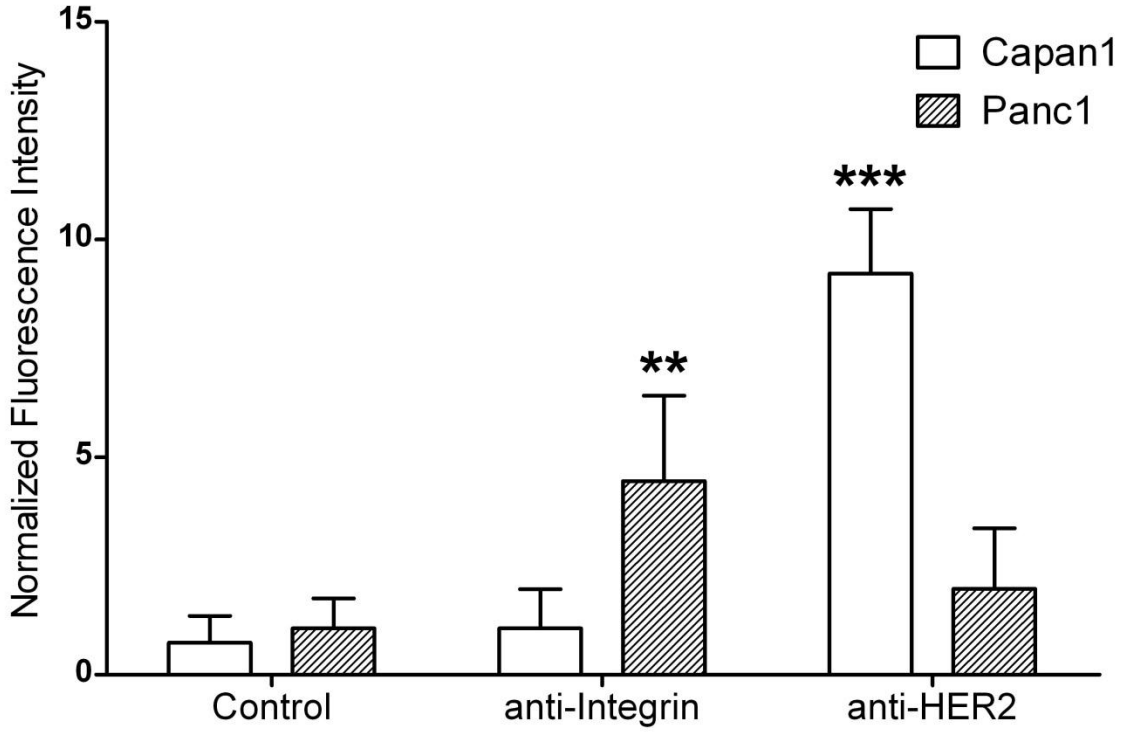

Figure 3.2. Flow cytometry for HER2 and $\alpha_v\beta_3$ integrin expression on pancreatic tumor cell lines. Differences in expression were compared to control (normal mouse IgG). PANC-1 had a significant difference in αvβ3 Integrin expression (** = $p < 0.001$) and CAPAN-1 had a significant difference in HER2 expression (*** = $p < 0.0001$) . Data expressed as mean ± standard error of the mean (SEM) (n=5).

respectively, and found to retain their affinities as shown in *Figure 3.3* and *Figure 3.4*. The affinities of the RGDfK containing HPMA copolymers were about an order of magnitude less when compared to free peptide controls (*Figure 3.3*). However, the possible multivalency effect of multiple peptides per polymer backbone is not accounted for in this in vitro assay. According to literature, there is no natural ligand that exists for HER2 receptors[41]. Therefore, a blocking experiment was conducted competing free KCCYSL with radiolabeled HPMA copolymer-KCCYSL-DTPA conjugates. Increasing concentrations in excess of 100x prevented the binding of HPMA copolymer-KCCYSL-DTPA, suggesting that the binding affinity is retained for HER2 receptors in vitro even when covalently bound to the copolymer backbone.

3.3.4. Radiolabeling and radiostability

HPMA copolymer complexation with ^{111}In was found to be reproducible and stable. Radiolabeling yields were on average 52.5±0.41% for all conjugates regardless of peptide ligand used. ^{111}In and DTPA coordination is well-known to be a stable complex[42]. *Figure 3.5* shows an example of the elution profile from a PD-10 column after incubation in mouse serum for 72 h. All other conjugates examined demonstrated similar stability profiles (data not shown).

3.3.5. Immunohistochemistry of pancreatic cells

Pancreatic tumors are well-known to exhibit a dense stromal matrix that is difficult to penetrate with anticancer drugs[28]. The nu/nu mouse subcutaneous xenograft tumor model used in this study was examined for a similar type of behavior by immunohistochemistry shown in *Figure 3.6*. Some of the typical signs of desmoplasia

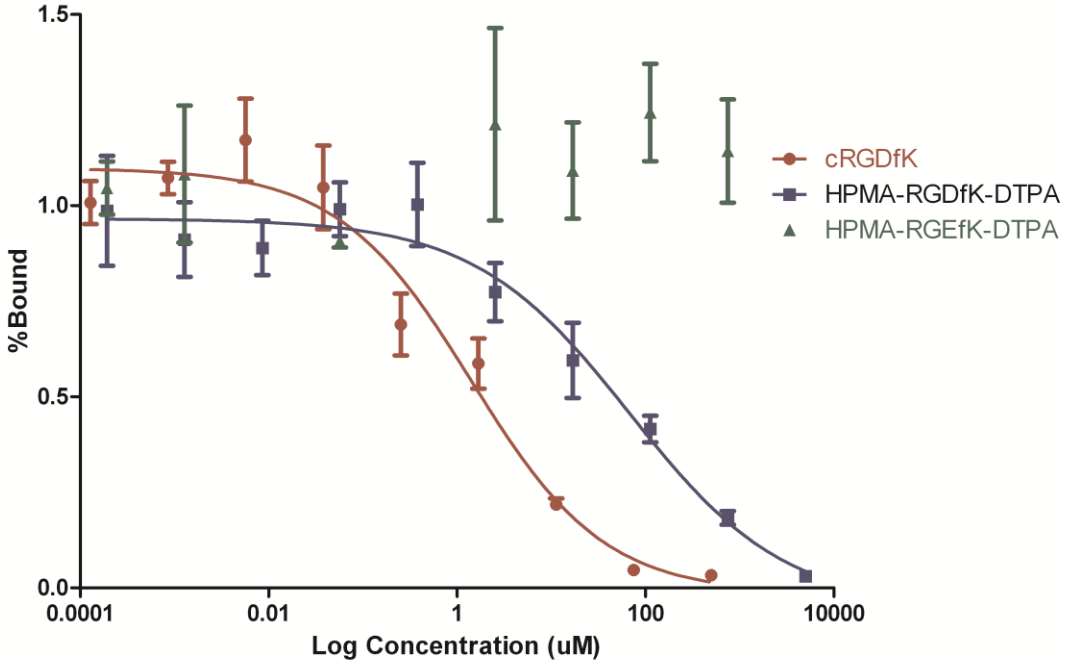

Figure 3.3. Competitive binding of HPMA-RGDfK-DTPA copolymers. Competitive binding performed against ^{125}I-Eichistatin with increasing concentrations of free peptide, targeting HPMA copolymer and nontargeted control (RGEfK). Assay performed in PANC-1 cell lines, and data expressed as the mean ± SEM performed in triplicate (n=3). The K_D value for cRGDfK and HPMA copolymer-RGDfK-DTPA was found to be 1.418 ± 0.550 μM and 67.83 ± 0.48 μM, respectively. Statistical significance was found between the estimated K_D values using a student t-test between cRGDfK and HPMA copolymer-RGDfK-DTPA ($p < 0.0001$).

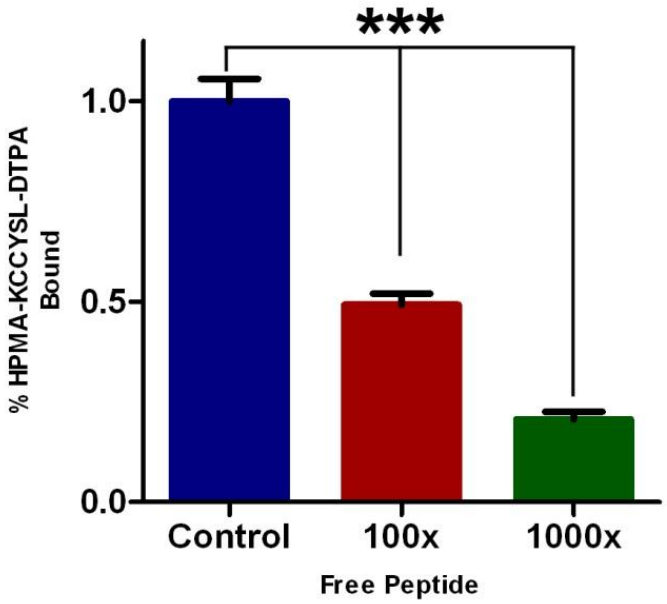

Figure 3.4. Blocking experiment with HPMA copolymer-KCCYSL-DTPA conjugates. Cells were incubated with either 100 or 1000 times excess free KCCYSL peptide (or KYLCSC for control) in order to prevent binding to the surface of CAPAN1 HER2 expressing cells in serum free media. Data are represented as the mean ± SEM (n=4). *** = $p < 0.0001$

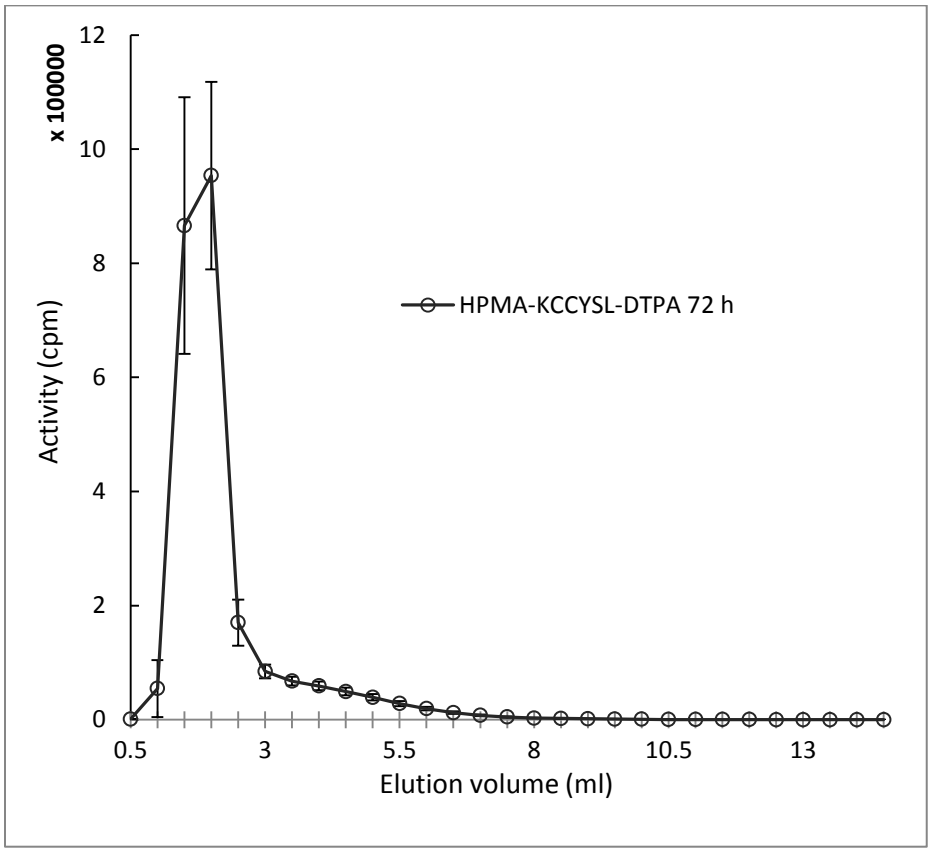

Figure 3.5. Radiostability of the ^{111}In labeled HPMA copolymers in vitro. Graph represents the typical elution profile from the PD-10 SEC separation for all HPMA copolymer-peptide-(^{111}In-DTPA) conjugates. No free label ($^{111}In^{+3}$) was detected for any of the conjugates tested. Data represented as a mean ± standard deviation (n=3).

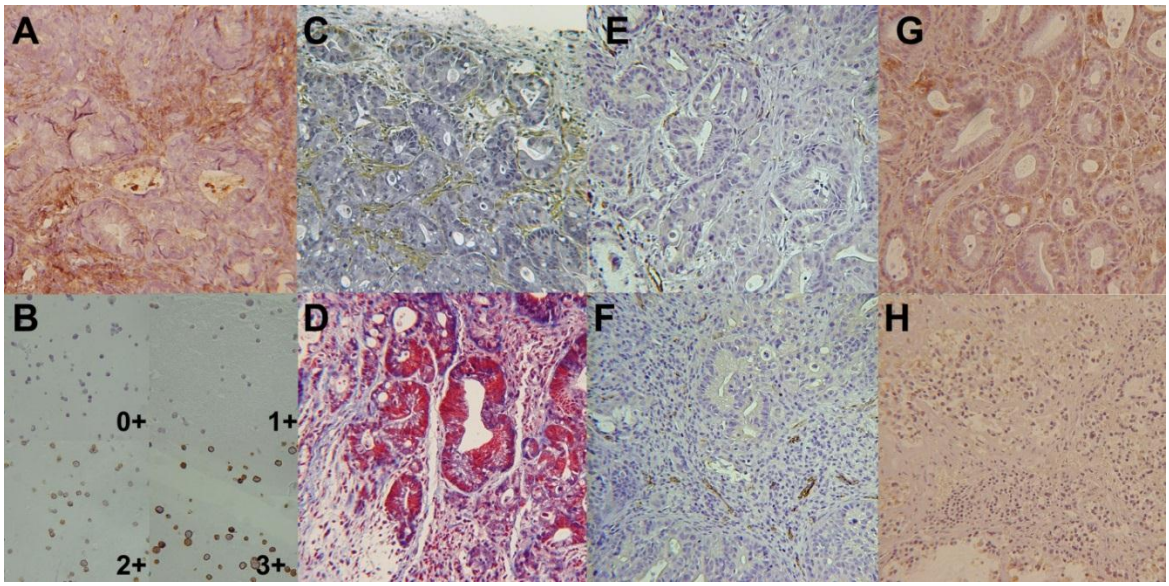

Figure 3.6. Immunohistochemistry of CAPAN1 tumors. A) HER2 staining. B) HER2 expression scale 2+ and 3+ considered high expression. C) Smooth muscle actin (SMA) reddish brown color. Expressed in desmoplasia of pancreatic tumors. D) Masson's Tri-chrome stain. Blue color is collagen fiber. E) CD31 staining of endothelial cells before hyaluronidase treatment. F) CD31 staining after hyaluronidase treatment showing evidence of vascularization of the tumor beginning to penetrate the tumor. G) Stain for hyaluronic acid (brown) before hyaluronidase treatment. H) Stain for hyaluronic acid (brown) after treatment. Also shows a breakdown of the normal organized structure or stromal collapse.

or dense extracellular matrix are exhibited by expression of collagen, smooth muscle actin, hyaluronic acid (HA) and an overall dense interstitial tissue between pancreatic ductal adenocarcinoma cell (PDAC) formations[4]. The excised xenograft CAPAN1 tumors from this study demonstrate a similar response when examined by immunohistochemistry (*Figure 3.6A*). High levels of HA have been associated with increased IFP which prevents diffusion of drugs into the tumor for anticancer therapy[4,31,43]. *Figure 3.6B* demonstrates evidence of the stromal barrier breakdown after intratumoral injections of hyaluronidase. The organized ductal formations were absent and decreased HA levels were observed by immunohistochemistry after treatment with hyaluronidase (*Figure 3.6B*). The dense interstitial tissue was also reduced in severity (*Figure 3.6B*). Increased levels of CD31 expression in the outer layers of the tumor shown in *Figure 3.6C* may also be evidence of initial tumor remodeling and neovascular penetration of the hyaluronidase treated tumors.

3.3.6. Biodistribution of targeted HPMA copolymer-conjugates

Biodistribution studies were conducted which compared the overall effects of both targeting and tumor stromal barrier breakdown. *Figure 3.7* shows the comparison of targeted conjugates against controls with and without hyaluronidase treatment. Overall differences in nontargeted organ uptake were similar except in the case of KYLCSC containing conjugates which showed increased uptake in the kidney, and increased uptake in the spleen and liver was observed with RGDfK-containing HPMA copolymer conjugates (*Figure 3.7A-B*). The increase in tumor concentrations of targeted conjugates and nontargeted conjugates of hyaluronidase treatments can also be observed in *Figure 3.7C-D*.

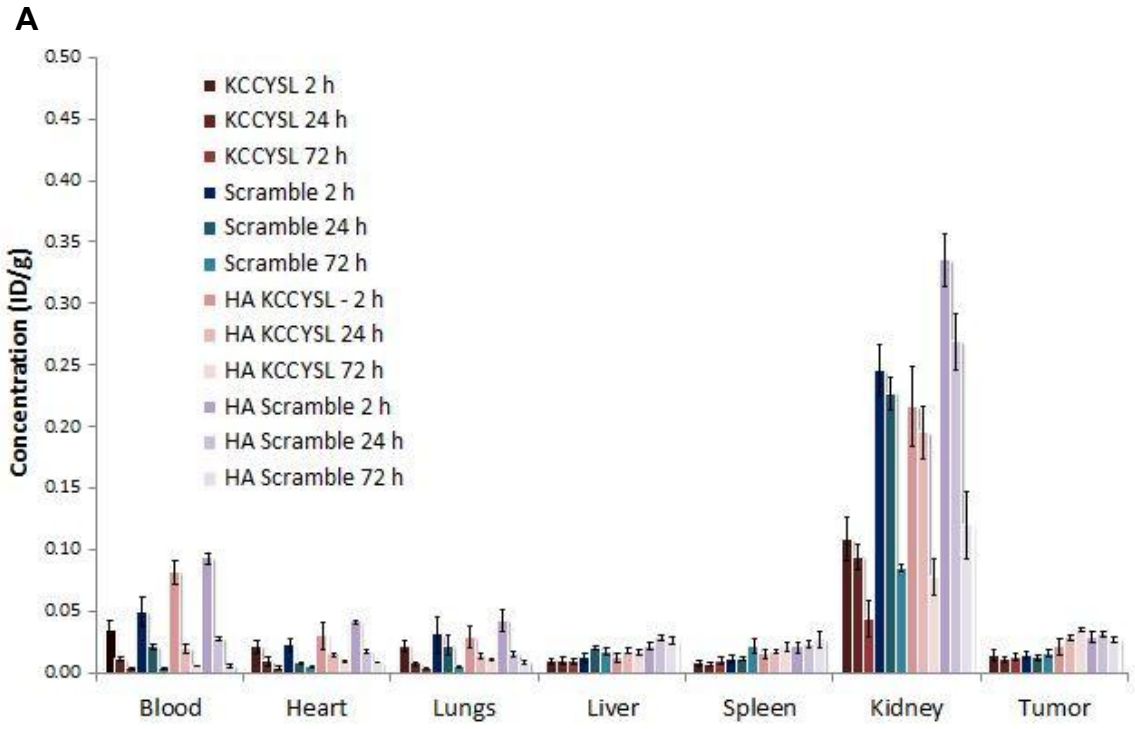

Figure 3.7. A) Biodistribution of HPMA copolymer conjugates. Comparison of HER2 targeted conjugates before and after hyaluronidase (HA) treatment. Data are represented as the mean ± SEM of n=3 for organs and n=6 for tumors. B)Comparison of integrin targeted conjugates before and after HA treatment. Data are represented as the mean ± SEM of n=3 for organs and n=6 for tumors. C) Bar graph showing statistical significance at 72 h postinjection between HER2 targeted conjugate and controls before and after HA treatment. Data are represented as the mean ± SEM of n=6. Stastical significance determined using one-way ANOVA. D) Bar graph showing the statistical significance at 72 h postinjection between integrin targeted conjugate and controls before and after HA treatment. Data are represented as the mean ± SEM of n=6. Stastical significance determined using one-way ANOVA.

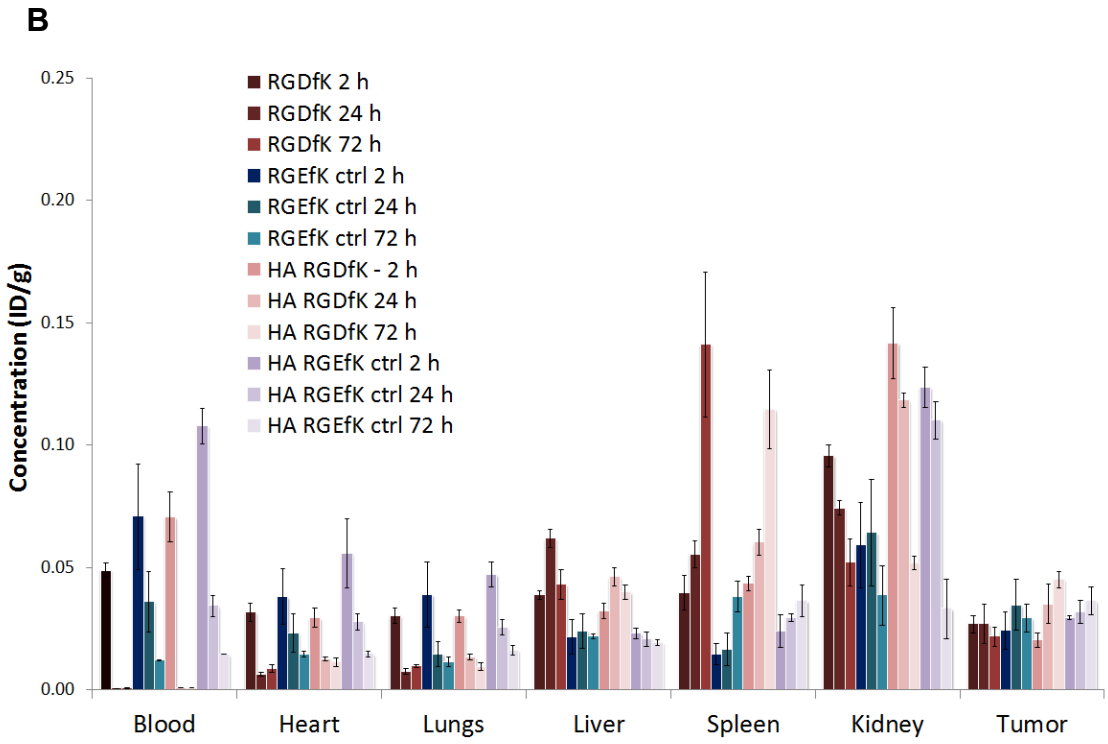

Figure 3.7. Continued

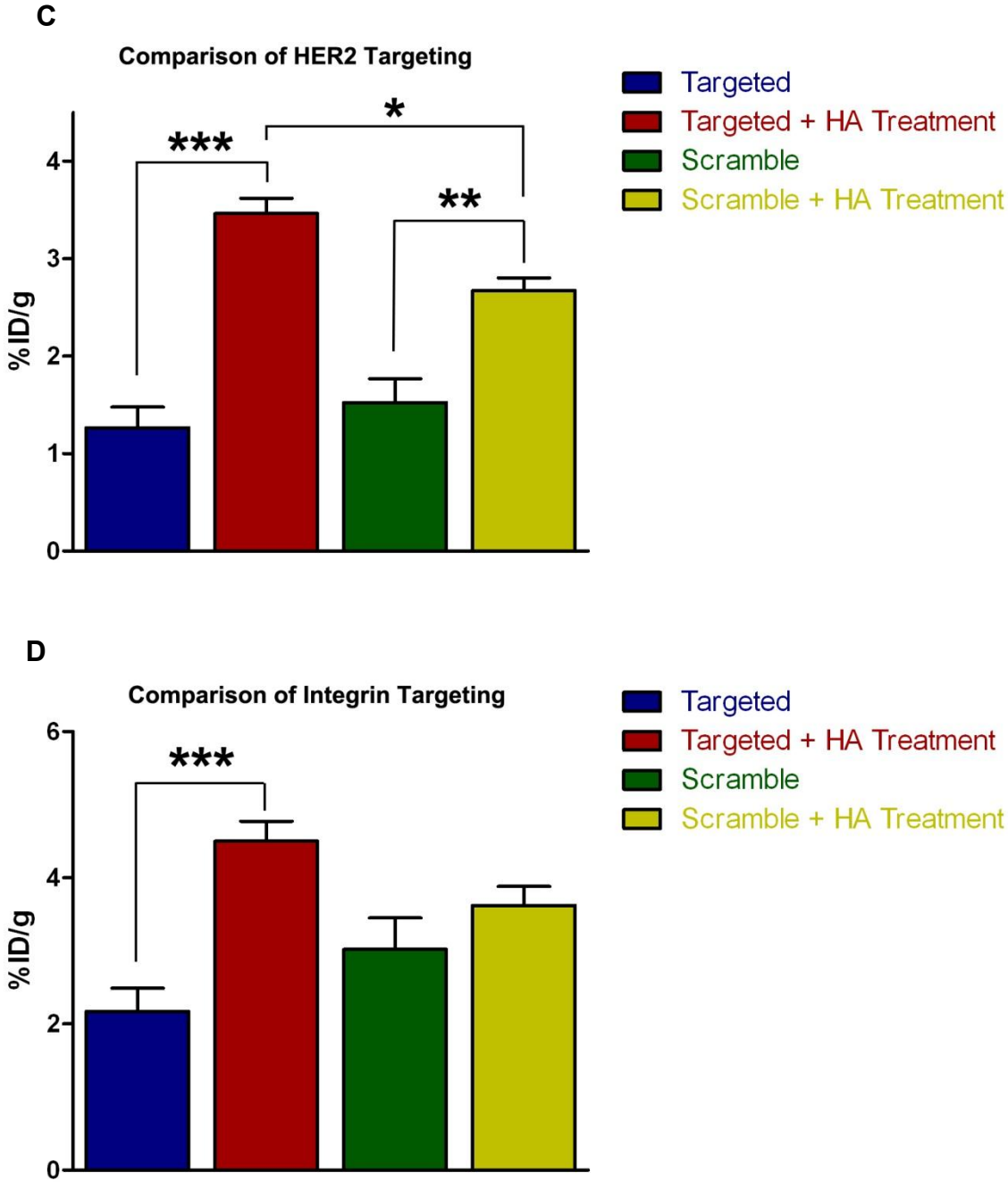

Figure 3.7. Continued

3.3.7. SPECT imaging of targeted HPMA copolymer conjugates

SPECT images revealed the overall fate of all conjugates studied overtime and support the necropsy biodistribution data (*Figure 3.8-3.9*). Clear evidence is shown in *Figure 3.9* of the overall increase of targeted polymer accumulation after the hyaluronidase treatment. The images also demonstrate the measureable increased accumulation due to targeting ligand on the HPMA copolymer backbone within the tumor and the overall accumulation of conjugates in other organs and tissues with respect to time.

3.4. Discussion

The goal of this study was to compare two strategies using macromolecular water-soluble HPMA copolymers for pancreatic tumor targeting. This study, as well as others, demonstrates that penetration is markedly decreased in pancreatic tumors because of the dense extracellular matrix surrounding the tumor cells[29,33]. Hyaluronic acid was selected as the target for stromal barrier breakdown, since previous work showed that increased IFP exhibited by dense hyaluronic acid within pancreatic tumors limits the penetration and diffusion of small molecule drugs[43]. Passive targeting exhibited by the EPR effect is suppressed by increased IFP[44,45]. By breaking down the hyaluronic acid, the IFP is decreased, thereby allowing for higher diffusion rates and penetration within the tumor and augmenting the EPR effect. The hyaluronidase treatment used by Provenzano utilized a PEGylated version of hyaluronidase for intravenous administration which increases stability of the enzyme in the blood stream and sufficient active enzyme activity within the tumor[4]. However, in these studies, hyaluronidase, was injected directly into the tumor in order to assure sufficient active enzyme reached the hyaluronic acid containing tumors.

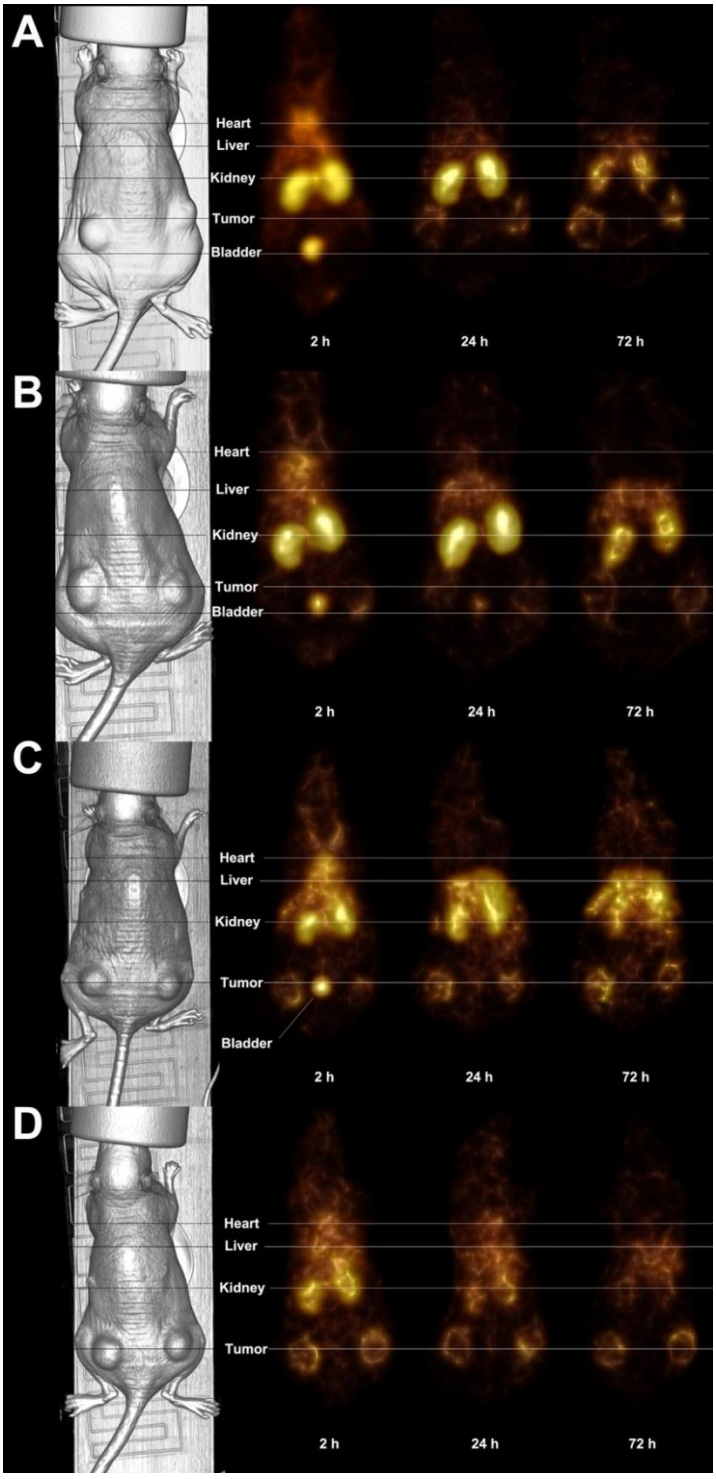

Figure 3.8. SPECT/CT imaging of conjugates treated with hyaluronidase. A) HPMA-KCCYSL-^{111}InDTPA. B) HPMA-KYLCSC-^{111}InDTPA. C) HPMA-RGDfK-^{111}InDTPA. D) HPMA-RGEfK-^{111}InDTPA. SPECT demonstrates the overall biodistribtion of the HPMA-conjugates over time. Targeted conjugates had an increasing concentration in tumors over time where nontargeted conjugates decreased or reduced in concentration with respect to time.

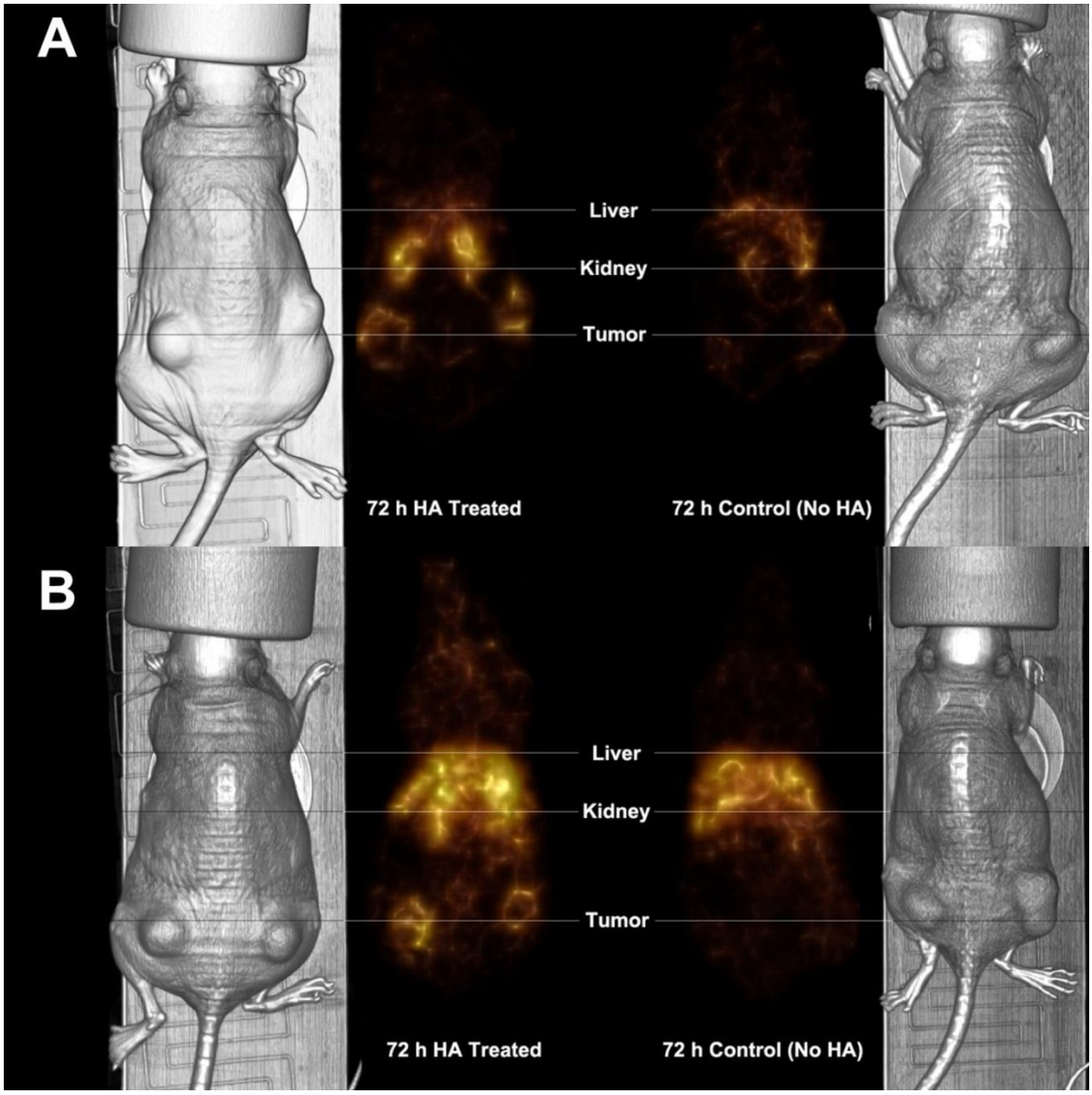

Figure 3.9. SPECT/CT images comparing hyaluronidase effects. SPECT images demonstrating the increase in tumor accumulation after treating with hyaluronidase. A) Comparison of tumor localization based on KCCYSL or HER2 targeting conjugate at 72 h postinjection. B) Comparison of tumor localization based on RGDfK or $\alpha_v\beta_3$ integrin targeting conjugates at 72 h postinjection.

Immunohistochemistry results provide evidence of both the presence of desmoplasia and stromal barrier breakdown. In this study, treatment with hyaluronic acid before administration of HPMA copolymer-targeted conjugates increased their overall accumulation in the tumor regardless of targeting ligand. This suggests that the xenograft tumor model used in the study still exhibits some of the desmoplastic properties of pancreatic cancer found in the clinical setting. Once the conjugates have entered the tumor region after stromal barrier breakdown, the active targeting ligands can interact with their receptors and effectively "stick" to their targeted sites within the tumor. Nontargeted conjugates were also found to increase in concentration in the tumor. This may be entirely because of the augmented EPR effect due to the lower IFP within the tumor. However, increases in diffusion rates in the tumor may cause the nontargeted HPMA copolymer conjugates to be flushed out of the tumor because they lack the ability to bind receptors within the tumor region. This idea is supported by the fact that no differences between targeted and nontargeted conjugates were found between targeted HPMA conjugates and their controls unless the barriers to diffusion were removed.

Previous experience with HPMA copolymer-RGDfK conjugates have shown active targeting potential or increased localization in many tumor types due to the increased expression of $\alpha_v\beta_3$ integrin related to angiogenesis[13,14,18]. However, it is known that pancreatic tumors have low vascularity when compared to other tumor types. Therefore, a second strategy utilizing HER2 targeting was selected based on its potential for a targeting strategy independent of the angiogenesis process. HER2 targeting is promising not only because of its overexpression in pancreatic tumors but other tumor types as well[46].

It appears that the HER2 strategy is superior to that of the integrin targeting strategy based on several observations. First, after hyaluronidase treatment, the HPMA copolymer-KCCYSL-DTPA conjugate was significantly different than its control at 72 h postinjection (*Figure 3.7C*). There was also no significant uptake in other nontargeted organs, suggesting that HER2 is a good strategy for targeting pancreatic tumors once the stromal barrier to macromolecular delivery is removed. The $\alpha_v\beta_3$ integrin targeted HPMA copolymer-RGDfK-DTPA shows a similar trend in increased accumulation in the tumor after hyaluronidase treatment but was not significantly different than controls (*Figure 3.7D*). This may be due to the fact that much of the HPMA copolymer-RGDfK-DTPA is rapidly cleared from the blood stream by the liver and the spleen between 2-24 h, therefore limiting the amount of polymer that can accumulate in the tumor when compared to the other conjugates (*Figure 3.7B*). The HPMA copolymer-RGDfK-DTPA is clearly being removed from the blood stream by the reticuloendothelial system.

The imaging modality used in the study is convenient because clinically used radionuclides with relatively long half-lives that match the biological half-life of HPMA copolymers are readily available. However, positron emission tomography (PET) imaging can provide much more quantitative and accurate imaging results than that of SPECT[47]. Several groups have recently started to investigate HPMA copolymers radiolabeled with PET isotopes[48-50]. However, the wide use of PET for HPMA copolymer imaging is limited due to the majority of clinically available positron emitting radionuclides having shorter half-lives which do not provide imaging information long enough to match the biological half-life of HPMA copolymer conjugates. A few isotope-producing facilities have the capabilities to produce longer lived isotopes but this lack of wide availability increases the costs, again making wide use logistically difficult. SPECT

imaging is widely used in the clinic for multiple procedures in cardiology, neurology and oncology and suitable in the short-term for development of image-guided delivery approaches.

Breaking stromal barriers for the delivery of macromolecular therapeutics provides a promising direction for targeted cancer therapy. Hyaluronidase is currently not the only stroma treating agent being investigated[33]. Recently, Abraxane® has been in clinical trials in conjunction with gemcitabine for pancreatic cancer treatment and has shown to cause stromal collapse and therefore increased drug accumulation in the tumor[51]. Hedgehog signal inhibitors can also influence the pancreatic stroma and have demonstrated increased drug accumulation[52]. These stromal treating agents have promise with increasing the concentration of macromolecular conjugates including targeted HPMA copolymers to pancreatic cancers and can be investigated in the near future. However, stromal disruption in tumors could also be detrimental. Breaking down the stroma potentially may lead to increased metastasis based on the fact that tumor cells rely on the stroma for their support structure. However, in the case of a hedgehog pathway inhibitor related to stromal treatment, metastasis was reduced in an orthotopic xenograft metastatic mouse model[53]. More in-depth studies related to increased metastasis must be conducted to understand the risks of treating the stroma with various antistromal agents.

3.5. Conclusion

This study demonstrates that pancreatic cancer targeting can be improved by macromolecular carriers such as HPMA copolymers when the dense stromal barrier is removed. It is further demonstrated that active targeting using the KCCYSL ligand increased tumor localization over time when hyaluronidase was used. Targeted HPMA

copolymers take advantage of passive accumulation to the tumor via the EPR effect which is augmented when stromal barriers are removed such as high intratumoral fluidic pressure. Further, HPMA copolymers complexed with radionuclides can be imaged for biodistribution. The imaging information can be utilized for predicting therapeutic delivery of a companion HPMA copolymer-drug conjugate. Antistromal agents have the potential to enhance efficacy of pancreatic cancer treatment. This strategy may open the door for enhanced delivery of polymer therapeutics.

3.6. References

1. American Cancer Society. Cancer Facts and Figures 2012. Atlanta, GA: American Cancer Society; 2012.

2. Hidalgo M. Pancreatic cancer. N Engl J Med. 2010; 362:1605-1617.

3. Hidalgo M. New insights into pancreatic cancer biology. Ann Oncol. 2012; 23 Suppl 10:x135-138.

4. Provenzano PP, Cuevas C, Chang AE, Goel VK, Von Hoff DD, Hingorani SR. Enzymatic targeting of the stroma ablates physical barriers to treatment of pancreatic ductal adenocarcinoma. Cancer Cell. 2012; 21:418-429.

5. Kopecek J, Kopeckova P. HPMA copolymers: origins, early developments, present, and future. Adv Drug Deliv Rev. 2010; 62:122-149.

6. Kopecek J. Polymer-drug conjugates: origins, progress to date and future directions. Adv Drug Deliv Rev. 2013; 65:49-59.

7. Noguchi Y, Wu J, Duncan R, et al. Early phase tumor accumulation of macromolecules: a great difference in clearance rate between tumor and normal tissues. Jpn J Cancer Res. 1998; 89:307-314.

8. Kopecek J, Kopeckova P, Minko T, Lu ZR, Peterson CM. Water soluble polymers in tumor targeted delivery. J Control Release. 2001; 74:147-158.

9. Larson N, Ray A, Malugin A, Pike DB, Ghandehari H. HPMA copolymer-aminohexylgeldanamycin conjugates targeting cell surface expressed GRP78 in prostate cancer. Pharm Res. 2010; 27:2683-2693.

10. Johnson RN, Kopeckova P, Kopecek J. Synthesis and evaluation of multivalent branched HPMA copolymer-Fab' conjugates targeted to the B-cell antigen CD20. Bioconjug Chem. 2009; 20:129-137.

11. Luo Y, Bernshaw NJ, Lu ZR, Kopecek J, Prestwich GD. Targeted delivery of doxorubicin by HPMA copolymer-hyaluronan bioconjugates. Pharm Res. 2002; 19:396-402.

12. Kopansky E, Shamay Y, David A. Peptide-directed HPMA copolymer-doxorubicin conjugates as targeted therapeutics for colorectal cancer. J Drug Target. 2011; 19:933-943.

13. Ray A, Larson N, Pike DB, et al. Comparison of active and passive targeting of docetaxel for prostate cancer therapy by HPMA copolymer-RGDfK conjugates. Mol Pharm. 2011; 8:1090-1099.

14. Greish K, Ray A, Bauer H, et al. Anticancer and antiangiogenic activity of HPMA copolymer-aminohexylgeldanamycin-RGDfK conjugates for prostate cancer therapy. J Control Release. 2011; 151:263-270.

15. Borgman MP, Aras O, Geyser-Stoops S, Sausville EA, Ghandehari H. Biodistribution of HPMA copolymer-aminohexylgeldanamycin-RGDfK conjugates for prostate cancer drug delivery. Mol Pharm. 2009; 6:1836-1847.

16. Zarabi B, Borgman MP, Zhuo J, Gullapalli R, Ghandehari H. Noninvasive monitoring of HPMA copolymer-RGDfK conjugates by magnetic resonance imaging. Pharm Res. 2009; 26:1121-1129.

17. Borgman MP, Coleman T, Kolhatkar RB, Geyser-Stoops S, Line BR, Ghandehari H. Tumor-targeted HPMA copolymer-(RGDfK)-(CHX-A"-DTPA) conjugates show increased kidney accumulation. J Control Release. 2008; 132:193-199.

18. Pike DB, Ghandehari H. HPMA copolymer-cyclic RGD conjugates for tumor targeting. Adv Drug Deliv Rev. 2010; 62:167-183.

19. Marchan S, Perez-Torras S, Vidal A, et al. Dual effects of beta3 integrin subunit expression on human pancreatic cancer models. Cell Oncol (Dordr). 2011; 34:393-405.

20. Cayrol C, Bertrand C, Kowalski-Chauvel A, et al. alphav integrin: a new gastrin target in human pancreatic cancer cells. World J Gastroenterol. 2011; 17:4488-4495.

21. Hosotani R, Kawaguchi M, Masui T, et al. Expression of integrin alphaVbeta3 in pancreatic carcinoma: relation to MMP-2 activation and lymph node metastasis. Pancreas. 2002; 25:e30-35.

22. Korc M. Pathways for aberrant angiogenesis in pancreatic cancer. Mol Cancer. 2003; 2:8.

23. Komoto M, Nakata B, Amano R, et al. HER2 overexpression correlates with survival after curative resection of pancreatic cancer. Cancer Sci. 2009; 100:1243-1247.

24. Huang ZQ, Buchsbaum DJ. Monoclonal antibodies in the treatment of pancreatic cancer. Immunotherapy. 2009; 1:223-229.

25. Safran H, Iannitti D, Ramanathan R, et al. Herceptin and gemcitabine for metastatic pancreatic cancers that overexpress HER-2/neu. Cancer Invest. 2004; 22:706-712.

26. Safran H, Steinhoff M, Mangray S, et al. Overexpression of the HER-2/neu oncogene in pancreatic adenocarcinoma. Am J Clin Oncol. 2001; 24:496-499.

27. Karasseva NG, Glinsky VV, Chen NX, Komatireddy R, Quinn TP. Identification and characterization of peptides that bind human ErbB-2 selected from a bacteriophage display library. J Protein Chem. 2002; 21:287-296.

28. Neesse A, Michl P, Frese KK, et al. Stromal biology and therapy in pancreatic cancer. Gut. 2011; 60:861-868.

29. Merika EE, Syrigos KN, Saif MW. Desmoplasia in pancreatic cancer. Can we fight it? Gastroenterol Res Pract. 2012; 2012:781765.

30. Stylianopoulos T, Wong C, Bawendi MG, Jain RK, Fukumura D. Multistage nanoparticles for improved delivery into tumor tissue. Methods Enzymol. 2012; 508:109-130.

31. Nugent LJ, Jain RK. Plasma pharmacokinetics and interstitial diffusion of macromolecules in a capillary bed. Am J Physiol. 1984; 246:H129-137.

32. Boucher Y, Jain RK. Microvascular pressure is the principal driving force for interstitial hypertension in solid tumors: implications for vascular collapse. Cancer Res. 1992; 52:5110-5114.

33. Garber K. Stromal depletion goes on trial in pancreatic cancer. J Natl Cancer Inst. 2010; 102:448-450.

34. Thompson CB, Shepard HM, O'Connor PM, et al. Enzymatic depletion of tumor hyaluronan induces antitumor responses in preclinical animal models. Mol Cancer Ther. 2010; 9:3052-3064.

35. Jacobetz MA, Chan DS, Neesse A, et al. Hyaluronan impairs vascular function and drug delivery in a mouse model of pancreatic cancer. Gut. 2013; 62:112-120.

36. Strohalm J, Kopecek J. Poly *N*-(2-hydroxypropyl) methacrylamide: 4. Heterogenous polymerization. Angewandte Makromolekulare Chemie. 1978; 70:109-118.

37. Subr V, Ulbrich K. Synthesis and properties of new *N*-(2-hydroxypropyl)-methacrylamide copolymers containing thiazolidine-2-thione reactive groups. React Funct Polym. 2006; 66:1525-1538.

38. Mitra A, Nan A, Papadimitriou JC, Ghandehari H, Line BR. Polymer-peptide conjugates for angiogenesis targeted tumor radiotherapy. Nucl Med Biol. 2006; 33:43-52.

39. Mitra A, Coleman T, Borgman M, Nan A, Ghandehari H, Line BR. Polymeric conjugates of mono- and bi-cyclic alphaVbeta3 binding peptides for tumor targeting. J Control Release. 2006; 114:175-183.

40. Kimura K, Sawada T, Komatsu M, et al. Antitumor effect of trastuzumab for pancreatic cancer with high HER-2 expression and enhancement of effect by combined therapy with gemcitabine. Clin Cancer Res. 2006; 12:4925-4932.

41. Brennan PJ, Kumagai T, Berezov A, Murali R, Greene MI. HER2/neu: mechanisms of dimerization/oligomerization. Oncogene. 2000; 19:6093-6101.

42. Maecke HR, Riesen A, Ritter W. The molecular structure of indium-DTPA. J Nucl Med. 1989; 30:1235-1239.

43. Brekken C, de Lange Davies C. Hyaluronidase reduces the interstitial fluid pressure in solid tumours in a non-linear concentration-dependent manner. Cancer Lett. 1998; 131:65-70.

44. Baxter LT, Jain RK. Transport of fluid and macromolecules in tumors. I. Role of interstitial pressure and convection. Microvasc Res. 1989; 37:77-104.

45. Boucher Y, Baxter LT, Jain RK. Interstitial pressure gradients in tissue-isolated and subcutaneous tumors: implications for therapy. Cancer Res. 1990; 50:4478-4484.

46. Tai W, Mahato R, Cheng K. The role of HER2 in cancer therapy and targeted drug delivery. J Control Release. 2010; 146:264-275.

47. Bailey DL. Positron emission tomography : basic sciences. New York: Springer, 2005.

48. Herth MM, Barz M, Jahn M, Zentel R, Rosch F. 72/74As-labeling of HPMA based polymers for long-term in vivo PET imaging. Bioorg Med Chem Lett. 2010; 20:5454-5458.

49. Yuan J, Zhang H, Kaur H, Oupicky D, Peng F. Synthesis and Characterization of Theranostic Poly(HPMA)-c(RGDyK)-DOTA-64Cu Copolymer Targeting Tumor Angiogenesis: Tumor Localization Visualized by Positron Emission Tomography. Mol Imaging. 2012; 12:203-212.

50. Herth MM, Barz M, Moderegger D, et al. Radioactive labeling of defined HPMA-based polymeric structures using [18F]FETos for in vivo imaging by positron emission tomography. Biomacromolecules. 2009; 10:1697-1703.

51. Von Hoff DD, Ramanathan RK, Borad MJ, et al. Gemcitabine plus nab-paclitaxel is an active regimen in patients with advanced pancreatic cancer: a phase I/II trial. J Clin Oncol. 2011; 29:4548-4554.

52. Olive KP, Jacobetz MA, Davidson CJ, et al. Inhibition of Hedgehog signaling enhances delivery of chemotherapy in a mouse model of pancreatic cancer. Science. 2009; 324:1457-1461.

53. Feldmann G, Fendrich V, McGovern K, et al. An orally bioavailable small-molecule inhibitor of Hedgehog signaling inhibits tumor initiation and metastasis in pancreatic cancer. Mol Cancer Ther. 2008; 7:2725-2735.

CHAPTER 4

IN VITRO EVALUATION OF HER2 TARGETED HPMA-COPOLYMERS FOR IMAGE-GUIDED DRUG DELIVERY IN PANCREATIC CANCER*

4.1. Introduction

Successful treatment of pancreatic cancer is in dire need of improvement. Patients have the abysmal prospect when diagnosed based on the current 5-year survival rate of only 6%[1]. Not only is there a low probability of survival but incidence rates have been increasing by 1.5% since 2004[1]. Many of the current therapies for the treatment of pancreatic cancer are designed as a one-size-fits-all approach. However, heterogeneity of the cancer patient population, tumor type, origin and microenvironment contribute to differences in response to any particular therapy. There remains a need to predict and assess therapies administered to patients in real-time and provide information of the potential efficacy and safety of drug conjugates. Advanced knowledge of a potentially successful treatment will provide better efficiency, efficacy and safety for anticancer drug therapies, thus individualizing treatment for each patient.

* Buckway B, Wang Y, Ray A, Ghandehari H. In vitro evaluation of HPMA-copolymers targeted to HER2 expressing pancreatic tumor cells for image guided drug delivery Macromol Biosci. (2013); Accepted.

One approach for accomplishing individualized medicine is to use image-guided drug delivery (IGDD). Imaging is being incorporated into cancer treatment at an ever growing rate[2]. It has the capability of providing clinicians information for diagnosis and potentially selecting a particular therapy based on the imaging results. This approach has been used in the clinic to improve cancer therapy. One example is the use of radioimmunotherapy for B-cell lymphomas such as Bexxar® and Zevalin®[3]. This radioimmunotherapy includes a two-part system. First, a patient is given an imaging version of the labeled CD-20 targeted antibody and imaged by gamma camera. Depending on the biodistribution data acquired, the patient is then qualified for the therapeutic radiolabeled antibody based on safety parameters defined in the imaging version. A similar approach can be used for drug conjugates. A multifunctional carrier that can carry both an imaging agent and a drug can be combined to provide both diagnostics and therapeutics in one carrier. This allows for real-time assessment of drug safety and potential efficacy.[4-7] Systems based on this technology can be of particular use for clinicians in selecting patients for anticancer therapies.

Macromolecular water soluble polymers such as *N*-(2-hydroxypropyl)-methacrylamide (HPMA) copolymers are known to increase the solubility of many hydrophobic drugs and exhibit passive targeting to tumor tissues due to the enhanced permeability and retention (EPR) effect[8,9]. HPMA copolymers are suitable for IGDD due to their biocompatibility, ability to control molecular weight and molecular weight distribution, and incorporation of multifunctional components such as drugs, imaging agents and active targeting ligands. The use of cancer-specific targeting ligands conjugated to the backbone of HPMA copolymers has been shown to increase its localization in the tumor tissue[10].

One potential target for pancreatic cancer that has recently been explored is HER2[11-13]. HER2 is a member of the human epidermal growth factor receptor family of tyrosine kinases. HER2 receptors are overexpressed in many cancer types, including pancreatic cancer. However, there exists a reported range (16-61%) of pancreatic tumors having high expression of HER2[14-18]. Recently, a small peptide ligand KCCYSL was reported to have selective specificity to HER2 receptors overexpressed in breast cancer tissues confirmed by in vivo imaging techniques[19]. KCCYSL can easily be conjugated to HPMA copolymers in a similar manner as described for other peptide ligands.

In vitro and in vivo imaging of HPMA copolymers has been performed for many studies[20]. Imaging agents such as fluorophores, MRI contrast agents and radionuclides have proven valuable in evaluating the uptake of HPMA copolymer conjugates in tumor cells and localization in animal models[20-23]. Nuclear medicine techniques such as single photon emission computerized tomography (SPECT) and positron emission tomography (PET) are advantageous based on their ability to provide high-resolution and quantifiable images of radionuclide labeled HPMA copolymer distribution in vivo[5]. For example, we have used gamma scintigraphy to monitor the tumor localization of targeted HPMA copolymers in various tumor animal models[5,24,25]. However, these studies were limited to planar gamma scintigraphy techniques which only give information on the localization but cannot be used quantitatively. ^{111}In is an optimal radionuclide to attach to the HPMA copolymers due to its clinical utility and accessibility, and its 2.8 day half-life which is sufficient for monitoring the biodistribution for a few days in vivo by SPECT/CT which can give more accurate and quantitative results.

Gemcitabine is the first line therapy for pancreatic cancer but suffers from poor stability in the blood stream[26]. It is a cytidine analogue and during cell division can

inhibit DNA chain elongation, thus triggering apoptosis[27]. This requires the drug to traverse the blood stream to the tumor site and migrate into the tumor cell for it to be effective. However, it is known that gemcitabine is rapidly metabolized in the blood stream to an inactive product. Another factor limiting gemcitabine efficacy is its dose-limiting toxicity associated with myelosuppression[26]. Gemcitabine delivery to the tumor cell may be improved when incorporated into the side chains of HPMA copolymers *via* a lysosomal degradable linker. Including this drug in the side chains of the copolymer can serve three purposes: First, it can prevent rapid metabolism in the blood stream because the HPMA copolymer can reduce the interactions of the drug with the enzymes responsible for its inactivation. Second, covalently bound gemcitabine can potentially prevent free drug from diffusing into the normal vasculature. This can limit the dose-limiting toxicity and allow for a higher amount of drug to be administered to the patient, thus improving efficacy. Third, site specific release can be achieved by attachment of targeting moieties and degradable spacers. This will ultimately improve the safety and efficacy profile of gemcitabine therapy in the treatment of pancreatic cancer. The goal of this study was to synthesize and characterize HPMA copolymers containing gemcitabine, chelator of $^{111}In^{3+}$, and KCCYSL in the side chains. To our knowledge, this is the first example of an HPMA copolymer simultaneously containing anticancer drug, tumor targeting peptide and imaging agent. A series of experiments were conducted to evaluate the radionuclide stability, drug release and targetability of these systems in vitro.

4.2. Materials and Methods

4.2.1. Chemicals

Gemcitabine HCl was obtained from LC Laboratories (Woburn, MA). Amino acids for peptide synthesis were obtained from AAPPTec (Louisville, KY). *N*-[(*R*)-2-Amino-3-(*p*-isothiocyanatophenyl)propyl]-*trans*-(S,S)-cyclohexane-1,2-diamine-*N,N-N',N',N''N''*-pentaacetic acid (*p*-SCN-CHX-A"-DTPA) was obtained from Macrocyclics (Dallas, TX). *N*-(3-Aminopropyl)methacrylamide hydrochloride (APMA) was acquired from Polysciences (Warrington, PA). 2,2'-Azobis[2-(2-imidazolin-2-yl)propane] dihydrochloride (VA-044) was obtained from Wako Chemicals (Richmond, VA). $^{111}InCl_3$ was obtained from the Intermountain Radiopharmacy (Salt Lake City, UT). All other reagents were of reagent grade and obtained from Sigma-Aldrich (St. Louis, MO).

4.2.2. Synthesis of comonomers

N-(2-hydroxypropyl)methacrylamide comonomer (HPMA) and *N*-methacryloylaminopropyl-2-amino-3-(isothiourea-phenyl)propyl-cyclohexane-1,2-diamine-*N,N-N',N',N'',N''*-pentaacetic acid (APMA-CHX-A"-DTPA) were synthesized according to published methods[28,29] (*Figure 4.1*) with results in Appendix A. The intermediate *N*-methacryloylglycylphenylalanylleucylglycine (MA-GFLG-OH) was synthesized *via* solid phase synthesis. Briefly, amino acids were sequentially added from N-terminus to C-terminus using a typical solid phase synthesis strategy[30]. The final addition involves the coupling of methacrylic acid to the peptide resin employing *O*-Benzotriazole-N,N,N',N'-tetramethyl-uronium-hexafluoro-phosphate (HBTU) as a coupling reagent. The MA-GFLG-OH was removed from the resin by treatment with trifluoroacetic acid in the presence of a polymerization inhibitor, *t*-octyl pyrocatechine.

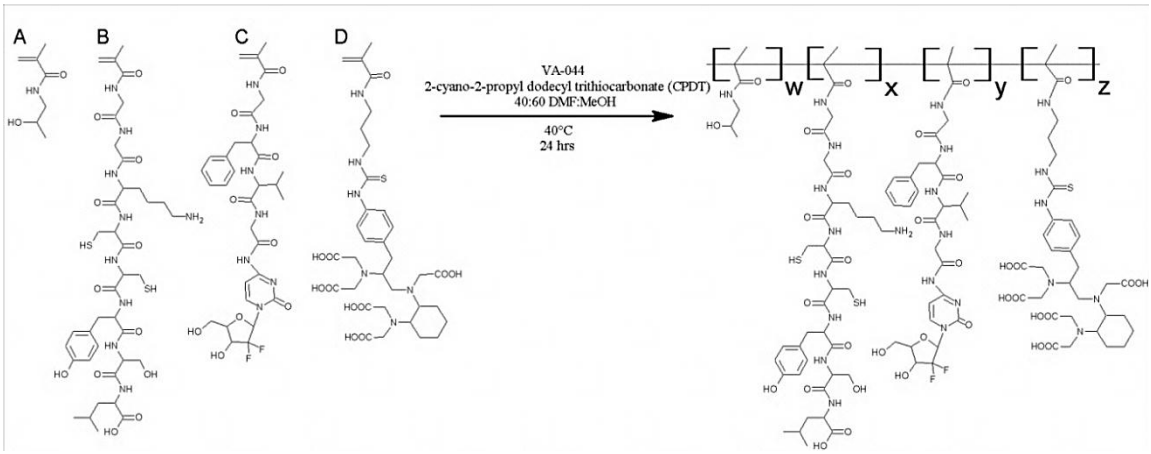

Figure 4.1. Comonomers used for the synthesis of the polymers and RAFT synthesis scheme. A) HPMA comonomer which affords water solubility constituting the main part of the backbone. B) MA-GG-KCCYSL comonomer used for active targeting of HER2 receptors. C) MA-GFLG-Gem comonomer capable of lysosomal release of gemcitabine within the tumor cell. D) APMA-CHX-A"-DTPA comonomer for chelation of $^{111}In^{3+}$ for imaging by SPECT/CT. For RAFT polymerization monomers were kept constant at 1M concentration with a ratio of [300:1:1] monomer:CPDT:VA-044.

MA-GFLG-OH was converted to *N*-methacryloylglycylphenylalanylleucylglycyl-*p*-nitrophenyl ester (MA-GFLG-ONp) according to published methods[31]. The final steps for synthesis of the drug-comonomer *N*-methacryloylglycylphenylalanylleucylglycyl-gemcitabine (MA-GFLG-Gem) were performed by aminolysis of the MA-GFLG-ONp with excess gemcitabine (1:1.5 ratio, respectively). The product was purified by column chromatography (silica gel, eluent: ethylacetate/methanol). The final product was confirmed by electrospray ionization mass spectrometry (ESI-MS) *m/z* calculated for $C_{32}H_{41}F_2N_7O_9$ 705.7062, found 705 $[M]^+$, 727 $[M+Na]^+$. Peptide comonomers *N*-methacryloylglycylglycyllysylcystylcystyltyrylserylleucine (MA-GG-KCCYSL) and *N*-methacryloylglycylgycyllysyltyrylleucylcystylserylcysteine (MA-GG-KYLCSC) were also synthesized *via* solid phase synthesis on a PS3 Peptide Synthesizer (Protein Technologies, Inc., Tucson, AZ) with addition of methacrylic acid as the final peptide residue as described above in the MA-GFLG-OH synthesis. Both products were confirmed by ESI-MS *m/z* calculated for $C_{38}H_{59}N_9O_{12}S_2$, 898.0582, found 898.3 $[M]^+$.

4.2.3. Polymerization of HPMA conjugates

Copolymerization was performed using the reversible addition-fragmentation chain transfer (RAFT) method in order to control the size and polydispersity[32]. Briefly, HPMA comonomer, MA-GFLG-Gem, MA-GG-KCCYSL (or MA-GG-KYLCSC for control) and APMA-CHX-A"-DTPA comonomers were combined with the initiator VA-044 and the chain transfer agent 2-cyano-2-propyl dodecyl trithiocarbonate (CPDT) in 40/60 DMF/methanol in a nitrogen-purged sealed glass ampule (*Figure 4.1*). The feed ratio of comonomers were kept constant at 83:10:5:2 (mol%), respectively. Pilot batches were synthesized in order to determine the optimal polymerization ratios of monomer,

CPDT and VA-044. Ultimately, a ratio of [300:1:1] monomers:CPDT:VA-044 with monomer concentration held constant at 1 M provided the desired results. The ampule was placed in a 40^{o}C oil bath for 24 h, after which the resulting polymer was collected by precipitation and washed with diethyl ether. The resulting copolymers' average molecular weight (M_w) and polydispersity (M_w/M_n) were estimated by size exclusion chromatography (SEC) using a Fast Protein Liquid Chromatography (FPLC) system (GE Healthcare, Piscataway, NJ) equipped with a Superose 12 column calibrated with fractions of known molecular weight HPMA homopolymers. Control conjugates with either the scrambled peptide sequence (KYLCSC), no targeting peptide or no drug were also synthesized in a similar manner.

4.2.4. Characterization of gemcitabine and peptide contents of HPMA copolymer conjugates

Gemcitabine content of the conjugates was determined by enzymatic release of free drug from the HPMA copolymer backbone as described previously[33]. Treated samples were subjected to HPLC analysis using a mobile phase consisting of deionized water with 1% trifluoroacetic acid (TFA) and acetonitrile (ACN) with 1% TFA according to the following gradient: 0 min, 2% ACN to 90% ACN over 20 min. HPLC analyses were performed with an Agilent Series 1100 HPLC (Agilent Technologies, Wilmington, DE, USA) equipped with an Alltima C18 5 µm 150 x 4.6 mm column and a photo diode array detector. A flow rate of 1.0 ml/min was utilized with an injection volume of 20 µl. UV absorbance of 267 nm was used for quantification of gemcitabine. Peptide content was determined by amino acid analysis performed in the University of Utah Core Research Facilities (Salt Lake City, UT).

4.2.5. Radiolabeling and stability of the conjugates

Each copolymer was dissolved in 400 µl of 1.0 M sodium acetate buffer pH 5.0 and added to 5.0 mCi of $^{111}InCl_3$ stock solution which was also previously treated with 200 µl of 1.0 M sodium acetate buffer pH 5.0. The reaction mixture was heated at 50ºC for 45 min after which 50 µl of 0.05 M EDTA solution was added to scavenge any free ^{111}In ions. The radiolabeled copolymer was then purified using Sephadex G-25 PD-10 columns (GE Life sciences, Piscataway, NJ). Radiostability was evaluated by incubating radiolabeled copolymer at 37ºC in the presence of mouse serum. Samples were collected at 24, 48 and 72 h and a comparison between ^{111}In labeled copolymers and free $^{111}In^{3+}$ was performed by size exclusion chromatography using PD-10 columns. Each fraction was subsequently measured using a Cobra II Auto-gamma-counter (Canberra Industries, Inc., Meriden, CT).

4.2.6. Cell lines

CAPAN-1 pancreatic adenocarcinoma cells (ATCC, Manassas, VA) were cultured in Iscove's Modified Dulbecco's Medium (IMDM) (ATCC, Manassas, VA) supplemented with 20% (v/v) fetal bovine serum (FBS) and 1:100 penicillin/streptomycin at 37ºC in a humidified atmosphere of 5% CO_2 (v/v). PANC-1 pancreatic duct carcinoma cells (ATCC, Manassas, VA) were cultured in Dulbecco's Modified Medium (DMM) (ATCC, Manassas, VA) supplemented with 10% FBS at 37ºC in a humidified atmosphere of 5% CO_2 (v/v). For all experimental procedures, the confluent cultures were harvested by treatment with TrypLE™ Express (Invitrogen, Grand Island, NY) and subsequent dilution in their respective medium or phosphate buffered saline (PBS).

4.2.7. Relative expression of HER2 by flow cytometry

Anti-HER2 (Neu) and normal mouse IgG_1 (negative control) monoclonal antibodies labeled with phycoerythrin were obtained from Santa Cruz Biotechnology (Santa Cruz, CA). Samples of CAPAN-1 and PANC-1 cells were removed, washed with fresh media followed by PBS and then incubated with antibodies for 30 min at 4°C. Cells were washed with PBS and then fixed in 1% formaldehyde in PBS. Samples were analyzed by flow cytometry using a FACScan System (BD Biosciences, San Jose, CA).

4.2.8. Affinity of KCCYSL-containing copolymers

Copolymers containing KCCYSL in the side chains were assayed by performing an in vitro blocking experiment. CAPAN-1 cells were harvested and resuspended in serum-free IMDM media. Each sample was combined with ^{111}In labeled KCCYSL copolymers and 100 and 1000 fold excess concentrations of free KCCYSL peptide or KYLCSC as control. The samples were incubated at 4ºC for 18 h and then cells were centrifuged and the supernatant removed. The cells were subsequently washed three times with saline until no further activity could be removed from the resulting cell pellet. The resulting cell pellet was then counted using a CAPTUS® 3000 Well Counting System (Capintec, Ramsey, NJ). The percent of HPMA copolymer conjugate bound to the cells relative to control was reported. The assay was conducted in triplicate.

4.2.9. Gemcitabine release in various media

The rate of gemcitabine release in vitro from copolymers was examined in buffer solutions or cell culture media. The release of the drug from copolymers was carried out by dissolving the polymers (3 mg/ml) each in acetate buffer solution (pH 5.0), phosphate

buffered saline (PBS) solution (pH 7.4), Dulbecco's Modified Eagle's Medium (DMEM) with 10% of fetal bovine serum (FBS) and Iscove's Modified Dulbecco's Medium (IMDM) with 20% of fetal bovine serum, respectively. The samples were kept at 37 °C. At scheduled time intervals, 20-60 μl solutions were withdrawn from the samples. Gemcitabine contents were analyzed by HPLC under the same conditions as described above.

4.2.10. Cytotoxicity of conjugates with gemcitabine in the side chains

The in vitro cell growth inhibition of gemcitabine and copolymers was evaluated using a Cell Counting Kit-8 (CCK-8) assay (Donjindo Molecular Technologies, Inc., Rockville, MD). Briefly, PANC-1 and CAPAN-1 cells were seeded into 96-well plates at an initial density of 2000 cells/well and allowed to adhere for 24 h. Stock solutions of free gemcitabine, conjugates and controls were prepared in dimethylsulfoxide (DMSO) and subsequent dilutions were done to a final concentration of 0.5% (v/v) in media. Seeded cells were incubated for 72 h with increasing concentrations of gemcitabine or copolymers in fresh media containing 0.5% (v/v) DMSO. The drug-containing media were removed and incubated in fresh media for another 48 h. The media were removed and 100 μl of medium solution containing 10% CCK-8 reagent was added. The cells were incubated at 37 °C for a further 1-4 h. Cell viability was obtained by scanning with a SpectraMax M2 microplate reader (Molecular Devices, Sunnyvale, CA) at 450 minus 630 nm. Each experiment was performed three times in triplicate.

4.3. Results and Discussion

HPMA copolymer conjugates containing gemcitabine, chelator of $^{111}In^{3+}$, and a HER2 targeting peptide were successfully synthesized by RAFT copolymerization techniques. The design criteria for a potentially translatable and successful IGDD system based on HPMA copolymers are as follows: First, the copolymer must be synthesized in a size-controlled and reproducible manner. Second, the polymer-drug constructs must have a biological half-life that allows enough circulation time in the blood stream in order to allow sufficient time to encounter and accumulate within the diseased tissue. The constructs on the other hand must be eliminated from the kidney in a timely manner in order to reduce background signal in the blood during imaging and reduce the longtime exposure of HPMA copolymer conjugates to nontargeted tissues in the body. Previous studies have shown that HPMA copolymers generally can be filtered through the kidney and excreted in the urine when the M_w is less than 45 kDa[9]. Therefore, the copolymer conjugates were synthesized around a size range of 20-30 kDa (*Table 4.1*). The final criteria needed in a successful IGDD HPMA copolymer system is stability of the drug and imaging components in conditions simulated to the blood stream and site-specific drug release within the targeted tissue. Each of these issues was examined as discussed below. Radiolabeling of the HPMA copolymers with ^{111}In was found to be quite efficient with a decay corrected radiochemical yield of 83.1 $\pm$ 0.2%. Stability was assessed in mouse serum as displayed in *Figure 4.2*. DTPA is known to be a stable chelator of ^{111}In and other radionuclides.[34] No free $^{111}In^{3+}$ was detected from the size exclusion column purifications over the 72 h. The results confirm that chelation with DTPA is stable. The HPMA copolymer-KCCYSL-DTPA conjugates contain the HER2 targeting peptide sequence discovered by Karasseva, et al.[19]. This peptide was included because of its

Table 4.1. Summary of the HPMA copolymer characteristics

Polymer	Monomer Feed Ratio[a] (mol%)	M_w [b] (kDa)	M_n [b] (kDa)	PDI (M_w/M_n)	Expected Peptide Content (wt%)	Measured Peptide Content[c] (wt%)	Expected Gemcitabine Content (wt%)	Measured Gemcitabine Content[d] (wt%)
HPMA-KCCYSL-Gem-DTPA	83:5:10:2	26.8	18.7	1.4	14.3	13.6	6.2	4.7
HPMA-KYLCSC[e]-Gem-DTPA	83:5:10:2	29.9	21.4	1.4	14.3	14.8	6.7	5.4
HPMA-Gem-DTPA	88:10:2	23.6	21.0	1.1	-	-	6.5	5.0
HPMA-KCCYSL-DTPA	93:5:2	20.4	16.8	1.2	18.4	19.9	-	-

[a)]Total monomer concentration 1M for RAFT polymerization at 40ºC for 24 h Solvent = 40:60 Dimethylformamide:Methanol
[b)]Estimated by size exclusion chromatography
[c)]Determined by amino acid analysis
[d)]Determined by enzymatic release followed by HPLC analysis
[e)]KYLCSC is nontargeted scramble peptide sequence

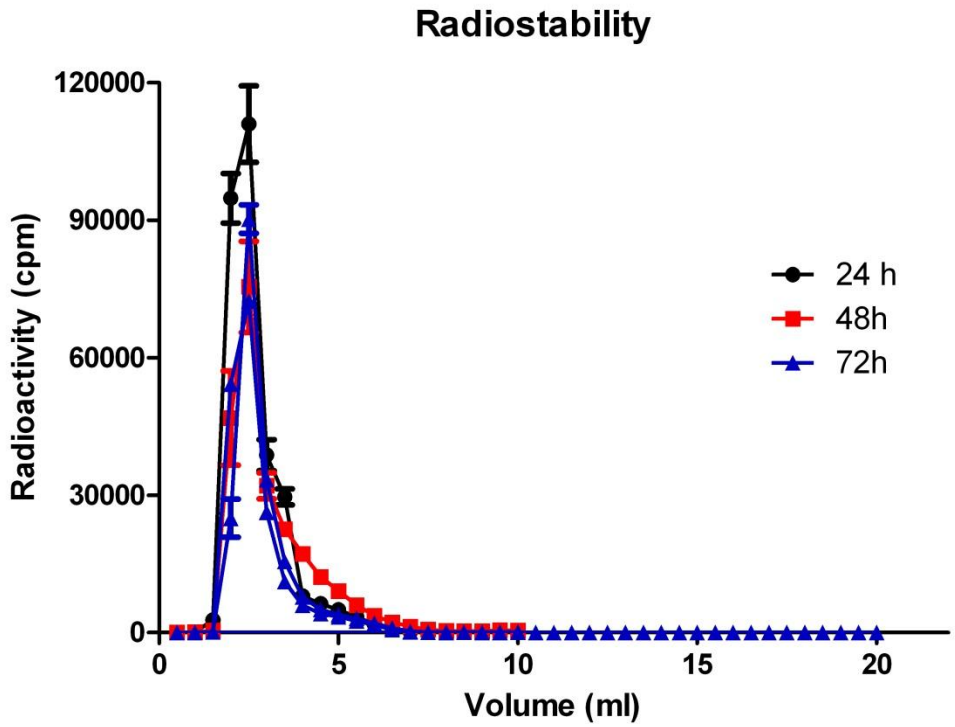

Figure 4.2. Stability of the [111-In] radiolabeled HPMA copolymer conjugate. HPMA copolymers were incubated in the presence of mouse serum for up to 72 h. After SEC purification, each fraction was measured. Each time point was performed in triplicate.

potential in targeting HER2 overexpressed in some tumor types such as pancreatic cancer. Several tumor cell lines have been reported to express different levels of HER2 as investigated by flow cytometry[35]. The results are shown in *Figure 4.3*. PANC-1 and CAPAN-1 were selected for our study based on their tumorogenicity and expression levels of HER2. CAPAN-1 was shown to have a significantly higher expression of HER2 than PANC-1 ($p < 0.001$) and control ($p < 0.0001$), which was consistent with previous reports[35]. No significant difference in HER2 expression was observed between PANC-1 and control antibodies, therefore PANC-1 cell line was used as a negative control for HER2 expression for in vitro assays.

The ability of the KCCYSL-containing HPMA copolymers to bind HER2 expressing cell lines was investigated, because the HPMA copolymer may change or prevent the affinity of the KCCYSL peptide contained on its side chains. No natural ligand is known for HER2 receptors that can be used in a competitive binding assay[36]. Therefore, a blocking experiment was performed where excess free peptide was incubated in the presence of ^{111}In labeled HPMA copolymer-KCCYSL-DTPA conjugates with CAPAN-1 cells in serum free media. *Figure 4.4* shows the results of the blocking study. In summary, binding of the CAPAN-1 cell lines known to express HER2 was effectively blocked when excess peptide was incubated in the presence of HPMA copolymer-KCCYSL-DPTA conjugates. Scramble peptide KYLCSC was used as a control and therefore suggests that the KCCYSL-containing copolymer retains a measurable binding affinity to the HER2 receptor.

Drug release was investigated in complete cell culture media and also in buffered solutions of pH 5.0 and 7.4. Results are shown in *Figure 4.5*. The conjugates were most stable in the low pH 5.0 media which is consistent with an amide bond formed between

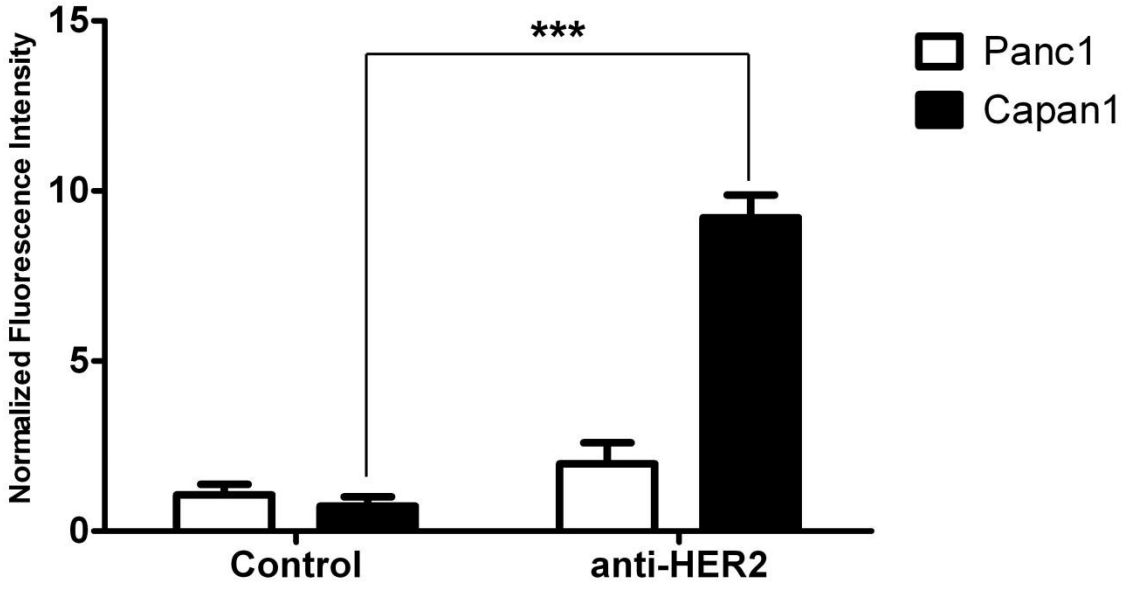

Figure 4.3. Relative expression of HER2 on pancreatic cancer cell lines. Only HER2 expression on CAPAN-1 cell lines showed a significant difference (*** = $p < 0.0001$) than that of control.

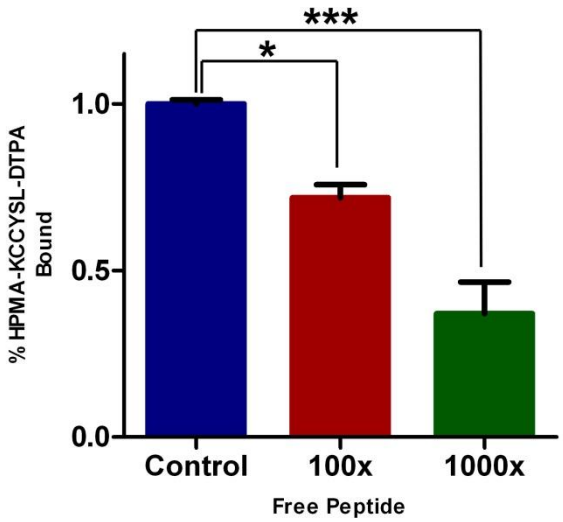

Figure 4.4. Binding affinity of HPMA copolymer-KCCYSL-DTPA conjugate. Control (blue bar) includes 1000 fold excess KYLCSC scramble peptide. Increasing amounts of 100 and 1000 fold excess of free KCCYSL peptide increasingly blocked the binding of HPMA-KCCYSL-DTPA. Data represented as the mean and SEM (n=3). Statistical significance performed using one-way ANOVA with Tukey's posttest (* = $p < 0.01$ and *** = $p < 0.001$).

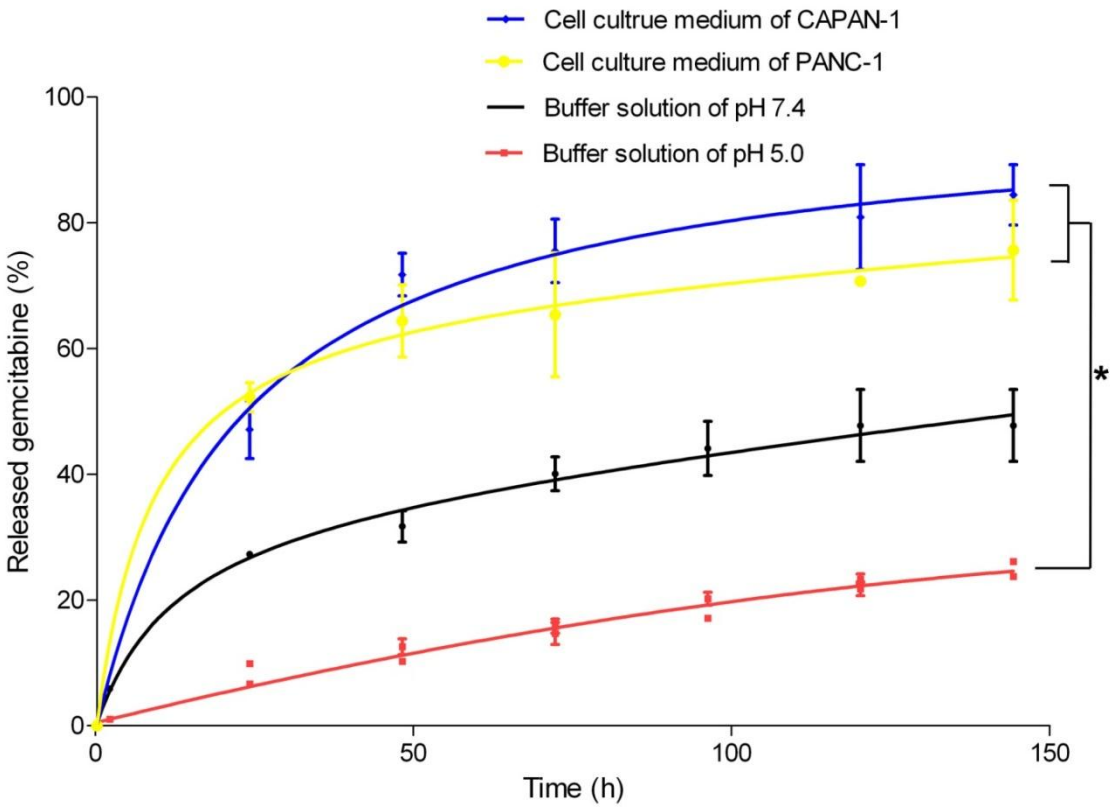

Figure 4.5 Gemcitabine release from the conjugates. Data expressed as the mean and SEM (n=3). Statistical significance performed using 1 way ANOVA with Tukey's post-test. * = $p < 0.01$.

the amide of the pyrimidine ring of gemcitabine and the C terminus of the GFLG linker. However, some drug instability was found in cell culture media. The amide bond may be unexpectedly less stable due to electron delocalization related to the pyrimidine ring of the drug. Another possible explanation for instability of the gemcitabine conjugation is the potential for the ester formation with the 5' OH of the gemcitabine structure. Esters are inherently less stable than amide bonds. It is possible that actually, both bond formations are occurring. Unfortunately, no techniques were currently available to accurately determine the type of bonds being formed. This includes NMR which would not be able to differentiate the differences of the protons on either structure. On another note, the drug released faster in cell culture media than PBS. This is consistent with previously reported results with an HPMA copolymer-docetaxel conjugate containing the same linker[33] and may be because there are various enzymes and proteins in the media. However, the HPMA copolymer-docetaxel conjugates with RGDfK ligands for targeting neovascular tissue demonstrated an enhanced anticancer effect, indicating that future in vivo experiments with targeted HPMA copolymers with gemcitabine may demonstrate a similar result. The stability of the gemcitabine conjugate is sufficient for drug delivery using HPMA copolymers, but perhaps could be improved by development of more stable linker chemistries.

Cytotoxicity of HPMA copolymer constructs was evaluated in both cell lines, including PANC-1 (negative HER2) and CAPAN-1 (positive HER2). Results are shown in *Figure 4.6* and calculated IC_{50} values are displayed in *Table 4.2*. IC_{50} values were consistently in the nM range, similar to results reported previously[35]. However, minor differences were observed between HER2 positive and HER2 negative cell lines, for

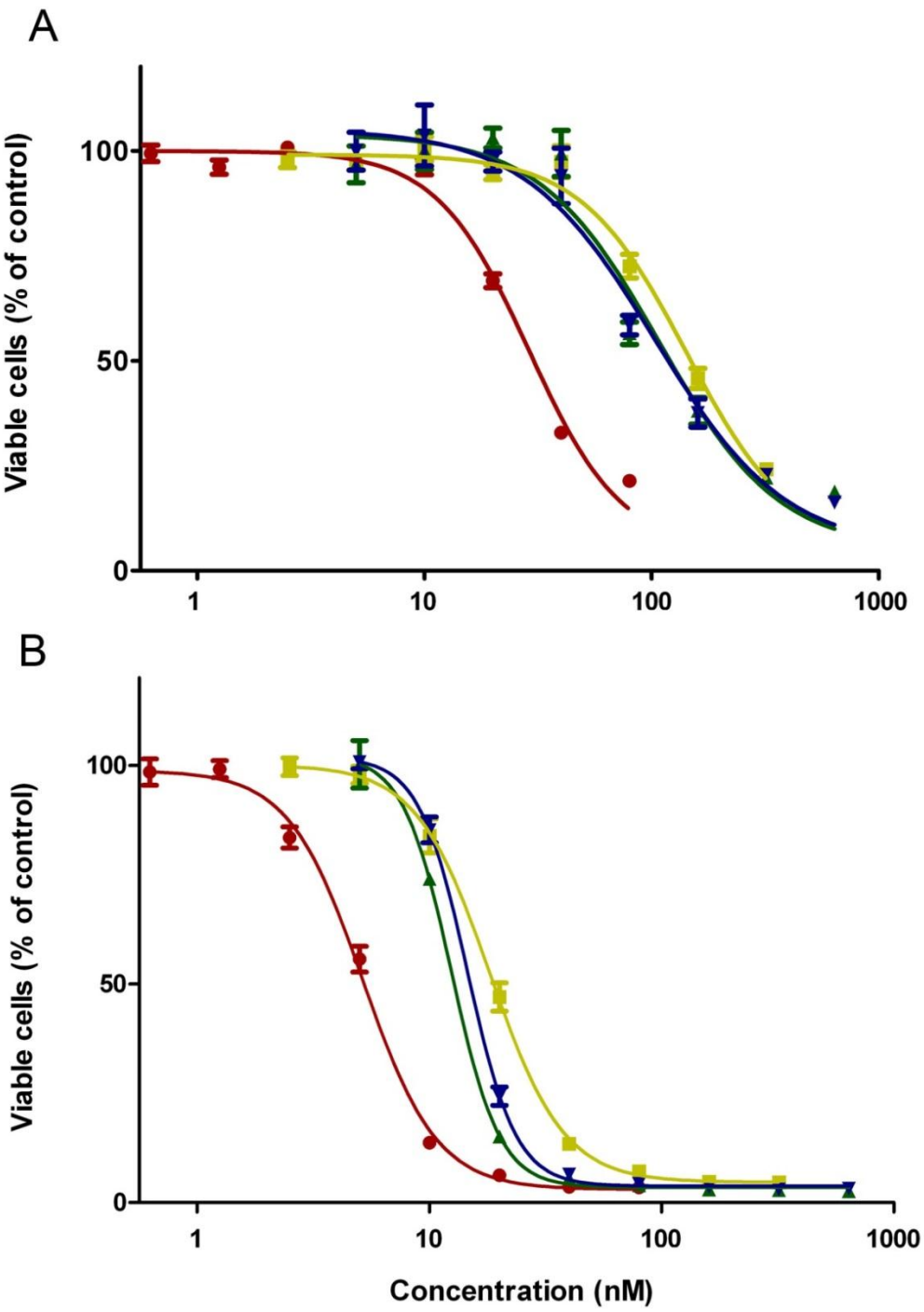

Figure 4.6. Cytotoxicity of HPMA copolymer conjugates containing gemcitabine. A) PANC-1 and B) CAPAN-1 graphs demonstrating the cytotoxicity of each HPMA copolymer species. Red circle is free Gemcitabine. Yellow square is HPMA copolymer-KCCYSL-Gem-DTPA. Green diamond is HPMA copolymer-KYLCSC-Gem-DTPA (scramble). Blue triangle is HPMA copolymer-Gem-DTPA. Data are represented as the mean and SEM (n=9).

Table 4.2. IC_{50} values of HPMA copolymer conjugates in HER2 negative and HER2 positive cell lines. Statistical analysis was performed within each cell line using one way ANOVA with Tukey's posttest. Free drug was statistically different than all three conjugates in both cell lines (*** = $p < 0.001$). HPMA conjugates were not statistically significant from each other.

Polymer	**PANC-1** IC_{50} **(nM)**	**CAPAN-1** IC_{50} **(nM)**
Gemcitabine (Free drug)	28.8***	5.3***
HPMA-KCCYSL-Gem-DTPA	142.0	18.2
HPMA-KYLCSC[a]-Gem-DTPA	108.0	12.4
HPMA-Gem-DTPA	104.0	14.6

[a)]KYLCSC is nontargeted scramble peptide sequence;

reasons that are not entirely clear. Data suggest that HER2 positive cell lines are more sensitive to gemcitabine therapy. Some studies have suggested that overexpression of HER2 in pancreatic cancer patients correlates with poor prognosis[37,38]. Regardless, more in-depth analysis is needed to validate this hypothesis. The results also show a difference between the free drug and the HPMA copolymer species. This is typical of HPMA copolymer-drug conjugates since the free drug enters the cell by passive diffusion compared to endocytosis of the conjugates by the macromolecular system. No significant difference was observed between the KCCYSL and KYLCSC (scrambled) peptides due to the fact that the drug is gradually released in the cell culture media over the 72 h. The available drug activity over this time frame is prolonged and therefore, local concentration of gemcitabine to a tumor cell may be lower, thus explaining the difference between the free drug and the polymer-drug conjugate.

The in vitro results demonstrate that gemcitabine activity is still retained when bound to the HPMA copolymer. However, the drug is gradually released in physiological media. Gemcitabine is rapidly metabolized in the bloodstream, thus losing its anticancer activity. Therefore, high doses must be administered to patients in order to achieve efficacy, but that in turn also increases toxicity such as myelosupression[26]. However, because the drug is released slowly from the conjugates, it should be protected from metabolic enzymes until encountering the tumor in the in vivo situation. Subsequent release once in the tumor environment may increase the local active concentration of gemcitabine, thus providing a potentially more efficacious and safe drug therapy. Active targeting of the drug to tumor cells under study did not show an increased efficacy. Reports in the literature regarding active and passive targeting of drugs are mixed[39]. In the current study, a possible explanation of lack of difference between actively or

passively targeted copolymers in terms of cytotoxicity is the premature release of the drug. Future in vivo studies will need to be conducted to evaluate the value of this targeting strategy in relevant preclinical animal models and perhaps to consider alternative targeting strategies for targeting pancreatic tumors.

4.4. Conclusion

HPMA copolymer–gemcitabine conjugates containing chelator of $^{111}In^{3+}$ and HER2 targeting peptides in the side chain were synthesized in a size and content-controlled manner. The conjugates showed efficacy against pancreatic tumor cell lines. However attachment of the targeting peptides did not improve cytotoxicity. Premature release of the free drug was observed that can in part contribute to cytotoxicity. In vitro radiostability of the ^{111}In complex was sufficient for imaging over a relevant time. These studies have set the stage for further optimization and evaluation of the constructs for image-guided delivery in pancreatic tumor models.

4.5. References

1. American Cancer Society. Cancer Facts and Figures 2012. Atlanta, GA: American Cancer Society; 2012.

2. Fass L. Imaging and cancer: a review. Mol Oncol. 2008; 2:115-152.

3. Goldsmith SJ. Radioimmunotherapy of lymphoma: Bexxar and Zevalin. Semin Nucl Med. 2010; 40:122-135.

4. Lammers T, Kiessling F, Hennink WE, Storm G. Nanotheranostics and image-guided drug delivery: current concepts and future directions. Mol Pharm. 2010; 7:1899-1912.

5. Mitra A, Nan A, Line BR, Ghandehari H. Nanocarriers for nuclear imaging and radiotherapy of cancer. Curr Pharm Des. 2006; 12:4729-4749.

6. Iyer AK, He J, Amiji MM. Image-guided nanosystems for targeted delivery in cancer therapy. Curr Med Chem. 2012; 19:3230-3240.

7. Fernandez-Fernandez A, Manchanda R, McGoron AJ. Theranostic applications of nanomaterials in cancer: drug delivery, image-guided therapy, and multifunctional platforms. Appl Biochem Biotechnol. 2011; 165:1628-1651.

8. Kopecek J, Kopeckova P. HPMA copolymers: origins, early developments, present, and future. Adv Drug Deliv Rev. 2010; 62:122-149.

9. Noguchi Y, Wu J, Duncan R, et al. Early phase tumor accumulation of macromolecules: a great difference in clearance rate between tumor and normal tissues. Jpn J Cancer Res. 1998; 89:307-314.

10. Kolhatkar R, Lote A, Khambati H. Active tumor targeting of nanomaterials using folic acid, transferrin and integrin receptors. Curr Drug Discov Technol. 2011; 8:197-206.

11. Larbouret C, Gaborit N, Chardes T, et al. In pancreatic carcinoma, dual EGFR/HER2 targeting with cetuximab/trastuzumab is more effective than treatment with trastuzumab/erlotinib or lapatinib alone: implication of receptors' down-regulation and dimers' disruption. Neoplasia. 2012; 14:121-130.

12. Buchler P, Reber HA, Buchler MC, et al. Therapy for pancreatic cancer with a recombinant humanized anti-HER2 antibody (herceptin). J Gastrointest Surg. 2001; 5:139-146.

13. Arya G, Vandana M, Acharya S, Sahoo SK. Enhanced antiproliferative activity of Herceptin (HER2)-conjugated gemcitabine-loaded chitosan nanoparticle in pancreatic cancer therapy. Nanomedicine. 2011; 7:859-870.

14. Huang ZQ, Buchsbaum DJ. Monoclonal antibodies in the treatment of pancreatic cancer. Immunotherapy. 2009; 1:223-229.

15. Safran H, Steinhoff M, Mangray S, et al. Overexpression of the HER-2/neu oncogene in pancreatic adenocarcinoma. Am J Clin Oncol. 2001; 24:496-499.

16. Safran H, Iannitti D, Ramanathan R, et al. Herceptin and gemcitabine for metastatic pancreatic cancers that overexpress HER-2/neu. Cancer Invest. 2004; 22:706-712.

17. Komoto M, Nakata B, Amano R, et al. HER2 overexpression correlates with survival after curative resection of pancreatic cancer. Cancer Sci. 2009; 100:1243-1247.

18. Yamanaka Y, Friess H, Kobrin MS, et al. Overexpression of HER2/neu oncogene in human pancreatic carcinoma. Hum Pathol. 1993; 24:1127-1134.

19. Karasseva NG, Glinsky VV, Chen NX, Komatireddy R, Quinn TP. Identification and characterization of peptides that bind human ErbB-2 selected from a bacteriophage display library. J Protein Chem. 2002; 21:287-296.

20. Lu ZR. Molecular imaging of HPMA copolymers: visualizing drug delivery in cell, mouse and man. Adv Drug Deliv Rev. 2010; 62:246-257.

21. Zarabi B, Borgman MP, Zhuo J, Gullapalli R, Ghandehari H. Noninvasive monitoring of HPMA copolymer-RGDfK conjugates by magnetic resonance imaging. Pharm Res. 2009; 26:1121-1129.

22. Zarabi B, Nan A, Zhuo J, Gullapalli R, Ghandehari H. HPMA copolymer-doxorubicin-gadolinium conjugates: synthesis, characterization, and in vitro evaluation. Macromol Biosci. 2008; 8:741-748.

23. Herth MM, Barz M, Moderegger D, et al. Radioactive labeling of defined HPMA-based polymeric structures using [18F]FETos for in vivo imaging by positron emission tomography. Biomacromolecules. 2009; 10:1697-1703.

24. Borgman MP, Coleman T, Kolhatkar RB, Geyser-Stoops S, Line BR, Ghandehari H. Tumor-targeted HPMA copolymer-(RGDfK)-(CHX-A"-DTPA) conjugates show increased kidney accumulation. J Control Release. 2008; 132:193-199.

25. Mitra A, Nan A, Ghandehari H, McNeill E, Mulholland J, Line BR. Technetium-99m-Labeled N-(2-hydroxypropyl) methacrylamide copolymers: synthesis, characterization, and in vivo biodistribution. Pharm Res. 2004; 21:1153-1159.

26. Hui YF, Reitz J. Gemcitabine: a cytidine analogue active against solid tumors. Am J Health Syst Pharm. 1997; 54:162-170; quiz 197-168.

27. Mini E, Nobili S, Caciagli B, Landini I, Mazzei T. Cellular pharmacology of gemcitabine. Ann Oncol. 2006; 17 Suppl 5:v7-12.

28. Strohalm J, Kopecek J. Poly *N*-(2-hydroxypropyl) methacrylamide: 4. Heterogenous polymerization. Angewandte Makromolekulare Chemie. 1978; 70:109-118.

29. Mitra A, Nan A, Papadimitriou JC, Ghandehari H, Line BR. Polymer-peptide conjugates for angiogenesis targeted tumor radiotherapy. Nucl Med Biol. 2006; 33:43-52.

30. Chan WC, White PD. Fmoc solid phase peptide synthesis : a practical approach. New York: Oxford University Press, 2000.

31. Fisher KD, Ulbrich K, Subr V, et al. A versatile system for receptor-mediated gene delivery permits increased entry of DNA into target cells, enhanced delivery to the nucleus and elevated rates of transgene expression. Gene Ther. 2000; 7:1337-1343.

32. Scales CW, Vasilieva YA, Convertine AJ, Lowe AB, McCormick CL. Direct, controlled synthesis of the nonimmunogenic, hydrophilic polymer, poly(N-(2-hydroxypropyl)methacrylamide) via RAFT in aqueous media. Biomacromolecules. 2005; 6:1846-1850.

33. Ray A, Larson N, Pike DB, et al. Comparison of active and passive targeting of docetaxel for prostate cancer therapy by HPMA copolymer-RGDfK conjugates. Mol Pharm. 2011; 8:1090-1099.

34. Maecke HR, Riesen A, Ritter W. The molecular structure of indium-DTPA. J Nucl Med. 1989; 30:1235-1239.

35. Kimura K, Sawada T, Komatsu M, et al. Antitumor effect of trastuzumab for pancreatic cancer with high HER-2 expression and enhancement of effect by combined therapy with gemcitabine. Clin Cancer Res. 2006; 12:4925-4932.

36. Rubin I, Yarden Y. The basic biology of HER2. Ann Oncol. 2001; 12 Suppl 1:S3-8.

37. Lammers T, Kiessling F, Hennink WE, Storm G. Drug targeting to tumors: principles, pitfalls and (pre-) clinical progress. J Control Release. 2012; 161:175-187.

CHAPTER 5

GOLD NANOROD-MEDIATED HYPERTHERMIA ENHANCES THE EFFICACY OF HPMA COPOLYMER-^{90}Y CONJUGATES IN TREATMENT OF PROSTATE TUMORS*

5.1. Introduction

Prostate cancer is the most frequently diagnosed cancer in the U.S.[1]. Typically, this disease affects men in their later years of life. With early screening, the majority of patients can be appropriately treated with much success. However, it remains difficult to treat when the cancer is found in late or advanced stages. Treatment options typically start with surgical resection followed by hormone therapy, chemotherapy, biologic therapy or radiation therapy. Each of these treatments can cause distal or local adverse effects that can lead to lesser quality of life. Therefore, there remains a need to develop novel methods to treat prostate cancer that minimize the potential for side effects.

Macromolecular systems for delivery of therapeutics have been shown to intrinsically target the tumor tissue via the enhanced permeability and retention (EPR) effect[2]. Leaky vasculature from angiogenesis due to the rapid tumor growth generates increased extravasation rates of macromolecules within the tumor region.

* Buckway B, Frazier N, Gormley AJ, Ray A, Ghandehari H. Gold nanorod-mediated hyperthermia enhances the efficacy of HPMA copolymer - ^{90}Y conjugates in treatment of prostate tumors. Nucl Med Biol. (2013); Submitted.

Macromolecules do not easily diffuse from the normal vessels because the gaps in vascular walls are largely tight and intact. Evidence suggests that increased concentrations of these delivery systems containing therapeutics improve the treatment of cancer[3, 4].

The use of radionuclides for imaging and as radiotherapeutics has been shown to be effective in the diagnosis and treatment of many cancer types[5]. Yet, radiotherapeutics for cancer treatment have had limited application. This is in part due to insufficient localization and the nonspecific uptake of radionuclides in the patient causing undesirable nontargeted tissue damage from radiation exposure. Several clinically approved radionuclides for therapy are conjugated to macromolecular tumor targeting monoclonal antibodies (MoAbs) in order to target only the specific diseased tissue[6]. However, tumor targets are heterogeneous in various patients and within individual tumors due to a variety of expression levels of the targeted antigen. One other shortfall of targeted delivery using MoAbs is that the target receptor is rarely only expressed on the targeted disease tissue which may lead to increased uptake in nonspecific tissues, thereby increasing the chance of treatment related toxicity. There remains a need to target tumors using other macromolecular systems.

Use of water-soluble polymers based on *N*-(2-hydroxypropyl)methacrylamide (HPMA) is one potential method to increase radiotherapeutic accumulation in the tumor[7-9]. HPMA copolymers are ideal macromolecular carriers for radionuclide delivery because of their ability to be synthesized in a size-controlled manner and presence of a variety of comonomers available to incorporate drugs, imaging agents or tumor targeting ligands[9-12]. Because of their macromolecular nature, they are also able to passively target tumors via the enhanced permeability and retention (EPR) effect[2]. However, the delivery

of HPMA copolymers and other macromolecules via the EPR effect has been variable from patient to patient[13]. Therefore, other methods must be considered to increase localization within the tumor.

Previous studies have shown the advantage of localized hyperthermia to increase HPMA copolymer conjugate localization and efficacy in treating prostate tumors[14-16]. Hyperthermia can be easily controlled and localized using plasmonic photothermal therapy (PPTT)[17]. PPTT uses the surface plasmon resonance of gold nanorods (GNR) when activated by the appropriate wavelength of light for controlled activation of heat[17]. Delivery of GNRs to the tumor is also based on passive accumulation and once localized to tumors can be irradiated by laser to augment the localization of subsequently injected polymer therapeutics[15].

The central hypothesis of this work is that by using localized hyperthermia with GNR-mediated plasmonic photothermal therapy, it is possible to enhance the delivery of HPMA copolymer-yttrium 90 conjugates to prostate tumors and improve radiotherapeutic efficacy. The overall design of the copolymer system described in this work includes side chain conjugated 1, 4, 7, 10-tetraazacyclododecane-1,4,7,10-tetraacetic acid (DOTA) for chelation of either ^{111}In for imaging of the biodistribution of the HPMA copolymers after hyperthermia treatment, or ^{90}Y for radiotherapeutic treatment of the tumor. ^{90}Y is a pure beta emitting isotope which is not an ideal imaging agent for γ-ray detection. Nuclear medicine techniques such as single photon emission computerized tomography (SPECT) offer relatively high-resolution and quantitative images[18,19]. Therefore, imaging of HPMA copolymer-^{111}In conjugate using SPECT should provide more detailed information as to the quantity and kinetics of tumor localization and enable correlation of

such localization with therapy. Correlation performed in this study between these two conjugates can give us a potential personalized therapy for use in treating prostate cancer.

5.2. Materials and Methods

5.2.1. Chemicals

N-(3-Aminopropyl)methacrylamide hydrochloride (APMA) was acquired from Polysciences (Warrington, PA). 1, 4, 7, 10-tetraazacyclododecane-1,4,7,10-tetraacetic acid mono (*N*-hydroxysuccinimide ester) (DOTA-NHS-ester) was obtained from Macrocyclics (Dallas, TX). 2,2'-Azobis[2-(2-imidazolin-2-yl)propane] dihydrochloride (VA-044) was obtained from Wako Chemicals (Richmond, VA). [^{90}Y]YCl_3 and [^{111}In]$InCl_3$ was obtained from the Intermountain Radiopharmacy (Salt Lake City, UT). All other reagents were of reagent grade and were obtained from Sigma-Aldrich (St. Louis, MO).

5.2.2. Comonomer synthesis and characterization

N-(2-hydroxypropyl)methacrylamide comonomer (HPMA) was synthesized according to published methods[20]. A brief description of the synthesis and characterization can be found in Appendix A. 1, 4, 7, 10-tetraazacyclododecane-1,4,7,10-tetraacetic acid mono (*N*-(3-aminopropyl)methacrylamide (APMA-DOTA) was synthesized by combining a molar ratio of 1.5:1 DOTA-NHS-ester to APMA in anhydrous dimethylformamide (DMF) with 10% diisopropylethylamine (DIPEA) and stirred overnight at room temperature. The crude product was precipitated and excessively washed in diethyl ether to form a white powder. The final comonomer

molecular weight was analyzed by electrospray ionization mass spectrometry *m/z* calculated for $C_{23}H_{40}N_6O_8$, 528.5991, found 527 $[M-H]^+$, 549 $[M+Na]^+$.

5.2.3. Synthesis of the HPMA copolymer conjugate

HPMA and APMA-DOTA were copolymerized by reversible addition-fragmentation chain transfer (RAFT) polymerization according to *Scheme 5.1*. The radical initiator used was 2,2'-Azobis[2-(2-imidazolin-2-yl)propane]dihydrochloride (VA-044) and the chain transfer agent 2-cyano-2-propyl dodecyl trithiocarbonate (CPDT). At a molar ratio of 300:1:0.67 monomers/CPDT/VA-044 in methanol with total concentration of 1M, monomers were polymerized at 50^{o}C for 24 h in a nitrogen-purged sealed ampule to control the size and polydispersity of the HPMA copolymers. The final product was obtained by precipitating in diethyl ether and the resulting white solid was dissolved in deionized water and subsequently dialyzed using a 3.5 kDa molecular weight cut off (MWCO) dialysis bag (Spectrum Laboratories, Inc., Rancho Dominguez, CA). The purified copolymer was obtained by lyophilization and analyzed by Fast Protein Liquid Chromatography (FPLC) system (GE Healthcare, Piscataway, NJ) equipped with a multi-angle light scattering (MALS) detector (Wyatt Technologies, Santa Barbara, CA). DOTA content was determined by analyzing gadolinium content (assuming a 1:1 ratio) after chelation according to previously described methods[21].

5.2.4. Radiolabeling with ^{111}In and ^{90}Y

HPMA copolymer-DOTA conjugate was labeled with radioisotopes according to previously published methods[22,23]. 10 mg of HPMA copolymer-DOTA conjugate was dissolved in 250 µl of 1.0 M sodium acetate buffer pH 5.0. 10 mCi of [^{111}In]$InCl_3$ or

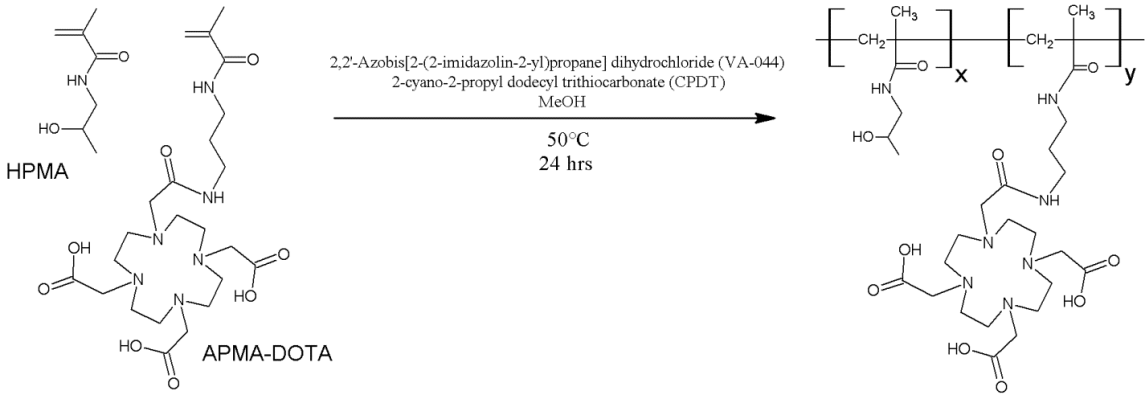

Scheme 5.1. RAFT polymerization of HPMA copolymer-DOTA

[^{90}Y]YCl_3 was also treated with 0.25 ml of 1.0 M sodium acetate buffer pH 5.0. Radioactive compounds were added to the HPMA copolymer-DOTA solution and incubated at 50^{o}C for 1.0 h with mixing under nitrogen. The solution was allowed to cool to room temperature, and then treated with 100 µl of 0.05 M ethylenediaminetetraacetic acid (EDTA) for about 10 min in order to remove free or loosely bound $^{111}In^{+3}$ or $^{90}Y^{+3}$ ions. Radioactive polymers were purified by Sephadex G25 PD-10 columns (GE Life Sciences, Piscataway, NJ). Radioactivity was measured using a CAPTUS 3000 multichannel analyzer (Canberra Industries, Inc., Meriden, CT). Radiostability was determined by incubating radiolabeled copolymers at 37^{o}C in the presence of mouse serum. Samples were collected at 24, 48 and 72 h and subjected to PD-10 column separation to determine the free radiolabel content.

5.2.5. Synthesis of PEGylated gold nanorods

Gold nanorods (GNRs) were synthesized using the seed-mediated growth method with an aspect ratio that correlates with a surface plasmon resonance (SPR) peak between 800 and 810 nm[24]. The light absorption profile was measured by UV spectrometry. The GNRs were then centrifuged and washed three times with deionized water to remove excess hexadecyltrimethylammonium bromide (CTAB). After washing, poly(ethylene glycol) (PEG) (methoxy-PEG-thiol 5 kD, Creative PEGWorks, Winston Salem, NC) was added to the GNR suspension and stirred for 1 h to allow for sufficient coating. The PEG-GNRs were then dialyzed (10k MWCO, Spectrum labs), centrifuged, washed and concentrated to remove any excess, unbound PEG. The final concentration of the PEG-GNRs was 1.2 mg/ml (OD = 120) and were stored at 4°C. Finally, the PEG-GNR solution was sterile filtered prior to use in vivo.

5.2.6. Animal tumor model

DU-145 prostate tumor cells (ATCC, Manassas, VA) were cultured in Eagle's Minimum Essential Medium (EMEM) (ATCC, Manassas, VA) supplemented with 10% (v/v) fetal bovine serum (FBS) at 37ºC in a humidified atmosphere of 5% CO_2 (v/v). Cell cultures were harvested at approximately 80% confluence by treatment with TrypLE™ Express (Invitrogen, Grand Island, NY) and subsequent dilution in phosphate buffered saline (PBS). Athymic Nu/Nu female mice were inoculated with 1 x 10^7 cells on both the left and right lower flanks of each mouse. Experiments were initiated after tumor diameters had reached 5–7 mm in diameter by external caliper measurement. All animal experiments were conducted under an approved protocol from the Institutional Animal Care and Use Committee at the University of Utah (Salt Lake City, UT).

5.2.7. Biodistribution of ^{111}In HPMA copolymer-DOTA conjugates

The general method of plasmonic photothermal therapy for moderate hyperthermia is demonstrated in *Figure 5.1*. Prostate tumor bearing mice were administered 9.6 mg/kg of PEGylated GNRs via lateral tail vein injection. After 48 h mice were injected with 300-350 μCi of ^{111}In labeled HPMA copolymer-DOTA conjugates and immediately treated on the right tumor with moderate hyperthermia as described previously[15]. Briefly, the right tumor of the mouse was irradiated by laser at a wavelength of 808 nm for 10 min. Temperature was measured using a needle point temperature probe near the center of the tumor and laser power was adjusted in order to maintain tumor temperature at 43±1^{o}C. The mouse was anesthetized by isofluorane via nose cone, immediately placed on the bed of an Inveon microPET/SPECT/CT multimodality scanner (Siemens Medical Solutions USA, Inc., Malvern, PA) and imaged

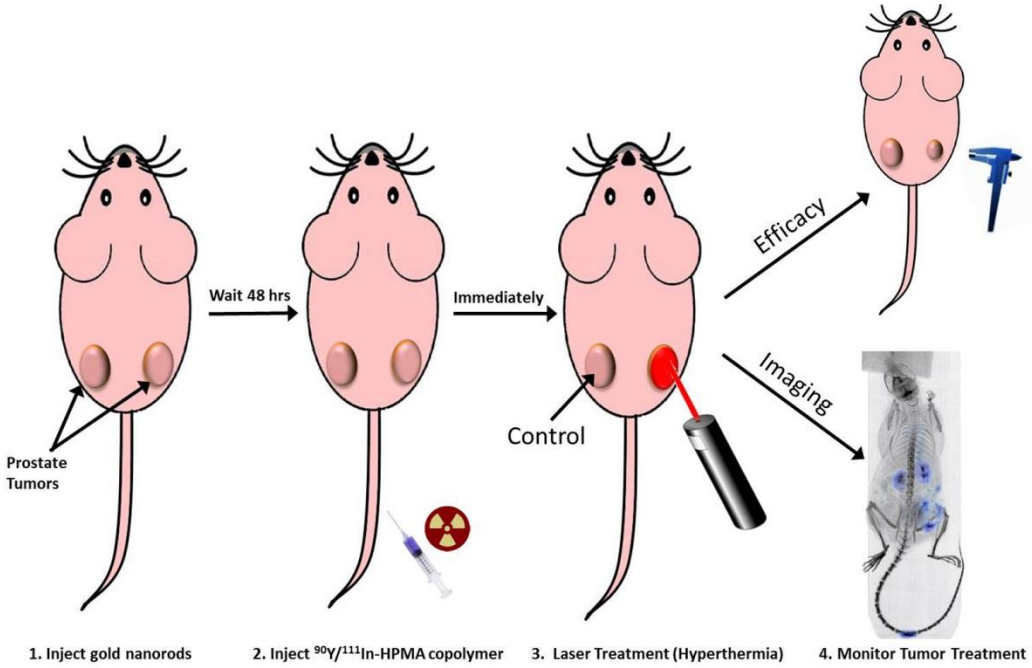

Figure 5.1. Methodology for combination radiotherapy and hyperthermia treatment in prostate tumor bearing mice.

by single photon emission computerized tomography (SPECT) for 4 h. SPECT scans were performed in 22-min frames with an X-Ray Computerized Tomography (CT) scan performed at the beginning and end of the 4-h SPECT series. A follow up static SPECT/CT scan was also conducted at 24 h the following day. After 24 h, the mouse was euthanized and organs collected (blood, heart, lung, liver, spleen, kidney and tumors). The organs were weighed and gamma counted using a CAPTUS 3000 well counter. SPECT images were analyzed using the Inveon Research Workplace software (Siemens Medical Solutions USA, Inc., Malvern, PA) with regions of interest (ROI) drawn respective to the tumors shown on the CT image with SPECT registration. The estimated average voxel intensity obtained from each ROI of each tumor was correlated to the gamma counted tissues excised at the 24-h time point of each mouse. Left and right tumor activity concentrations estimated from the imaging data were compared to determine differences in pharmacokinetic and biodistribution profiles related to the hyperthermia treatment using GraphPad Prism Software (La Jolla, CA). The area under the curve (AUC) was determined using the trapezoid method via the same software.

5.2.8. Combination radiotherapy and hyperthermia treatment

Prostate tumor animal models treated with PEGylated GNRs were prepared as described above and injected with 250 μCi of ^{90}Y labeled HPMA copolymer-DOTA conjugates via the lateral tail vein injection. The right tumor of the mouse was subjected to moderate hyperthermia as described above. A saline (hyperthermia only) control group was also treated in a similar manner. Left and right tumor ellipsoid volumes were estimated by external caliper measurement of the length and width of each tumor twice weekly. Tumor volumes were normalized to measurement on day 0 of treatment. Animal

tumor weights were monitored. At the end of the 40-day study, the mice were euthanized and heart, lung, liver, spleen, kidney and both tumors were collected and incubated in 10% neutral buffered formalin for 48 h. The tissues were subsequently sliced into 5 μm slices and hematoxylin and eosin (H&E) stained by the Histology Department at ARUP Laboratories (Salt Lake City, UT). Tissue slides were analyzed for toxicity related to radioactive exposure from the ^{90}Y HPMA copolymer-DOTA conjugate treatment. Tumor tissues were also investigated for evidence of radiotherapeutic damage.

5.2.9. Statistical analysis

Animal study results were analyzed for statistical significance using one-way ANOVA with Tukey's posttest and biodistribution results between tumor treatments were analyzed by the student T-test using GraphPad Prism Software (La Jolla, CA).

5.3. Results and Discussion

The overall goal for this study was to evaluate a polymer containing both an imaging agent and a radiotherapeutic in conjunction with localized hyperthermia. The polymer was designed to reduce nonspecific uptake, allow urinary clearance and assure sufficient uptake within the tumor mass. Characteristics of the copolymers are shown in *Table 5.1*. A polymer of less than 45 kDa was desired in order for glomerular filtration of of the HPMA copolymer in the body[2]. The DOTA content was expected to be 10 wt% based on the feed content of the copolymer (2.0 mol%). DOTA content was sufficient for ^{111}In and ^{90}Y radiolabelling demonstrated by the radioactive content shown in *Table 5.1*.

DOTA has been shown to be a stable chelator for both radioisotopes[22,25]. ^{111}In is a common γ-emitting radionuclide used in the clinic for SPECT imaging[26]. ^{90}Y as a beta

Table 5.1. HPMA copolymer-DOTA characteristics

Polymer Characteristics	Result
M_w[a]	27.7 kDa
M_n[a]	25.5 kDa
PDI[a]	1.09
APMA-DOTA feed ratio	2.0 mol%
^{111}In content[b]	571 μCi/mg
^{90}Y content[b]	356 μCi/mg

a) Determined by MALS
b) Determined by γ-counter at end of synthesis

emitting radionuclide has been clinically used for radiotherapeutic treatment of tumors[27]. ^{111}In and ^{90}Y have similar half-lives (2.80 and 2.67 days, respectively) that correspond to the potential biological half-life of HPMA copolymer construct. This allowed sufficient monitoring by imaging and radioactivity exposure for treatment of the tumor. The imaging construct based on ^{111}In allowed image-based biodistribution and pharmacokinetic profiles that can predict therapeutic safety and efficacy of the ^{90}Y radiotherapeutic construct. Stability of the ^{90}Y with HPMA copolymer-DOTA conjugate in the presence of serum is shown in *Figure 5.2*. The ^{90}Y labeled conjugate was ~93% stable over 72 h in mouse serum after separation on the PD-10 column. This could be caused by radiolysis of some of the label due to the high beta energy of ^{90}Y and lack of any scavenger in the formulation.

The results from the animal imaging study of the ^{111}In labeled HPMA copolymer-DOTA conjugate demonstrate increased localization in the tumor with moderate hyperthermia. *Figure 5.3* demonstrates that hyperthermia-treated tumors (right tumor) have a marked increased localization of the HPMA copolymer over time. It also demonstrates that the most off-target overall exposure in the animal is likely the kidneys. Based on the ^{111}In imaging version of the HPMA copolymer, the right tumor received a higher average exposure of beta particle emission than that of the left tumor due to hyperthermia treatment. Time activity concentration curves determined from image analysis was performed for each tumor (hyperthermia treated and control). Average voxel intensity from SPECT/CT images were calibrated based on the necropsied tissue counts of both tumors of each mouse collected at the 24-h time point (n = 3) (*Figure 5.3E*). Radioactivity exposure to the tumor was measured by calculating the AUC for 0-4 h and 4-24 h using the trapezoidal method. The hyperthermia-treated tumor $AUC_{0\text{-}4\ h} = 1990 \pm$

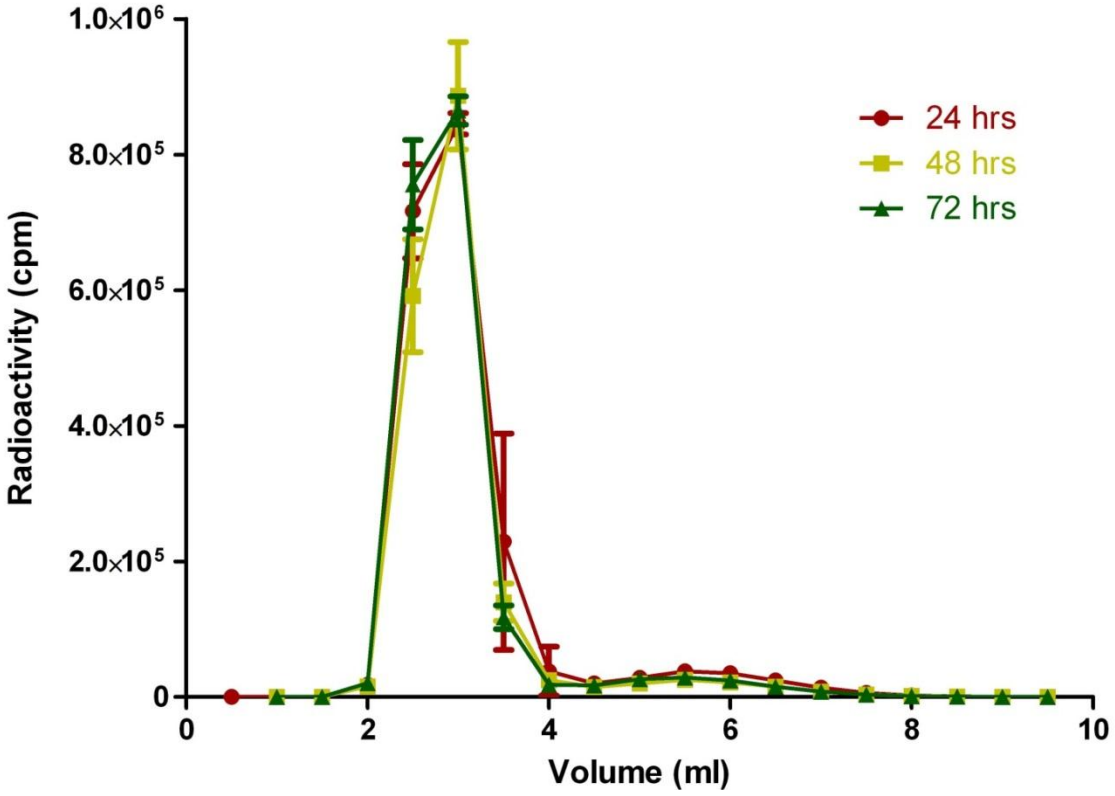

Figure 5.2. Radiostability of the ^{90}Y labeled HPMA copolymer-DOTA. Data are represented as the mean ± standard error of the mean (SEM) (n=3). An average amount of approximately 93% was observed as macromolecular in size corresponding to the radiolabeled HPMA copolymer.

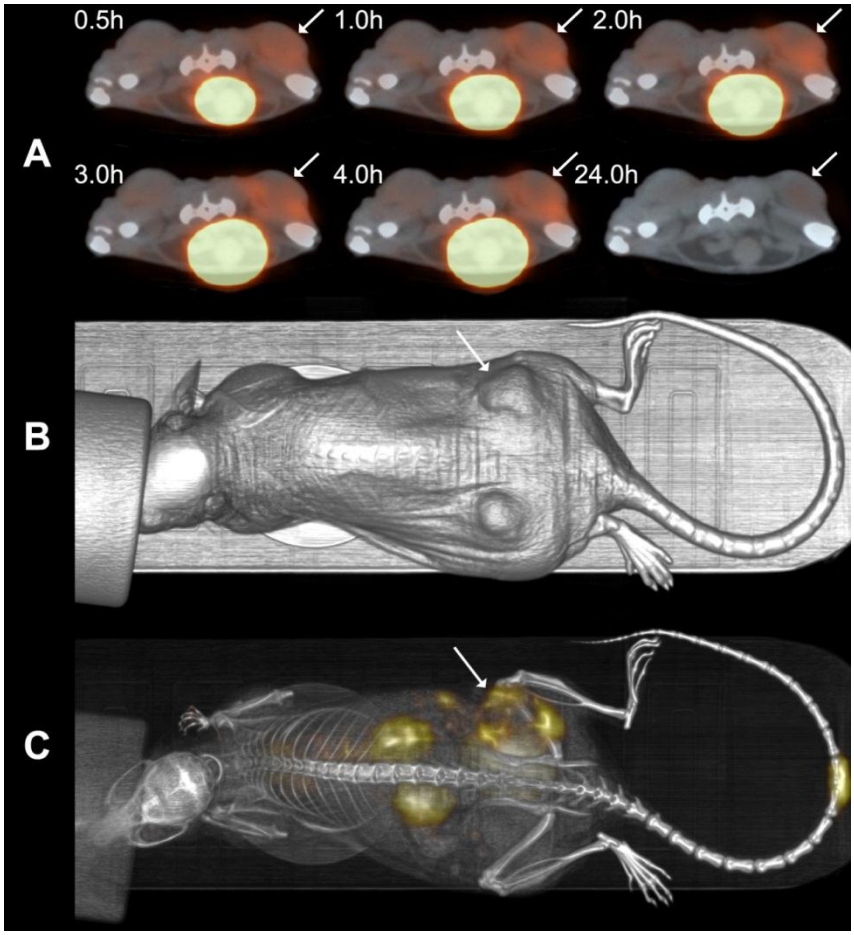

Figure 5.3. Biodistribution and pharmacokinetic analysis of ^{111}In labeled HPMA copolymer-DOTA. A) Serial 22-min axial scans showing a comparison of the right (hyperthermia-treated) and left tumors on the dorsal region of the animal injected 300 μCi of ^{111}In-HPMA copolymer while under isofluorane. The large bright spot central to the anterior side of the animal is a result of a large accumulation in the bladder demonstrating the eventual clearance of the HPMA copolymer conjugates. Arrows denote hyperthermia treated tumor. B) CT image of the mouse showing the lower dorsal placement of the tumors. C) Whole body planar image at approximately 4 h postinjection. D) Biodistribution and pharmacokinetic analysis of ^{111}In labeled HPMA copolymer-DOTA. Time activity graph showing the curve fits for the calculations of AUC for each tumor. Red line represents the right (hyperthermia) tumor and the blue line represents the left (control) tumor. Data represented as the mean ± SEM (n=3). The hyperthermia treated tumor $AUC_{0\text{-}4\ h}$ = 1990 %ID·min/g and $AUC_{4\text{-}24\ h}$ = 9107 %ID·min/g. The control tumors $AUC_{0\text{-}4\ h}$ = 648.5 %ID·min/g and $AUC_{4\text{-}24\ h}$ = 2994 %ID·min/g. The dashed lines represent the elimination phases in which the accuracy is limited based on limited data points for analysis. E) The biodistribution data from the γ-counting of each individual organ at 24 h postinjection. Data represented as the mean ± SEM (n=3).

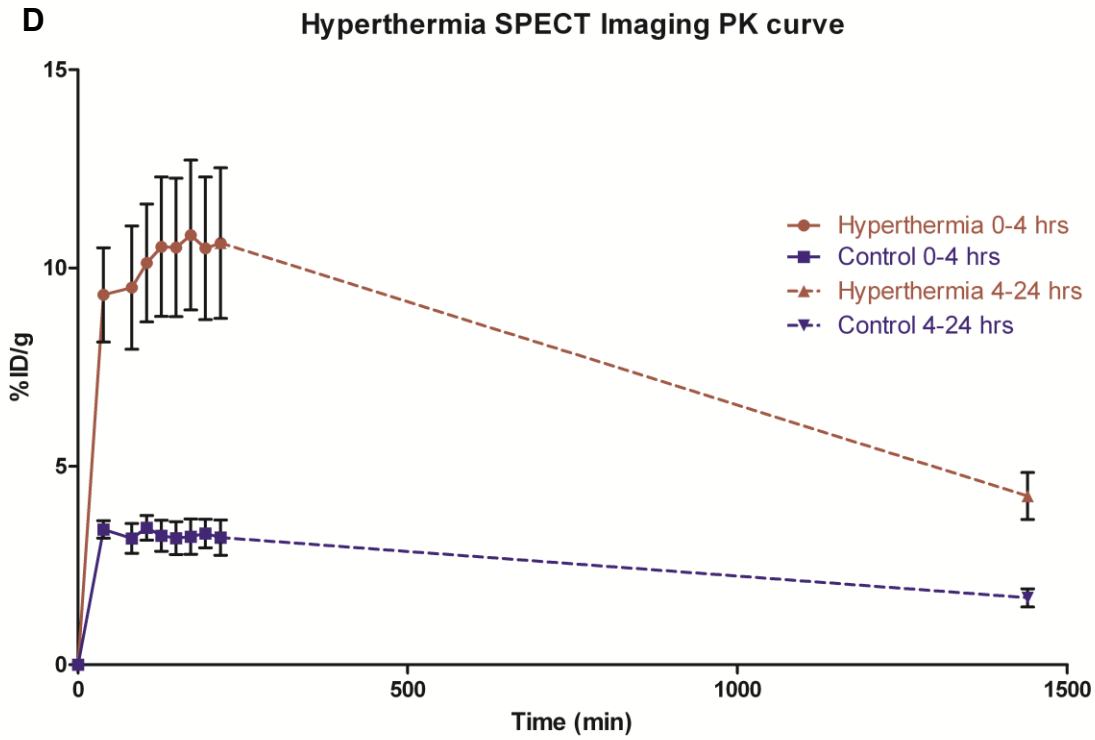

Figure 5.3. Continued

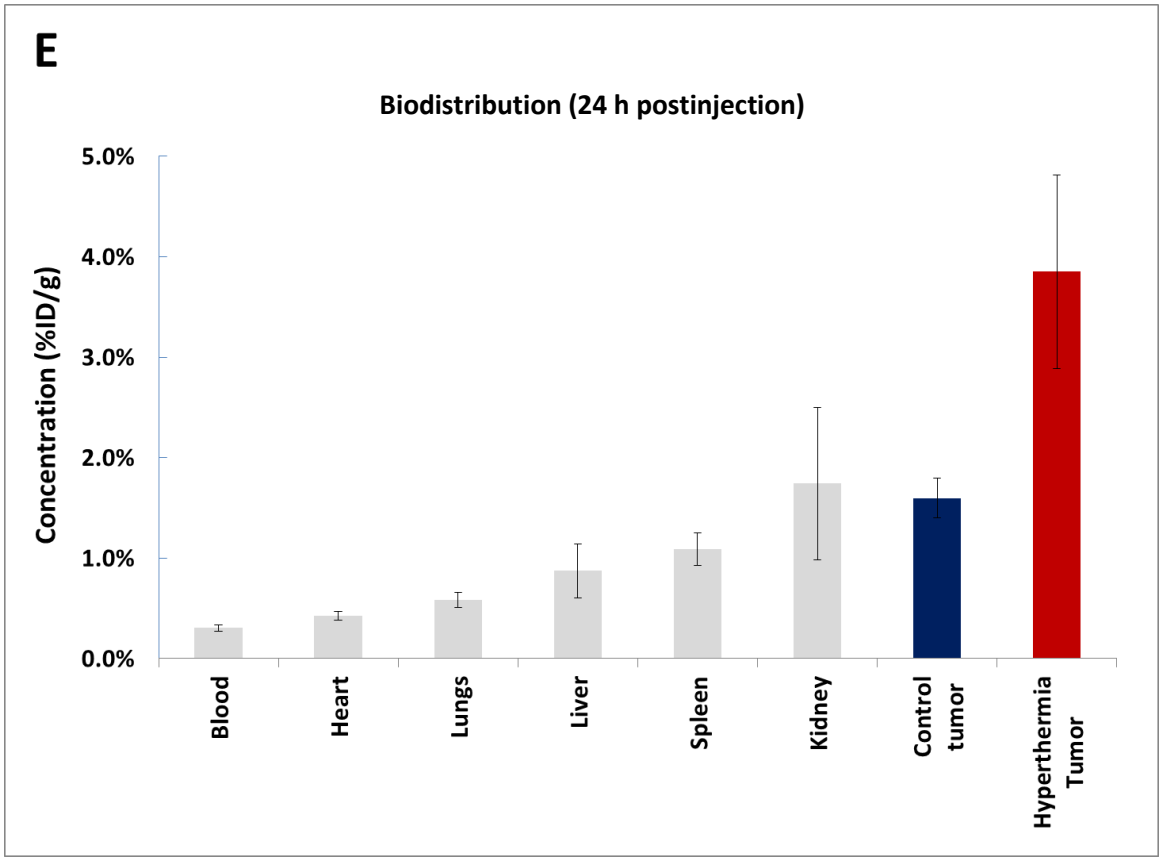

Figure 5.3. Continued

310 %ID·min/g and $AUC_{4\text{-}24\ h}$ = 9107 ± 1512 %ID·min/g. The control tumors $AUC_{0\text{-}4\ h}$ =648.5 ± 62.4 %ID·min/g and $AUC_{4\text{-}24\ h}$ = 2994 ± 391 %ID·min/g. The amount of exposure is about 3 times higher for the hyperthermia-treated animals during both periods of 0-4 and 4-24 h. The accuracy during elimination phase (4-24 h) is limited based on the lack of data points between 4-24 h. However, the AUC ratios between both regions of the time activity curve are very similar ($AUC_{0\text{-}4\ h}$ ratio = 3.07 and $AUC_{4\text{-}24\ h}$ = 3.04), suggesting that the elimination phase fit is relatively accurate as we should expect the ratio of exposure to the tumors to be the same. SPECT imaging is known to have limitations in absolute quantitation and is normally considered semiquantitative due to a lack of ability to correct for scattering, attenuation and other related factors that can skew imaging results. The data from this imaging study compare the left and right tumors of the same animal and can therefore represent a fairly accurate comparison. Overall, the imaging data analysis clearly demonstrates an increased accumulation of the radiolabeled polymer. This overall increase in exposure to the hyperthermia treated tumor can be related to the beta emitting ^{90}Y radiolabeled HPMA construct and effectively explain the efficacy results discussed below.

The efficacy study shows the clear advantage of using moderate hyperthermia to improve the delivery and efficacy of ^{90}Y radiotherapy (*Figure 5.4*). Radiotherapy was only effective in the tumor treated with hyperthermia. This is expected due to the fact that we see more of the radiolabeled copolymers localizing in the tumor over time. Hyperthermia increases blood flow and perfusion to the tumor[28,29], thus potentially augmenting the EPR effect and localization of HPMA copolymers. It is also possible that the increased perfusion to the tumor region may sensitize the tumor to the effects of radiation. This can be due to the increased oxygenation of the tumor delivered from the

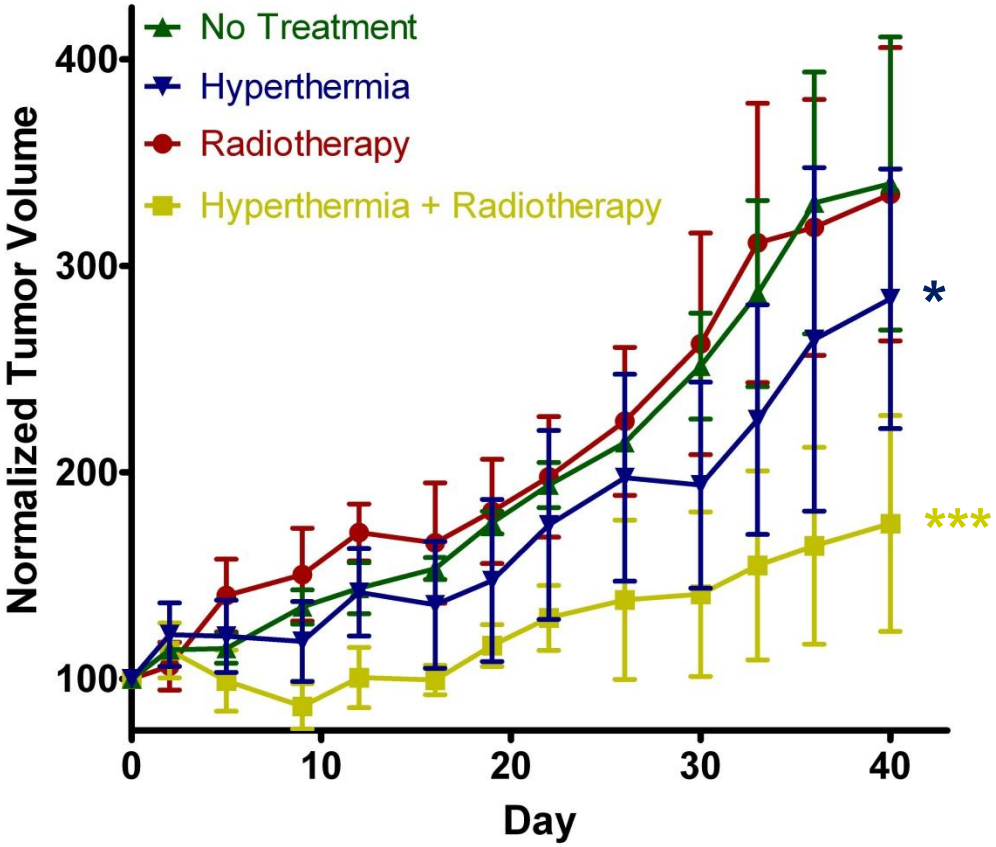

Figure 5.4. Efficacy of ^{90}Y HPMA copolymer-DOTA conjugates. Efficacy data for 40 days treatment comparing radiotherapy and hyperthermia combinations. No Treatment (Green) and hyperthermia (Blue) data are represented as mean ± SEM (n=3). Radiotherapy (Red) and hyperthermia + radiotherapy (Yellow) are represented as mean ± SEM (n=5). Statistical significance was analyzed by repeated measure ANOVA using Tukey's posttest with hyperthermia (Blue) group (*) statistically different ($p < 0.01$) than control and radiotherapy alone. The combination hyperthermia + radiotherapy (yellow) group (***) was also found to be statistically different ($p < 0.0001$) than all other groups.

increased blood flow. Hyperthermia alone to the tumors using PPTT also had a significant effect but to a lesser extent. This is similar to results conducted in a similar study performed previously[16]. Despite the mild temperature increase in the overall tumor measured by the needle thermal couple, the local temperature near the gold nanorods may be higher and cause some vascular damage and disruption. This may lead to temporary starvation of the tumor that demonstrates reduced tumor growth and could explain the efficacy related to hyperthermia alone. Interestingly, the radiotherapy alone had no efficacy in this study. This can be explained based on the fact that the biodistribution studies in *Figure 5.3* show much less accumulation of the radioactivity in the tumors. The fact that hyperthermia has the potential to sensitize tumors to radiotherapy also is supported based on these results.

The normalized animal weights shown in *Figure 5.5* demonstrate that the treatment was well tolerated. Histological analysis displayed in *Figure 5.6* also demonstrates the lack of damage to the primary organs of the mice. From the biodistribution studies, the normal tissue/organ most exposed to radiation was the kidneys (*Figure 5.3*). However, kidney samples showed a normal structure of both glomerulus and proximal tubule regions. Possible evidence of radiation damage to the tumor is demonstrated in *Figure 5.6F-H* due to increased fibrosis, vacuolization and increased number of apoptotic bodies. These effects are similar to results found in previous studies using ^{90}Y radiotherapy[30,31]. Further analysis was performed by comparing the differences in the amounts of necrotic tissue in the treated tumors versus nontreated tumors shown in *Figure 5.7*. Some of the necrotic tissue is a result of rapid tumor growth in this animal model. Therefore, areas of necrosis from treatment were measured using image analysis software and compared to control mice. Necrosis in the combination radiotherapy and

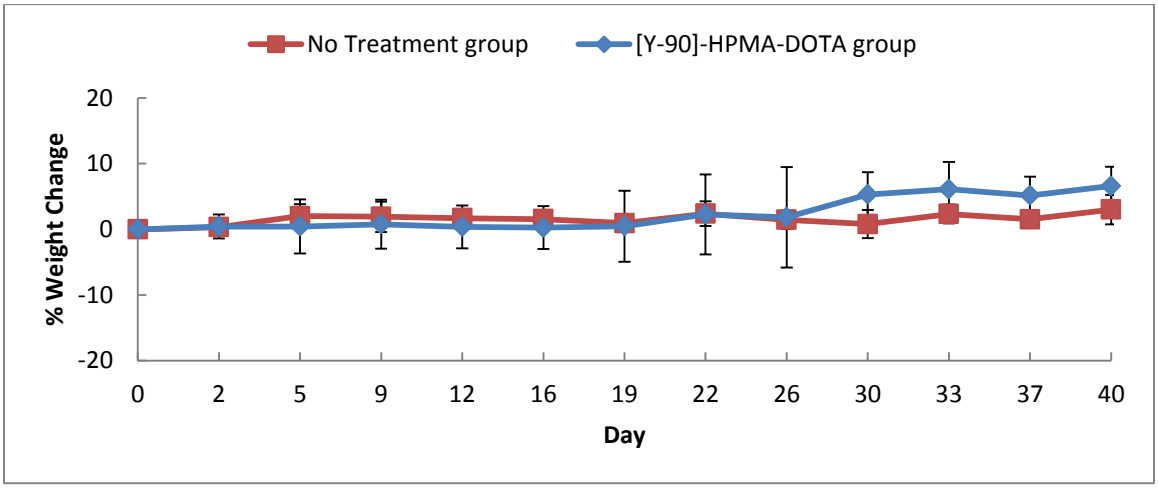

Figure 5.5. Normalized animal weight change. No treatment effect related to weight-loss was observed on either group of animals. No treatment group includes both no treatment and hyperthermia alone groups and the [Y-90]-HPMA-DOTA group includes both radiotherapy alone and combination groups from *Figure 5.4*.

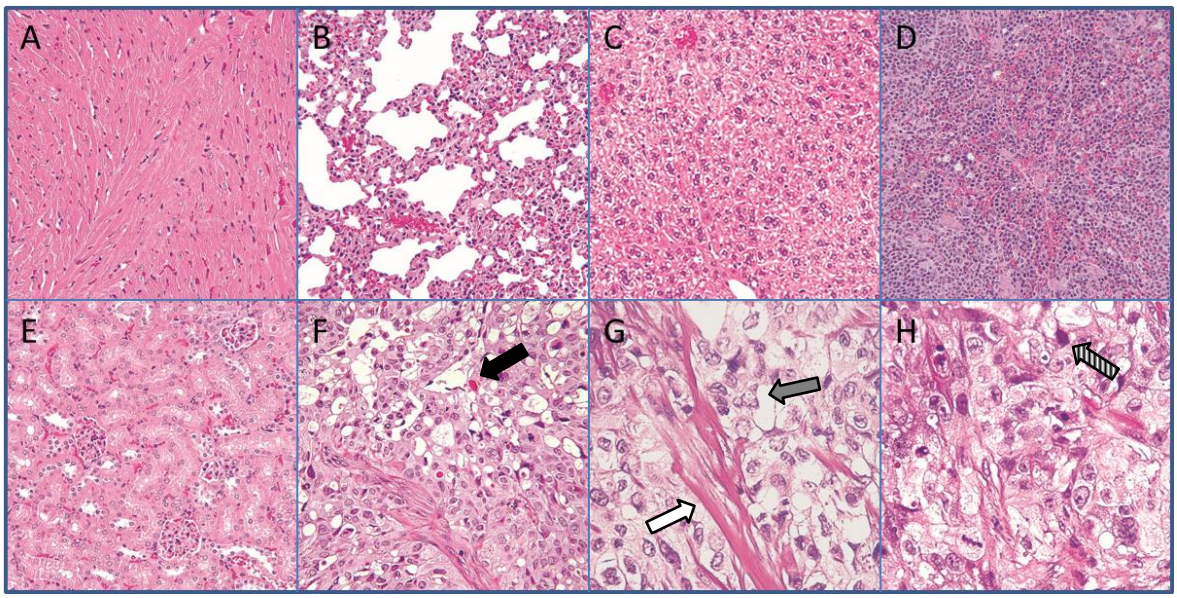

Figure 5.6. Representative Histology samples removed at the end of the 40-day study and stained using H&E staining. Organs showed no difference compared to controls. Arrows represent potential types of evidence for radiation related effects from ^{90}Y-HPMA copolymer-DOTA and hyperthermia treatment.

A) Heart (magnification 40x)
B) Lung (40x)
C) Liver (40x)
D) Spleen (40x)
E) Kidney (40x)
F) Radiotherapy-treated tumor (40x)
G) Radiotherapy-treated tumor (100x)
H) Radiotherapy-treated tumor (100x)

Solid black arrow = thanatosome infiltration
White arrow = Fibrosis
Grey arrow = Vacuole formation
Striped arrow = Apoptotic bodies

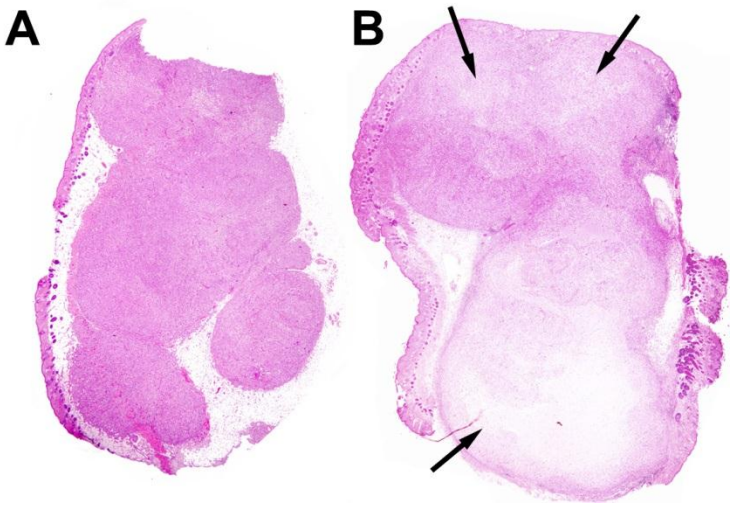

Figure 5.7. Histological comparison of necrosis. H&E stained tumor slices representative of: A) normal mouse tumor and B) radiotherapy + hyperthermia-treated tumor. Arrows represent areas of necrosis.

hyperthermia treated group was found to be approximately 5 times greater than that of control. This increase in levels of tissue damage is a result of the treatment and explains effects observed in the efficacy results (*Figure 5.4*.)

This study demonstrates the enhanced efficacy to prostate cancer treatment with ^{90}Y HPMA copolymers in combination with gold nanorod mediated hyperthermia. One of the advantages of this system compared to other macromolecular radiotherapeutics that have been developed is the increased localization by external trigger and without increasing nontargeted tissue uptake. The size of HPMA copolymers used in this study were designed to eventually eliminate from the body but have sufficient circulation time to distribute into the hyperthermia treated tumors. However, the EPR effect of HPMA copolymers and other macromolecules has been shown to be enhanced by using larger molecular weight carriers based on longer circulation times due to their inability to be filtered through the pores in the glomerulus of the kidney. This may be detrimental because the longer the conjugates remain in the body, the more likely the radiolabel can be released and distributed to undesirable organs and cause toxicity. However, recent large degradable HPMA copolymers have shown eventual clearance due to enzymatically cleavable spacers in the backbone of the polymer construct[32]. These conjugates showed a marked increase in tumor localization compared to small molecular weight systems and suggest that radiotherapeutic delivery could also be enhanced using this method.

The radionuclides used in this study for HPMA copolymer delivery of radiotherapeutics are similar to those used in the clinic for image-guided therapy. Bexxar® and Zevalin® are monoclonal antibodies used in the delivery of both radioisotopes for imaging and therapy[6]. Imaging of these therapies using SPECT is utilized to predict safety of the subsequently administered radiotherapeutic version. The

HPMA copolymer system developed in this study could be used in a similar way for prostate cancer. The imaging version could be used to visualize any nonspecific uptake that may exist in a particular patient and could also be used to measure the amount localized in the tumor. The ^{111}In labeled HPMA copolymer imaging version provides information about the quantity localized in the prostate tumor. This quantitation is useful in determining the dose required for efficacy of the ^{90}Y labeled HPMA copolymers used for radiotherapy. This strategy can potentially provide the prostate cancer patient with a personalized therapy that increases the efficiency, safety and efficacy of anticancer treatment.

5.4. Conclusion

The HPMA copolymers radiolabeled with ^{90}Y for combination radiotherapy and hyperthermia were found to be effective in treatment of prostate tumors in a mouse model. HPMA copolymers were successfully monitored by SPECT imaging for biodistribution effects related to hyperthermia. The radioactive treatment was found to be primarily accumulated in the tumor. Histological examination of the various organs did not show evidence of any radioactive related toxicity. Overall, the conjugates were proven to be potentially safe and efficacious for treatment of prostate cancer.

5.5. References

1. American Cancer Society. Cancer Facts and Figures 2012. Atlanta, GA: American Cancer Society; 2012.

2. Noguchi Y, Wu J, Duncan R, Strohalm J, Ulbrich K, Akaike T, et al. Early phase tumor accumulation of macromolecules: a great difference in clearance rate between tumor and normal tissues. Jpn J Cancer Res 1998; 89:307-14.

3. Maeda H, Bharate GY, and Daruwalla J. Polymeric drugs for efficient tumor-targeted drug delivery based on EPR-effect. Eur J Pharm Biopharm 2009; 71:409-19.

4. Maeda H, Sawa T, and Konno T. Mechanism of tumor-targeted delivery of macromolecular drugs, including the EPR effect in solid tumor and clinical overview of the prototype polymeric drug SMANCS. J Control Release 2001; 74:47-61.

5. Kramer-Marek G and Capala J. The role of nuclear medicine in modern therapy of cancer. Tumour Biol 2012; 33:629-40.

6. Goldsmith SJ. Radioimmunotherapy of lymphoma: Bexxar and Zevalin. Semin Nucl Med 2010; 40:122-35.

7. Kopecek J. Polymer-drug conjugates: origins, progress to date and future directions. Adv Drug Deliv Rev 2013; 65:49-59.

8. Kopecek J, Kopeckova P, Minko T, and Lu Z. HPMA copolymer-anticancer drug conjugates: design, activity, and mechanism of action. Eur J Pharm Biopharm 2000; 50:61-81.

9. Lu ZR. Molecular imaging of HPMA copolymers: visualizing drug delivery in cell, mouse and man. Adv Drug Deliv Rev 2010; 62:246-57.

10. Kopecek J and Kopeckova P. HPMA copolymers: origins, early developments, present, and future. Adv Drug Deliv Rev 2010; 62:122-49.

11. Mitra A, Nan A, Line BR, and Ghandehari H. Nanocarriers for nuclear imaging and radiotherapy of cancer. Curr Pharm Des 2006; 12:4729-49.

12. Pike DB and Ghandehari H. HPMA copolymer-cyclic RGD conjugates for tumor targeting. Adv Drug Deliv Rev 2010; 62:167-83.

13. Lammers T, Kiessling F, Hennink WE, and Storm G. Drug targeting to tumors: principles, pitfalls and (pre-) clinical progress. J Control Release 2012; 161:175-87.

14. Gormley AJ, Larson N, Banisadr A, Robinson R, Frazier N, Ray A, et al. Plasmonic photothermal therapy increases the tumor mass penetration of HPMA copolymers. J Control Release 2013; 166:130-8.

15. Gormley AJ, Larson N, Sadekar S, Robinson R, Ray A, and Ghandehari H. Guided delivery of polymer therapeutics using plasmonic photothermal therapy. Nano today 2012; 7:158-67.

16. Larson N, Gormley AJ, Frazier N, and Ghandehari H. Synergistic enhancment of cancer therapy using a combination of heat shock protein targeted HPMA copolymer-drug conjugates and gold nanorod induced hyperthermia. J Control Release; In Press

17. Huang X, Jain PK, El-Sayed IH, and El-Sayed MA. Plasmonic photothermal therapy (PPTT) using gold nanoparticles. Laser Med Sci 2008; 23:217-28.

18. Alberini JL, Edeline V, Giraudet AL, Champion L, Paulmier B, Madar O, et al. Single photon emission tomography/computed tomography (SPET/CT) and positron emission tomography/computed tomography (PET/CT) to image cancer. J Surg Oncol 2011; 103:602-6.

19. Weissleder R. Molecular imaging: principles and practice. Shelton, CT: People's Medical Pub. House-USA, 2010.

20. Strohalm J and Kopecek J. Poly N-(2-hydroxypropyl) methacrylamide: 4. Heterogenous polymerization. Angew. Makromol. Chem. 1978; 70:109-18.

21. Zarabi B, Borgman MP, Zhuo J, Gullapalli R, and Ghandehari H. Noninvasive monitoring of HPMA copolymer-RGDfK conjugates by magnetic resonance imaging. Pharm Res 2009; 26:1121-9.

22. Kukis DL, DeNardo SJ, DeNardo GL, O'Donnell RT, and Meares CF. Optimized conditions for chelation of yttrium-90-DOTA immunoconjugates. J Nucl Med 1998; 39:2105-10.

23. Mitra A, Nan A, Papadimitriou JC, Ghandehari H, and Line BR. Polymer-peptide conjugates for angiogenesis targeted tumor radiotherapy. Nucl Med Biol 2006; 33:43-52.

24. Nikoobakht B, Burda C, Braun M, Hun M, and El-Sayed MA. The quenching of CdSe quantum dots photoluminescence by gold nanoparticles in solution. Photochem Photobiol 2002; 75:591-7.

25. Liu S, Pietryka J, Ellars CE, and Edwards DS. Comparison of yttrium and indium complexes of DOTA-BA and DOTA-MBA: models for (90)Y- and (111)In-labeled DOTA-biomolecule conjugates. Bioconjug Chem 2002; 13:902-13.

26. Biersack HJ. Clinical nuclear medicine. Berlin ; New York: Springer, 2007.

27. Goffredo V, Paradiso A, Ranieri G, and Gadaleta CD. Yttrium-90 (90Y) in the principal radionuclide therapies: an efficacy correlation between peptide receptor radionuclide therapy, radioimmunotherapy and transarterial radioembolization therapy. Ten years of experience (1999-2009). Crit Rev Oncol Hematol 2011; 80:393-410.

28. Griffin RJ, Dings RP, Jamshidi-Parsian A, and Song CW. Mild temperature hyperthermia and radiation therapy: role of tumour vascular thermotolerance and relevant physiological factors. International Journal of Hyperthermia : the Official Journal of European Society for Hyperthermic Oncology, North American Hyperthermia Group 2010; 26:256-63.

29. Song CW, Park HJ, Lee CK, and Griffin R. Implications of increased tumor blood flow and oxygenation caused by mild temperature hyperthermia in tumor treatment. International Journal of Hyperthermia: the Official Journal of European Society for Hyperthermic Oncology, North American Hyperthermia Group 2005; 21:761-7.

30. Huang J, Chunta JL, Amin M, Lee DY, Grills IS, Wong CY, et al. Detailed characterization of the early response of head-neck cancer xenografts to irradiation using (18)F-FDG-PET imaging. Int J Radiat Oncol Biol Phys 2012; 84:485-91.

31. Stone HB, Coleman CN, Anscher MS, and McBride WH. Effects of radiation on normal tissue: consequences and mechanisms. Lancet Oncol 2003; 4:529-36.

32. Zhang R, Luo K, Yang J, Sima M, Sun Y, Janat-Amsbury MM, et al. Synthesis and evaluation of a backbone biodegradable multiblock HPMA copolymer nanocarrier for the systemic delivery of paclitaxel. J Control Release 2013; 166:66-74.

CHAPTER 6

CONCLUSIONS AND FUTURE DIRECTIONS

6.1. Conclusions

Image-guided therapy can substantially impact treatment of cancer. Already more and more patients are being imaged using state-of-the-art techniques and modalities to accurately diagnose, stage and monitor treatment of cancer[1,2]. Novel targeted treatments are also on the horizon. There are more than 40 targeted therapeutic agents for oncology that are being evaluated in the clinic today[3]. There is an increasing focus on approaches which combine both therapeutic efficacy and safety with imaging. A few novel treatments have incorporated a theranostic approach which should not only accelerate their eventual approval but potentially take larger steps to increase the survival and quality of life of cancer patients[4].

The realization of these technologies can be further enhanced with development of nanomaterials which serve as a platform for the combined delivery of cancer targeting moieties, therapeutics and imaging agents. Several challenges still remain for wide-spread approval of nanomedicines in the clinic. Their ability to target the specific disease in humans has been variable[5]. Variations in tumor heterogeneity have resulted in lack of targeting in clinical trials[6]. Also the reproducible and cost-effective manufacture under

regulatory requirements of these nano-sized constructs is still a remaining challenge[7]. Therefore, much more research into addressing these needs is warranted.

The work presented in this dissertation is an attempt to solve some of the issues related to tumor treatment with image-guided nanomaterials. The focus of Chapters 3 and 4 was on the challenging issues of image-guided drug delivery to pancreatic tumors. In Chapter 3, two targeting approaches were examined which have shown promise in other cancers[8-12]. Validation of the targets was performed in vitro in order to assure that a viable targeting strategy was selected. Nano-sized HPMA copolymers were developed containing the two targeting agents along with ^{111}In for real-time imaging of tumor localization and biodistribution of the conjugates. Careful consideration for their design was taken in order to optimize the desired pharmacokinetic profile that may have success as imaging agents for pancreatic cancer. However, the main barrier to the delivery of small drugs and macromolecules alike in pancreatic cancer is the dense stromal tissue[13]. This study attempted to address this issue by removing a stromal component, hyaluronic acid (HA). HA has been reported to increase the intratumoral fluidic pressure (IFP) of tumors which prevents the diffusion and penetration of macromolecules into solid tumors[14]. In this study, after successful treatment of HA with hyaluronidase, increased tumor localization and active targeting was observed, thereby confirming recent research which has shown that breakdown of the stromal barrier can improve the treatment of pancreatic cancer[13-16].

Chapter 4 focused on the development of an image-guided drug delivery based on HPMA copolymers for pancreatic cancer targeting. A HER2 targeting strategy was selected in the development of this conjugate based on the targeting potential observed

from the studies in Chapter 3. Conjugates were successfully synthesized and characterized with targeting ligand (KCCYSL), drug (gemcitabine) and imaging agent (^{111}In) along with the relevant control systems. The conjugate's design was tailored for an optimal pharmacokinetic profile allowing sufficient time for localization to the tumor but eventual clearance through the kidney. Each component was carefully evaluated to assure their assigned functionality was not compromised by conjugation to the HPMA copolymer backbone. Binding affinity of the targeted ligand was conserved as well as drug activity. Radioactive labeling and stability was also found to be sufficient for potential SPECT imaging studies. However, premature release of the drug in cell-culture media was observed, even though drug activity against positive and negative HER2 cell lines was maintained. This led to concerns on whether the selected drug linker chemical attachment was ideal for this particular image-guided drug delivery system. However, similar types of targeted HPMA copolymer conjugates with premature drug release demonstrated successful increased anticancer efficacy in vivo[12]. Therefore, potential future studies in vivo may be possible but product yields were unfortunately poor. Thus, these studies were limited to in vitro evaluation because the polymerization of the complex conjugates with four different components (HPMA, targeting ligand, drug and imaging agent) posed a significant challenge in polymerization yields.

For Chapter 5, the image-guided therapeutic approach was taken to a slightly different direction. A promising image-guided radiotherapeutic HPMA platform in combination with gold nanorod (GNR)-mediated hyperthermia was developed in a different tumor model. The prostate tumor model was selected in this study. External laser irradiation of GNRs produces hypethermia via surface plasmon resonance. A

prostate tumor mouse model was treated with simple ^{90}Y radiolabeled HPMA copolymers for externally triggered targeted delivery via localized GNR mediated hyperthermia. The combination of both hyperthermia and radiotherapy was found to be efficacious in treating the tumor. Histological analysis revealed increased necrosis in treated tumors with respect to controls. SPECT imaging of an ^{111}In radiolabeled HPMA copolymer backbone demonstrated increased localization in the treated tumors. Organs with significant but minor exposure to the radioactivity did not show any recognizable toxicity from histological analysis. The utilization of both an imaging and therapeutic version of the same HPMA copolymer could potentially be used in an image-guided approach for selection and qualification. This study proved the potential for image-guided approach using radiotherapeutic HPMA copolymers in conjunction with externally controlled tumor targeting.

6.2. Future Directions

These three studies in Chapters 3-5 represent the current progress in the realization of an HPMA copolymer for image-guided therapeutics. The progress made has been significant, especially in regards to utilization of imaging techniques for biodistribution in relation to these studies. The goal of translation of HPMA copolymers for image-guided therapeutics is still distant. The following paragraphs suggest a few ideas that can potentially take this promising area to the next level.

The most obvious direction for the studies related to pancreatic cancer is the need for more translatable animal models. Although, in Chapter 3, the stromal barrier was validated to some degree even in the subcutaneous xenograft animal tumor model, the

tumor vascularity and desmoplastic reaction in actual pancreatic tumors is still different[13]. Several animal tumor models for pancreatic cancer are more clinically relevant and would provide a better assessment of the targeted approach and delivery of both imaging and drug to tumors[13]. One such model is the genetically engineered mice which spontaneously form pancreatic tumors[17]. These tumor models have vascular density and desmoplastic reactions near levels observed in the clinic for humans.

More viable targeting approaches must be developed for pancreatic cancer. In Chapter 3, two targeting strategies were selected based on expression levels in pancreatic cancer, the availability of targeting ligands and previously validated results. However, due to the heterogeneity of pancreatic tumors, more targets must be discovered for ligand-directed targeting of macromolecules. One such receptor that may be promising is epidermal growth factor receptor 1 (EGFR). This receptor has been found to be even more highly expressed on pancreatic tumors than HER2[18]. However, a selection of ligands that are able to be conjugated to the HPMA copolymer backbone without significantly changing its hydrophilic properties were not available. Many antibodies and fragments are available that bind EGFR, but these structures may not be capable of loading on the copolymer in high numbers. Many groups are using phage display techniques to find novel ligands for cancer targets[19-22]. Research could be focused on finding validated targets for pancreatic cancer. Once more ligands are discovered for these targets, they can be evaluated for active targeting of HPMA copolymers for image-guided therapeutic delivery.

Further development of better methods for site-specific release of drugs like gemcitabine within the tumor is needed. The strategy used in studies in Chapter 4 was

based on GFLG peptide linkers that are cleaved once the HPMA copolymers enter the lysosome of the targeted cell. The amide linkage between the base amine of gemcitabine C-terminus of GLFG was found to be slightly unstable. However, more options are needed based on the unexpected premature release in vitro of the gemcitabine amide linkage to the GFLG spacer. Other strategies for delivery based on pH or other protease specific targets warrant investigation. For an ideal image-guided drug delivery system, the drug conjugate should be completely stable until released in the targeted cell. The specificity of this need is yet to be discovered and further development of site-specific release mechanisms would be very advantageous for the delivery of anticancer drugs such as gemcitabine.

A future direction for these studies is the clinical translation of the hyperthermia in combination with radiotherapeutic HPMA copolymers. The current delivery method for hyperthermia utilizes GNRs with laser irradiation for localized heat production. This particular method may have many challenges to overcome in order to be used in the clinic. First is that the penetration of laser near-infrared light for activation is limited to about centimeter of tissue. Another challenge is that the long-term toxic effects of gold nanorods in the body have yet to be investigated. However, there are other methods already available clinically to deliver localized hyperthermia. High-intensity focused ultrasound (HIFU) can precisely deliver mild controlled hyperthermia to tumors which is not limited by depth or material deposition such as GNR-mediated hyperthermia[23]. HIFU for the delivery of macromolecules such as radiotherapeutic HPMA copolymers has enormous research potential. This image-guided delivery is potentially the easiest to translate based on the simplicity of the chemistry of HPMA copolymers for

radiotherapeutics synthesized in Chapter 5 and all components have been in the clinic[24-26]. Clearly more in-depth studies are still needed preclinically for translation.

The field of theranostics is growing and image guidance is becoming a realizable area of focus. Future work in this area can have a substantial impact on a disease that requires pre-assessment for therapy. Although that future has yet to be realized with clinically approved nanoparticle platforms, it is likely that theranostic approaches will transform personalized medicine.

6.3. References

1. Kurdziel K, Ravizzini G, Croft B, Tatum J, Choyke P, Kobayashi H. The evolving role of nuclear molecular imaging in cancer. Expert Opin Med Diagn. 2008; 2:829-842.

2. Fass L. Imaging and cancer: a review. Mol Oncol. 2008; 2:115-152.

3. National Cancer Institute. Targeted cancer therapies. Available from URL: http://www.cancer.gov/cancertopics/factsheet/Therapy/targeted [accessed April 8, 2013].

4. Lee DY, Li KC. Molecular theranostics: a primer for the imaging professional. AJR Am J Roentgenol. 2011; 197:318-324.

5. Bae YH, Park K. Targeted drug delivery to tumors: myths, reality and possibility. J Control Release. 2011; 153:198-205.

6. Duncan R. Development of HPMA copolymer-anticancer conjugates: clinical experience and lessons learnt. Adv Drug Deliv Rev. 2009; 61:1131-1148.

7. Desai N. Challenges in development of nanoparticle-based therapeutics. AAPS J. 2012; 14:282-295.

8. Deutscher SL, Figueroa SD, Kumar SR. In-labeled KCCYSL peptide as an imaging probe for ErbB-2-expressing ovarian carcinomas. J Labelled Comp Radiopharm. 2009; 52:583-590.

9. Greish K, Ray A, Bauer H, et al. Anticancer and antiangiogenic activity of HPMA copolymer-aminohexylgeldanamycin-RGDfK conjugates for prostate cancer therapy. J Control Release. 2011; 151:263-270.

10. Kumar SR, Gallazzi FA, Ferdani R, Anderson CJ, Quinn TP, Deutscher SL. In vitro and in vivo evaluation of ^{64}Cu-radiolabeled KCCYSL peptides for targeting epidermal growth factor receptor-2 in breast carcinomas. Cancer Biother Radiopharm. 2010; 25:693-703.

11. Pike DB, Ghandehari H. HPMA copolymer-cyclic RGD conjugates for tumor targeting. Adv Drug Deliv Rev. 2010; 62:167-183.

12. Ray A, Larson N, Pike DB, et al. Comparison of active and passive targeting of docetaxel for prostate cancer therapy by HPMA copolymer-RGDfK conjugates. Mol Pharm. 2011; 8:1090-1099.

13. Neesse A, Michl P, Frese KK, et al. Stromal biology and therapy in pancreatic cancer. Gut. 2011; 60:861-868.

14. Provenzano PP, Cuevas C, Chang AE, Goel VK, Von Hoff DD, Hingorani SR. Enzymatic targeting of the stroma ablates physical barriers to treatment of pancreatic ductal adenocarcinoma. Cancer Cell. 2012; 21:418-429.

15. Garber K. Stromal depletion goes on trial in pancreatic cancer. J Natl Cancer Inst. 2010; 102:448-450.

16. Merika EE, Syrigos KN, Saif MW. Desmoplasia in pancreatic cancer. Can we fight it? Gastroenterol Res Pract. 2012; 2012:781765.

17. Hruban RH, Adsay NV, Albores-Saavedra J, et al. Pathology of genetically engineered mouse models of pancreatic exocrine cancer: consensus report and recommendations. Cancer Res. 2006; 66:95-106.

18. Mendelsohn J. The molecular basis of cancer. 3rd ed. Philadelphia, PA: Saunders/Elsevier, 2008.

19. Cutler CS, Chanda N, Shukla R, et al. Nanoparticles and phage display selected peptides for imaging and therapy of cancer. Recent Results Cancer Res. 2013; 194:133-147.

20. Deutscher SL. Phage display in molecular imaging and diagnosis of cancer. Chem Rev. 2010; 110:3196-3211.

21. Karasseva NG, Glinsky VV, Chen NX, Komatireddy R, Quinn TP. Identification and characterization of peptides that bind human ErbB-2 selected from a bacteriophage display library. J Protein Chem. 2002; 21:287-296.

22. Koivunen E, Arap W, Rajotte D, Lahdenranta J, Pasqualini R. Identification of receptor ligands with phage display peptide libraries. J Nucl Med. 1999; 40:883-888.

23. Hijnen NM, Heijman E, Kohler MO, et al. Tumour hyperthermia and ablation in rats using a clinical MR-HIFU system equipped with a dedicated small animal set-up. Int J Hyperthermia. 2012; 28:141-155.

24. Goffredo V, Paradiso A, Ranieri G, Gadaleta CD. Yttrium-90 (90Y) in the principal radionuclide therapies: an efficacy correlation between peptide receptor radionuclide therapy, radioimmunotherapy and transarterial radioembolization therapy. Ten years of experience (1999-2009). Crit Rev Oncol Hematol. 2011; 80:393-410.

25. Goldsmith SJ. Radioimmunotherapy of lymphoma: Bexxar and Zevalin. Semin Nucl Med. 2010; 40:122-135.

26. Kopecek J, Kopeckova P. HPMA copolymers: origins, early developments, present, and future. Adv Drug Deliv Rev. 2010; 62:122-149.

APPENDIX

COMONOMER SYNTHESES AND CHARACTERIZATION

A.1. *N*-(2-hydroxypropyl)methacrylamide (HPMA)

A.1.1. HPMA synthesis

Synthesis was performed according to literature methods[1]. Briefly, 1-amino-2-propanol dissolved in 560 ml of acetonitrile was placed in an acetone-ice bath at less than -5ºC. 1 mg of inhibitor was added to the reaction. 100 g of methacryloyl chloride (MA-Cl) was added dropwise to the mixture. The reaction was allowed to stir for 30 min after the last amount of MA-Cl was added. The solid formed during the reaction was removed and the excess acetonitrile was evaporated by rotor evaporation. The final product was obtained by recrystallization in acetone overnight at -20ºC.

A.1.2. HPMA characterization

The resulting white solid was characterized by electrospray ionization mass spectroscopy (ESI-MS) *m/z* calculated for $C_7H_{13}NO_2$, 143.1836, found 178 $[M - Cl]^-$ and ^1H nuclear magnetic resonance (NMR) spectroscopy (400 MHz, CD_3OD) shown in *Figure A.1*.

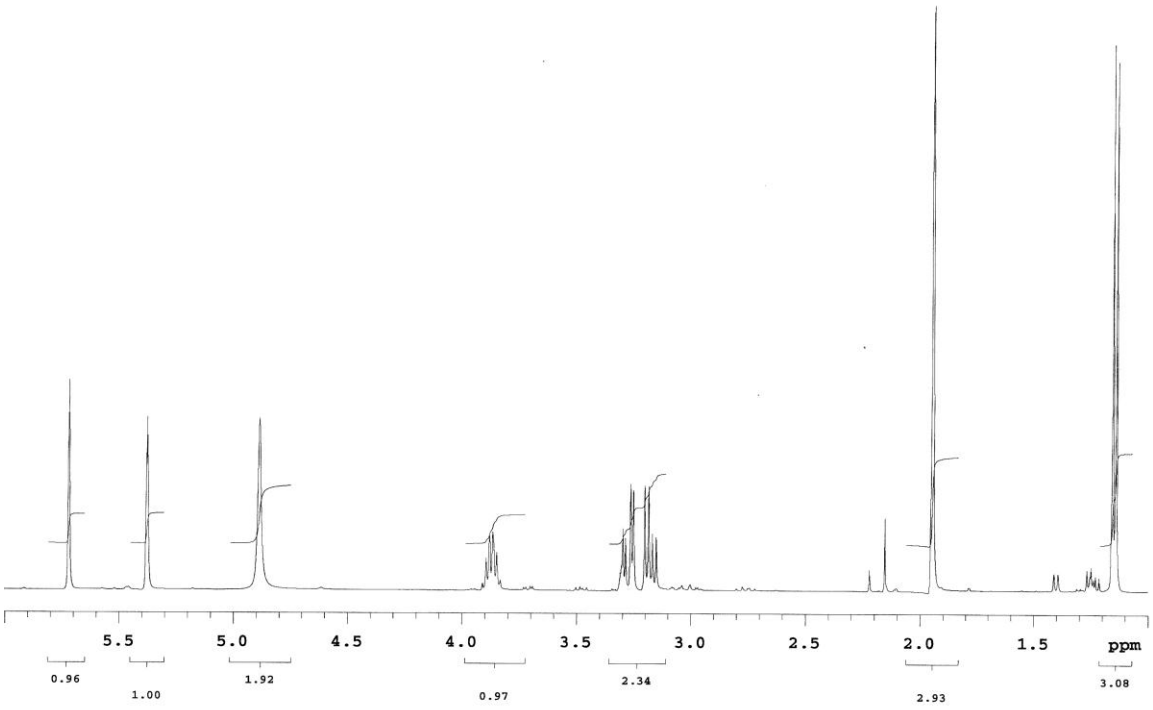

Figure A.1. NMR of HPMA monomer

A.2. *N*-methacryloylglycylglycyl thiazolidine-2-thione (MA-GG-TT)

A.2.1. MA-GG-TT synthesis

Synthesis was performed as described previously[2]. Briefly, a solution of 2 g of *N*-methacryloylglyclglycine (MA-GG-OH) and 1.33 g of 1,3-thiazolidine-2-thione (TT) were dissolved in 10 ml of cooled anhydrous dimethylformamide (DMF). The solution was cooled to -20ºC and then 2.48 g of *N,N'*-dicyclohexylcarbodiimide (DCC) in 10 ml of DMF (also cooled to -20 ºC) was added slowly, followed by 55 mg of 4-dimethylaminopyridine (DMAP). The solution was stirred overnight at 5ºC. 60 µl of acetic acid was added and stirred at room temperature for 1 h. The solution was filtered and the filtrate collected and excess solvent removed by rotor evaporation. The resulting yellow oil was recrystallized in a 1:1 acetone/ether solution.

A.2.2. MA-GG-TT characterization

The resulting yellow solid was collected and analyzed by ESI-MS *m/z*, calculated for $C_{11}H_{15}N_3O_3S_2$, 301.3851, found 322 $[M + Na]^+$ and ^1H NMR (400 MHz, d6-DMSO) shown in *Figure A.2*.

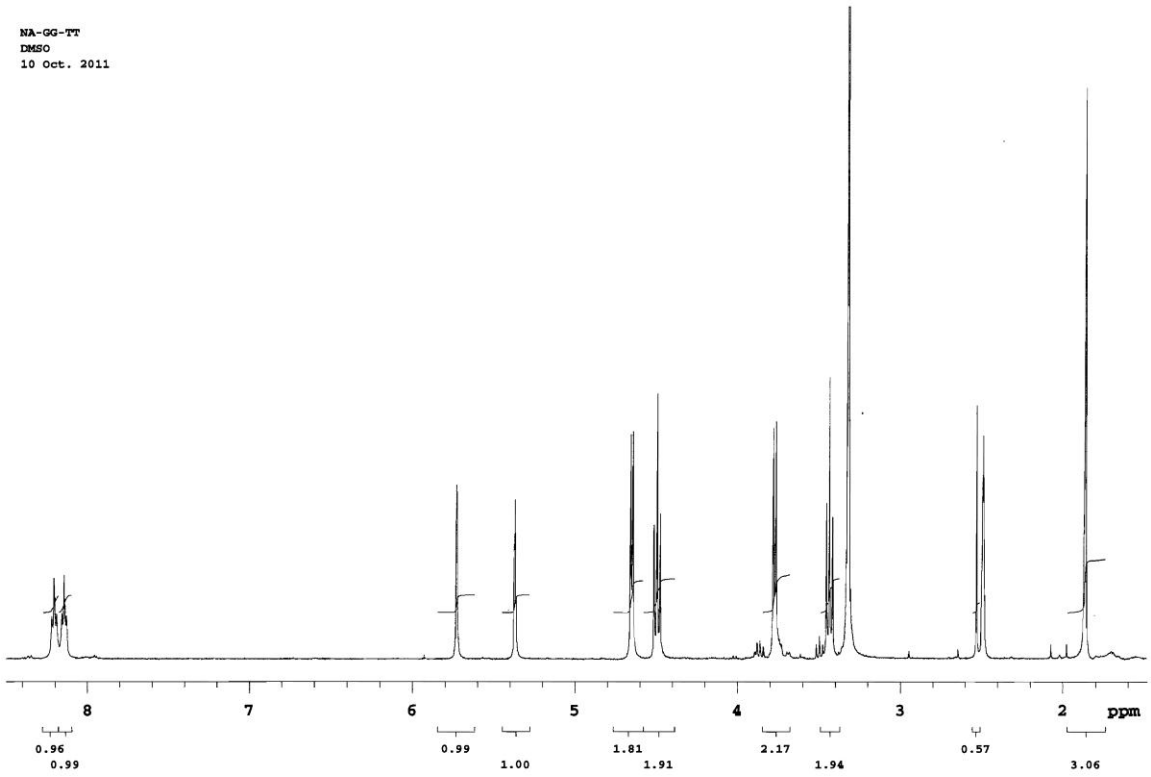

Figure A.2. NMR of MA-GG-TT.

A.3. *N*-methacryloylaminopropyl-2-amino-3-(isothiourea-phenyl)propyl-cyclohexane-1,2-diamine-N,N-N',N',N'',N''-pentaacetic acid (APMA-CHX-A"DTPA)

A.3.1. APMA-CHX-A"DTPA synthesis

Synthesis was performed according to literature methods[3]. Briefly, *N*-(3-aminopropyl)methacrylamide (APMA) was combined with *N*-[(R)-2-amino-3-(*p*-isothiocyanato-phenyl)propyl]-*trans*-(S,S)-cyclohexane-1,2-diamine-*N,N,N",N"*-pentaacetic acid (*p*-SCN-CHX-A"-DTPA) and diisopropylethylamine in a 1:1:5 molar ratio in DMF. The solution was purged with nitrogen, sealed and stirred for 24 h at room temperature. The final product was collected by precipitation, excessively washed with diethyl ether and recrystallized in acetone.

A.3.2. APMA-CHX-A"DTPA characterization

The resulting slightly yellow solid was collected and analyzed by ESI-MS *m/z*, calculated for $C_{33}H_{48}N_6O_{11}S$, 736.8328, found 735 $[M - H]^+$.

A.4. References

1. Strohalm J, Kopecek J. Poly *N*-(2-hydroxypropyl) methacrylamide: 4. Heterogenous polymerization. Angewandte Makromolekulare Chemie. 1978; 70:109-118.

2. Subr V, Ulbrich K. Synthesis and properties of new *N*-(2-hydroxypropyl)-methacrylamide copolymers containing thiazolidine-2-thione reactive groups. React Funct Polym. 2006; 66:1525-1538.

3. Mitra A, Nan A, Papadimitriou JC, Ghandehari H, Line BR. Polymer-peptide conjugates for angiogenesis targeted tumor radiotherapy. Nucl Med Biol. 2006; 33:43-52.